

LINEAR AND NONLINEAR OPTICAL PULSED  
RESPONSE OF CO<sub>2</sub> LASER AMPLIFIERS

by

PAUL WALTER HOFF

S. B., Massachusetts Institute of Technology  
(1966)

S. M., Massachusetts Institute of Technology  
(1966)

Submitted in Partial Fulfillment of the  
requirements for the Degree of  
Doctor of Philosophy  
at the  
Massachusetts Institute of Technology  
June 1970

Signature of Author:

\_\_\_\_\_  
Department of Electrical Engineering, May 11, 1970

Certified by:

\_\_\_\_\_  
Thesis Supervisor

Accepted by:

\_\_\_\_\_  
Chairman, Departmental Committee on Graduate Students

Archives



LINEAR AND NONLINEAR OPTICAL PULSED  
RESPONSE OF CO<sub>2</sub> LASER AMPLIFIERS

by

PAUL WALTER HOFF

Submitted to the Department of Electrical Engineering at the Massachusetts Institute of Technology on May 11, 1970, in partial fulfillment of the requirements for the degree of Doctor of Philosophy.

ABSTRACT

The linear and nonlinear optical response of a CO<sub>2</sub> laser amplifier has been measured for pulse inputs which have risetimes shorter than or comparable to the inverse bandwidth of the medium. The pulsed response behavior was predicted theoretically by integrating density matrix equations.

The theoretical linear (small-signal) response of a laser amplifier to a rectangular pulse signal input was derived. The linear step response was measured experimentally, and by comparison with the derived theoretical response, the bandwidth of the amplifier was directly measured.

The amplifier response was also studied for extremely intense fast risetime pulse inputs. At low amplifier gas pressures, the output pulses had faster risetimes than the input pulses, and the lagging edge of the pulse was absorbed leading to active pulse sharpening. The amplification was not bandwidth limited. At high gas pressures, no absorption of the lagging edge was observed because of rotational relaxation. The nonlinear pulse amplification results were also predicted theoretically.

Thesis Supervisor: Hermann A. Haus

Title: Professor of Electrical Engineering

## ACKNOWLEDGEMENTS

I wish to thank Professor Hermann A. Haus for the impetus and aid he provided me in doing this work. It was only through his knowledge and patience that this work came into being. I also wish to thank Thomas J. Bridges of Bell Telephone Laboratories who was a Visiting Professor at M. I. T. during 1967. His guidance, experimental advice, and friendship provided much needed aid. Frank Barrows provided valuable technical aid and designed much of the experimental equipment. Charles K. Rhodes kindly provided a program for computing the nonlinear pulse response at low pressures. I also wish to thank T. Kenneth Gustafson and Eugene Stark for a program to evaluate the nonlinear pulse response at high pressures. Professor Zimmermann and Ralph Sayers aided in obtaining space allocations and financial support which came from the Joint Services Electronics Program, the M. I. T. Sloan Fund for Basic Research, and a research grant from the Air Force Cambridge Research Laboratories.

## TABLE OF CONTENTS

	Page
ABSTRACT . . . . .	2
ACKNOWLEDGEMENTS . . . . .	3
LIST OF FIGURES . . . . .	6
CHAPTER I INTRODUCTION . . . . .	8
CHAPTER II THEORETICAL LINEAR RESPONSE OF LASER AMPLIFIERS . . . . .	13
Equations of motion of the density matrix.	14
Linear amplification on line center for homogeneous broadened line. . . . .	22
Linear amplification off line center for homogeneous broadened line. . . . .	28
Linear amplification with inhomogeneous broadening. . . . .	33
CHAPTER III EXPERIMENTAL SMALL-SIGNAL STEP RESPONSE AND MEASUREMENT OF BANDWIDTH . . . . .	39
The GaAs electro-optic modulator. . . . .	39
The multipass amplifier. . . . .	44
Sources of experimental error. . . . .	53
CHAPTER IV NONLINEAR AMPLIFICATION IN A LASER AMPLIFIER . . . . .	55
High pressure nonlinear amplification. . . . .	55
Low pressure nonlinear amplification. . . . .	57
Intermediate pressure nonlinear amplification.	57
Theoretical model for high pressure nonlinear amplification. . . . .	57

	Page
Theoretical model for low pressure nonlinear amplification. . . . .	65
Comparison with analytic $\pi$ -pulse solutions.	74
Effect of nonuniform electric field. . .	74
CHAPTER V      NONLINEAR PULSE AMPLIFICATION	
EXPERIMENT . . . . .	76
Experimental limitations on intense short pulse production. . . . .	85
Low pressure amplification results and computer matching of curves. . . .	88
High pressure amplification results and computer matching of curves. . . .	95
CHAPTER VI     CONCLUSIONS . . . . .	99
APPENDIX A     PROGRAM TO EVALUATE LINEAR STEP RESPONSE . . . . .	101
APPENDIX B     CALCULATION OF AMPLIFIER BANDWIDTH FROM COLLISION CROSS SECTION MEASUREMENTS . . . . .	102
APPENDIX C     PROGRAM TO EVALUATE NONLINEAR PULSE RESPONSE . . . . .	104
REFERENCES . . . . .	112
BIOGRAPHICAL NOTE . . . . .	115

## LIST OF FIGURES

Figure		Page
2-1	Impulse response for linear amplification. . . . .	25
2-2	Linear step response for constant gain with varying bandwidth. . . . .	29
2-3	Linear step response for constant bandwidth with varying gain. . . . .	30
2-4	Off resonance linear amplification. . . . .	32
2-5	Inhomogeneous amplification. . . . .	35
3-1	Linear experiment schematic. . . . .	40
3-2	Gallium arsenide crystal. . . . .	42
3-3	Multipass mirrors. . . . .	46
3-4	Masks for multipass mirrors. . . . .	47
3-5	Experimental step response. . . . .	49
3-6	Fitting of experimental step response with theoretical step response. . . . .	51
3-7	Experimentally measured bandwidth versus pressure.	52
4-1	Rotational relaxation. . . . .	56
4-2	Theoretical high pressure pulse amplification. . . . .	60
4-3	Population for Figure 4-2. . . . .	63
4-4	Population for Figure 4-5. . . . .	66
4-5	Theoretical high pressure pulse amplification with rotational relaxation. . . . .	67
4-6	Degenerate amplification. . . . .	69
4-7	Theoretical low pressure pulse amplification. . . . .	72
4-8	Comparison between pulse amplification for P(20) and single level. . . . .	73
5-1	Schematic of nonlinear experiment. . . . .	78
5-2	Operation of cavity-dumping scheme. . . . .	79

Figure		Page
5-3	Experimental cavity intensity and GaAs voltage versus time. . . . .	81
5-4	Experimental dumped pulse and cavity intensity versus time. . . . .	81
5-5	Multiple exposure of Figure 5-3. . . . .	82
5-6	Spontaneous mode locking. . . . .	82
5-7	Detector circuit. . . . .	84
5-8	Voltage pulser for GaAs . . . . .	86
5-9	Experimental low pressure amplification result. .	89
5-10	Figure 5-9 with detector characteristics taken into account. . . . .	90
5-11	One computer matching fit for Figure 5-10. . .	92
5-12	Second experimental low pressure amplification result with computer matching fit. . . . .	94
5-13	Figure 5-11 with larger input intensity. . . .	96
5-14	Experimental high pressure amplification result with computer matching fit. . . . .	97

## CHAPTER I

### INTRODUCTION

Ever since its advent five years ago, the CO<sub>2</sub> laser has commanded a great deal of interest both as a research tool and as a commercially useable laser. Its high gain (in excess of 3 db/meter), ease of construction, high power, and ability to be Q-switched recommend it for a variety of tasks. In this work we are interested in the short pulse behavior of CO<sub>2</sub> lasers both as oscillators and amplifiers; as oscillators to be able to generate short CO<sub>2</sub> laser pulses, and as amplifiers to determine what limits the amplification of short pulses. It is in conjunction with this second goal that we have examined some of the basic physical mechanisms which occur in the CO<sub>2</sub> laser, such as the effects of multiple degeneracy upon amplification, saturation broadening, and bandwidth limited amplification. In the course of the investigation we have determined a way to measure the bandwidth directly when amplifying low intensity pulses, and can achieve pulse amplification at frequencies greater than the bandwidth in conjunction with pulse shaping when intense pulses are amplified.

Since the experimental portion of this work was concerned with generation, amplification, and measurement of these short pulses, it was considered beyond the scope of this work to construct any CO<sub>2</sub> laser amplifiers capable of producing high cw power levels such as those constructed by Miles and associates. Rather, the experimental emphasis here was placed upon the use of GaAs electro-optic modulators to generate pulses much shorter than the more standard methods used to generate them.



The motivation for studying short pulse amplification arises mainly from the fact that the  $\text{CO}_2$  laser, because of its high gain and the long lifetime of its upper state, can be Q-switched to generate short intense pulses. That is, the Q of the laser cavity is lowered to prevent oscillation, permitting the population inversion to be at its nonsaturated level, and then the Q is raised to a high value for a short period of time causing a brief intense pulse to be emitted. The existence of these pulses raises questions concerning their production and use; for example, is it better to make a long laser cavity with high gain to generate more intense pulses, or is it better to create a pulse of sufficient intensity and then amplify it for greater intensity? Studies here indicate that the pulse length of a Q switch increases with the length of an oscillator and that the peak intensity does not grow as quickly, whereas much greater peak intensities and pulse shortening may be obtained with the use of an oscillator-amplifier combination. An example of the need for knowledge of short  $\text{CO}_2$  pulses arises from preliminary studies of  $\text{CO}_2$   $10.6 \mu$  radars, which originally generated interest because of the atmospheric window at this wavelength. Shorter pulses improve the resolution of the radar, so again the problem is how to create short pulses without sacrificing the energy in the pulse.

Interest in short  $\text{CO}_2$  pulses also arises from the possibility of their use in second harmonic generation. If a pulse of sufficient intensity propagates through certain nonlinear materials, second harmonic radiation can be generated at a high efficiency. This work has applications in frequency measurements of visible radiation; the frequency of  $\text{CO}_2$  can be measured by mixing it with previously measured longer wavelength  $\text{H}_2\text{O}$  lines. Once the frequency of  $\text{CO}_2$  is known, second

harmonic generation can be used to get into the visible and measure the frequencies of some of the shorter wavelength lasers, such as He-Ne.

The work here was made possible only by novel schemes of short pulse generation for both low level and intense pulses. As a rule, we found no new interesting effects to occur unless the peak pulse power was realized in a time comparable to the inverse bandwidth of the medium. However, pulses produced by conventional means are limited in their buildup time by the bandwidth of the medium. In this work, we have utilized a voltage controlled polarization switch (GaAs with a Ge polarizer) to produce pulses of both small and large intensities that have risetimes significantly less than the bandwidth of the medium.

It was because other workers have had such problems in generating short pulses that this field of research has not been adequately explored. Although some authors<sup>1, 2, 3, 4</sup> have considered the problem of an intense pulse propagating through an amplifying medium, no one has done experiments to study some of their more interesting conclusions. More recently, picosecond pulses in neodymium doped glass lasers<sup>5</sup> have been produced and amplified. While interesting effects due to fast, intense pulses were observed, no attempt was made to match these with a descriptive theory. In addition, the work was not performed in CO<sub>2</sub> or even another gas laser, so many results we hoped to see were not present in this work. In addition, the bandwidth in glass lasers is so large that the pulses necessary to achieve the type of effects discussed here are so short as to not be easily detected. Currently, these picosecond pulses are being detected by photographing double resonant fluorescence in a dye and measuring the length of space these pulses occupy. However, in CO<sub>2</sub> lasers these pulses are in the nanosecond range and can be readily

measured on an oscilloscope.

Recently much work has been done on an effect known as "self-induced transparency" (a mechanism whereby a pulse may propagate through an absorbing medium without energy loss). Although this work is extremely interesting, it (1) does not study propagation in an amplifying medium, (2) considers pulses only much shorter than the inverse bandwidth, and (3) is not done in  $\text{CO}_2$ . Quite recently though, people have looked for self-induced transparency by shining  $\text{CO}_2$  laser radiation through sulfur hexafluoride ( $\text{SF}_6$ ),<sup>6</sup> but again this is not an amplifying medium. In addition, much controversy surrounds this work, since little is known about  $\text{SF}_6$  and its transitions. Other workers have used  $\text{SF}_6$  as a saturable absorber placed internally in a  $\text{CO}_2$  laser cavity for self-induced Q-switching.<sup>7</sup> This is only of interest here as a possible means of producing an intense pulse for nonlinear amplification purposes. However, work has been reported similar to reference 6, where an inertial effect in the population is supposedly observed.<sup>8</sup> But the reported effects could be due to off resonance absorption rather than saturation of the absorber in a time comparable to the bandwidth.

The only work done for intense pulse amplification of  $\text{CO}_2$  laser radiation in a  $\text{CO}_2$  laser amplifier was for an input pulse where the energy necessary to cause saturation was not achieved until the pulse was much larger than  $T_2$ , the inverse bandwidth.<sup>9</sup> That is, the amplifier was simply saturated and there was no ringing in the population (an effect which we hope will lead to achieving pulse sharpening).

As far as can be determined, no one has ever theoretically calculated or measured any parameters of low-level, short pulse amplification. In this work, we theoretically determine the impulse response, numerically

calculate the step response, and compare this to experimentally measured low-level step response.

## CHAPTER II

### THEORETICAL LINEAR RESPONSE OF LASER AMPLIFIERS

To describe adequately the behavior of laser amplifiers to pulses short compared with the inverse bandwidth of the medium, one must use a density matrix description of the material. One starts with Maxwell's and Schrodinger's equations and uses them to describe the interaction of an electromagnetic field with an ensemble of quantum systems which, in addition, experience relaxation described by appropriate time constants. This approach, which is a good deal more complicated than rate equations, is necessitated here by the fact that we are considering time responses of the quantum systems in which the macroscopic polarization cannot follow "instantaneously" the electric field. If pulses longer than the inverse bandwidth were to be considered, a rate equation approach could be used.

Although density matrix equations can be written in various degrees of complexity, the following assumptions will be used here in describing the linear fast time response of the laser amplifier:

- (1) A plane electromagnetic wave will be assumed. As long as the pulse amplification is not so strong as to cause changes in the electric field within a wavelength or so of propagation, the diffraction of a linearly amplified beam is the same in the medium as it would be in free space. Since a detector measures power, the spatial integral of the square of the electric field, and the electric field is everywhere amplified the same amount, the plane wave assumption is valid for linear amplification. However, for nonlinear amplification,

different intensities experience different amplification, the diffraction of the beam can be significantly different in the medium than in free space, and the plane wave assumption presents problems.

Now consider the linear amplification of an input pulse with an arbitrary transverse intensity distribution; the output beam will only be affected by the uniform gain the medium imparts to the beam. Therefore, a plane wave may be substituted for the arbitrary intensity distribution.

- (2) A two-level system will be assumed. Again, the results obtained under this assumption are immediately generalizable to a multilevel medium, but are not extendable to the nonlinear case. In the case of a  $\text{CO}_2$  laser operating on a P(20) transition, there are 20 different dipole moments contributing to the amplification process. In the nonlinear case, the quantum system behaves as a two-level system with an average dipole moment only for times longer than the inverse bandwidth.
- (3) Homogeneous broadening is assumed. This may appear to be improper in a  $\text{CO}_2$  laser where the homogeneous and inhomogeneous bandwidths (Doppler broadening in this case) are comparable; however, it will be shown that for a high gain system the linear amplification is virtually the same for either broadening mechanism.

### Equations of motion

The motion of the particles of the system is given by the time rate of change of the density matrix,<sup>1</sup> which is given by

$$\dot{\rho} = i/\hbar[\rho, H] = i/\hbar(\rho H - H\rho)$$

or in the notation of individual matrix elements

$$\dot{\rho}_{mn} = i/\hbar \sum_k (\rho_{mk} H_{kn} - H_{mk} \rho_{kn}) \quad (2-1)$$

where H is the complete Hamiltonian of the system and  $\rho$  is Hermitian,

i. e.,  $\rho_{ij} = \rho_{ji}^*$ . Equation (2-1) expanded reduces to

$$\dot{\rho}_{12} = (\dot{\rho}_{21})^* = \frac{i}{\hbar} [-(\rho_{22} - \rho_{11})H_{12} + \rho_{12}(H_{22} - H_{11})] \quad (2-2)$$

$$(\dot{\rho}_{22} - \dot{\rho}_{11}) = \frac{2i}{\hbar} (\rho_{21}H_{12} - \rho_{12}H_{21}) \quad (2-3)$$

where we now resort to perturbation theory to let

$$H = H_0 + V \quad V = -\bar{E} \cdot \bar{P}$$

with  $\bar{E}$  being the classical electric field and  $\bar{P}$  the polarization.  $H_0$  is a diagonal matrix and  $\bar{P}$  pure off-diagonal

$$H_0 = \begin{vmatrix} H_{11}^0 & 0 \\ 0 & H_{22}^0 \end{vmatrix} \quad \bar{P} = \begin{vmatrix} 0 & \bar{P}_{12} \\ \bar{P}_{21} & 0 \end{vmatrix}$$

with

$$H_{22}^0 - H_{11}^0 = H_{22} - H_{11} = \hbar\omega_m > 0$$

and

$$H = \begin{vmatrix} H_{11} & -\bar{E} \cdot \bar{P}_{12} \\ -\bar{E} \cdot \bar{P}_{21} & H_{22} \end{vmatrix}$$

By adding in phenomenological relaxation terms, (2-2) and (2-3) become

$$\begin{aligned} (\dot{\rho}_{22} - \dot{\rho}_{11}) &= \frac{-2i}{\hbar} (\rho_{21} \bar{E} \cdot \bar{P}_{12} - \rho_{12} \bar{E} \cdot \bar{P}_{21}) \\ &\quad - \frac{(\rho_{22} - \rho_{11}) - (\rho_{22}^e - \rho_{11}^e)}{T_1} \end{aligned} \quad (2-4)$$

$$(\dot{\rho}_{21})^* = \dot{\rho}_{12} = \frac{i}{\hbar} [(\rho_{22} - \rho_{11}) \bar{E} \cdot \bar{P}_{12} + \rho_{12} \hbar \omega] - \frac{\rho_{12}}{T_2} \quad (2-5)$$

Note that the relaxation term  $T_1$  describes the relaxation of the levels to their equilibrium value. This may be inadequate to describe relaxation between rotational levels in a  $\text{CO}_2$  laser amplifier, but for linear amplification this term is not important. The off-diagonal relaxation term,  $T_2$ , often called "the phase interruption time," describes the decay of the polarization. By solving these equations in the steady state, one finds the homogeneous (Lorentzian in shape) linewidth,  $\Delta\nu_n$ , to be equal to  $\frac{1}{\pi} T_2$ .

If we now consider the molecular dipole moment  $P_{12}$ ,  $P_{21}$  to be real and depend only on the state of the molecules under consideration

$$\bar{P}_{12} = \bar{P}_{21} = \mu$$

and a sinusoidal electric field which is linearly polarized

$$\bar{E} = E \cos [\omega t - kz + \varphi(z, t)] = \frac{1}{2} [E_+ e^{i(\omega t - kz)} + E_+^* e^{-i(\omega t - kz)}]$$

and in-phase rotating off-diagonal density matrix elements,

$$\rho_{12} = \rho_{12}(t) e^{i(\omega t - kz)} \quad \rho_{21} = \rho_{21}(t) e^{-i(\omega t - kz)}$$



for (2-4) we arrive at

$$\begin{aligned} (\dot{\rho}_{22} - \dot{\rho}_{11}) &= \frac{-i}{\hbar} (\rho_{21} E_+ - \rho_{12} E_+^*) \mu - \frac{(\rho_{22} - \rho_{11}) - (\rho_{22}^e - \rho_{11}^e)}{T_1} \\ &\quad - \frac{i}{\hbar} \left[ \rho_{21} E_+ e^{-2i(\omega t - kz)} - \rho_{12} E_+^* e^{2i(\omega t - kz)} \right] \mu \end{aligned}$$

The double frequency terms oscillate so fast compared to the other terms that they average to zero over short times or, in other words, they do not couple effectively; hence we shall drop these double-frequency terms

$$(\dot{\rho}_{22} - \dot{\rho}_{11}) = \frac{-i}{\hbar} (\rho_{21} E_+ - \rho_{12} E_+^*) \mu - \frac{(\rho_{22} - \rho_{11}) - (\rho_{22}^e - \rho_{11}^e)}{T_1} \quad (2-6)$$

If we proceed in a similar manner on (2-5)

$$\begin{aligned} \dot{\rho}_{12} &= \left[ i\omega \rho_{12} + \rho_{12} \right] e^{i(\omega t - kz)} \\ &= \frac{i}{\hbar} \left[ (\rho_{22} - \rho_{11}) \frac{E_+}{2} \mu + \rho_{12} \hbar \omega_m - \frac{\rho_{12}}{T_2} \right] e^{i(\omega t - kz)} \\ &\quad + \frac{i}{\hbar} (\rho_{22} - \rho_{11}) \frac{E_+}{2} \mu e^{-i(\omega t - kz)} \end{aligned}$$

divide by the exponential, drop the double-frequency term, and define

$$\Omega = (\omega - \omega_m)$$

$$\dot{\rho}_{12} = \frac{i}{\hbar} (\rho_{22} - \rho_{11}) \frac{E_+}{2} \mu - i\Omega \rho_{12} - \frac{\rho_{12}}{T_2} \quad (2-7)$$

and

$$\dot{\rho}_{21} = \frac{-i}{\hbar} (\rho_{22} - \rho_{11}) \frac{E_+}{2} \mu + i\Omega\rho_{21} - \frac{\rho_{21}}{T_2} \quad (2-8)$$

We must now consider the propagation of the electromagnetic field in the laser amplifier. The two pertinent Maxwell equations are given by

$$\nabla \times \bar{E} = -\mu_e \frac{\partial \bar{H}}{\partial t} \quad (2-9)$$

$$\nabla \times \bar{H} = \frac{\partial \bar{D}}{\partial t} \quad (2-10)$$

with the definition

$$\bar{D} = \epsilon \bar{E} + \bar{P}$$

Under the assumption that we have sinusoidal fields, we can describe the electric field and polarization by

$$\bar{E}(z, t) = \frac{1}{2} \left[ \bar{E}_+ e^{i(\omega t - kz)} + \bar{E}_- e^{-i(\omega t - kz)} \right] \quad (2-11)$$

$$\bar{P}(z, t) = \frac{1}{2} \left[ \bar{P}_+ e^{i(\omega t - kz)} + \bar{P}_- e^{-i(\omega t - kz)} \right] \quad (2-12)$$

where  $\bar{E}_+ = \bar{E}_-^*$ . We have from (2-11)

$$\begin{aligned} \frac{\partial \bar{E}}{\partial t} &= \frac{1}{2} e^{i(\omega t - kz)} \left[ i\omega \bar{E}_+ + \dot{\bar{E}}_+ \right] \\ &+ \frac{1}{2} e^{-i(\omega t - kz)} \left[ -i\omega \bar{E}_- + \dot{\bar{E}}_- \right] \end{aligned}$$

$$\begin{aligned}
\frac{\partial^2 \mathbf{E}}{\partial t^2} &= \frac{1}{2} e^{i(\omega t - kz)} \left[ -\omega^2 \mathbf{E}_+ + 2i\omega \dot{\mathbf{E}}_+ \right] \\
&+ \frac{1}{2} e^{-i(\omega t - kz)} \left[ -\omega^2 \mathbf{E}_- - 2i\omega \dot{\mathbf{E}}_- + \ddot{\mathbf{E}}_- \right] \\
\frac{\partial^2 \mathbf{E}}{\partial z^2} &= \frac{1}{2} e^{i(\omega t - kz)} \left[ -k^2 \mathbf{E}_+ - 2ki \frac{\partial \mathbf{E}_+}{\partial z} + \frac{\partial^2 \mathbf{E}_+}{\partial z^2} \right] \\
&+ \frac{1}{2} e^{-i(\omega t - kz)} \left[ -k^2 \mathbf{E}_- + 2ki \frac{\partial \mathbf{E}_-}{\partial z} + \frac{\partial^2 \mathbf{E}_-}{\partial z^2} \right] \\
\frac{\partial^2 \mathbf{P}}{\partial t^2} &= \frac{1}{2} e^{i(\omega t - kz)} \left[ -\omega^2 \mathbf{P}_+ + 2i\omega \dot{\mathbf{P}}_+ + \ddot{\mathbf{P}}_+ \right] \\
&+ \frac{1}{2} e^{-i(\omega t - kz)} \left[ -\omega^2 \mathbf{P}_- - 2i\omega \dot{\mathbf{P}}_- + \ddot{\mathbf{P}}_- \right]
\end{aligned}$$

From (2-9), in the conventional fashion we can show

$$\nabla \times \nabla \times \bar{\mathbf{E}} = -\nabla^2 \bar{\mathbf{E}} = -\mu_e \frac{\partial^2 \bar{\mathbf{D}}}{\partial t^2} = \mu_e \frac{\partial^2 \bar{\mathbf{P}}}{\partial t^2} + \epsilon \mu_e \frac{\partial^2 \bar{\mathbf{E}}}{\partial t^2} \quad (2-13)$$

If we assume no non-linearities, then we can simply take the positive frequency term, letting  $\epsilon \mu_e = 1/c^2$ . We see that (2-13) reduces to

$$\begin{aligned}
-\omega^2 \mu_e \mathbf{P}_+ + 2i\omega \mu_e \dot{\mathbf{P}}_+ - \frac{\omega^2}{c^2} \mathbf{E}_+ + \frac{2i\omega}{c^2} \dot{\mathbf{E}}_+ \\
+ \frac{1}{c^2} \ddot{\mathbf{E}}_+ + k^2 \mathbf{E}_+ + 2ki \frac{\partial \mathbf{E}_+}{\partial z} - \frac{\partial^2 \mathbf{E}_+}{\partial z^2} = 0
\end{aligned} \quad (2-14)$$

If  $\omega/c = k$  and we use the slow wave approximation, that is, that

$$P_+ \gg \frac{1}{\omega} \dot{P}_+ \gg \frac{1}{\omega^2} \ddot{P}_+ \quad E_+ \gg \frac{1}{\omega} \dot{E}_+ \quad E_+ \gg \frac{i}{k} \frac{\partial E_+}{\partial z}$$

then the reduced form of (2-14) is

$$\frac{1}{c} \frac{\partial E_+}{\partial t} + \frac{\partial E_+}{\partial z} = - \frac{i\omega^2 \mu_e}{2k} P_+ = - \frac{i\omega}{2\epsilon c} P_+$$

We can relate the polarization to the density matrix formulation by

$$\begin{aligned} P(x, t) &= N \langle P \rangle = N \text{Tr} \{ \rho P \} = +n\mu(\rho_{12} + \rho_{21}) \\ &= +n\mu \left[ \rho_{12} e^{i(\omega t - kz)} + \rho_{21} e^{-i(\omega t - kz)} \right] \end{aligned}$$

Therefore,

$$\frac{1}{c} \frac{\partial E_+}{\partial t} + \frac{\partial E_+}{\partial z} = - \frac{\omega n \mu i}{\epsilon c} \rho_{12} \quad (2-15)$$

For convenience let us introduce the following normalizations

(1) The normalized electric field:

$$F = \frac{\sqrt{\epsilon} E_+}{\sqrt{\hbar \omega_m \Delta N_e}} \quad (2-16)$$

(2) The normalized macroscopic polarization current:

$$K = \frac{i T_n \omega_m \mu n \rho_{12}}{\sqrt{2\epsilon} \sqrt{\hbar \omega_m \Delta N_e}} \quad (2-17)$$

(3) The normalized population inversion;

$$N = \frac{\rho_{22}^e - \rho_{11}^e}{\rho_{22}^e + \rho_{11}^e} \quad (2-18)$$

(4) The normalized time:

$$T = \frac{t}{T_n}$$

(5) The normalized distance:

$$Z = \frac{z}{c T_n}$$

where  $\Delta N_e = n(\rho_{22}^e - \rho_{11}^e)$  is the equilibrium inversion and  $T_n$  a normalization time.

The equations (2-6), (2-7), and (2-15), which describe the interaction, then become

$$\frac{\partial F}{\partial T} + \frac{\partial F}{\partial Z} = -K \quad (2-19)$$

$$\frac{\partial K}{\partial T} = -ANF - i\Omega K - \frac{K}{T_2} \quad (2-20)$$

$$\frac{\partial N}{\partial T} = 2(F^* K + FK^*) - \frac{N-1}{T_1} \quad (2-21)$$

where now  $\Omega = T_n (\omega - \omega_m)$  and  $A = \mu^2 \Delta N_e \omega_m T_n^2 / 2\hbar\epsilon = \alpha c T_n^2 / 2T_2$ , where  $\alpha$  is the low signal power gain coefficient.

The following points are of interest about these equations:

- (1) if  $\partial K/\partial T$  can be neglected compared with  $K/T_2$ , we obtain the rate equation;
- (2) there are actually five real equations, since  $F$  and  $K$  are complex; however, if  $\omega_f = \omega_m$ , the amplification is at line center, and  $F$  and  $K$ , if initially real, remain real;
- (3) for linear amplification, by definition  $N = 1$ , and the equation for  $\partial N/\partial T$  is not employed;
- (4) for linear or nonlinear amplification, the boundary condition imposed on this set of partial differential equations is the electric field at  $z = 0$  as a function of time, or at  $t = 0$  as a function of  $z$ ;
- (5) since the pulse is propagating in one dimension in space and another in time, it is convenient to define a new variable:  $n = T + Z$  for use in numerical integration techniques.

#### Linear amplification on line center for homogeneous broadened line

In this case both  $F$  and  $K$  are real,  $\Omega = 0$ ; the equations of interest are:

$$\frac{\partial F}{\partial T} + \frac{\partial F}{\partial Z} = -K \quad (2-22)$$

$$\frac{\partial K}{\partial T} = -AF - \frac{K}{T_2} \quad (2-23)$$

Furthermore, we are concerned with obtaining the solution to a low-level step of radiation propagating through the medium since this is the experiment we are able to perform. To obtain this step response

we may solve the above equations exactly for the impulse response. Let us put the following boundary condition on the above equation

$$F_+(Z, 0) = \mu_0(Z)$$

The equations may be solved using a Fourier transform in time and a Laplace transform in space.<sup>10</sup> Hence, we define

$$F(Z, T) = \int_{-\infty - i\sigma}^{\infty - i\sigma} d\omega' e^{-i\omega' T} \int_{-\infty}^{\infty} d\beta e^{i\beta Z} F(\omega', \beta)$$

and the Fourier transform of the initial condition becomes

$$F(\beta, 0) = \frac{1}{2\pi}$$

Solving for the transform we find from equation (2-22) and (2-23)

$$i(\omega' - \beta) F - F(\beta, 0) = -K$$

$$(i\omega' + \frac{1}{T_2})K = -AF$$

The transform of the electric field becomes

$$F(\beta, \omega') = \frac{1}{2\pi i \left\{ (\omega' - \beta) + \frac{A}{\omega' - \frac{i}{T_2}} \right\}}$$

The inverse transform of this cannot be taken directly because of an essential singularity which cannot be evaluated when the contour integral of the inverse transform is deformed. However, using the technique of reference 10, we can find an analytic solution of the impulse response

which can be verified by direct substitution.

$$F = \mu_0(T - Z) + \exp\left(\frac{T - Z}{T_2}\right) \left\{ \left(\frac{AZ}{T - Z}\right)^{\frac{1}{2}} I_1 \left[ 2(AZ)^{\frac{1}{2}} (T - Z)^{\frac{1}{2}} \right] \right\} \quad T > Z$$

$$= 0 \quad T < Z$$

$I_1$  is a modified Bessel Function of first order.

For ease of understanding it is convenient to write the previous equation without the normalized variables defined in equations (2-16), (2-17), and (2-18). The electric field impulse response then becomes, with  $T_n = t_2$ :

$$E = \mu_0(ct - z) + \exp\left(-\frac{t - \frac{z}{c}}{t_2}\right) \left(\frac{zA}{t - \frac{z}{c}}\right)^{\frac{1}{2}} \frac{1}{c^{3/2} t_2} \cdot I_1 \left[ \frac{2}{t_2} \left(\frac{zA}{c}\right)^{\frac{1}{2}} \left(t - \frac{z}{c}\right)^{\frac{1}{2}} \right] \quad t > \frac{z}{c}$$

(2-24)

$$= 0 \quad t < \frac{z}{c}$$

The constant A is now defined as

$$A = \frac{\alpha c t_2}{2}$$

where again  $\alpha$  is the low signal gain coefficient. Figure 2-1 shows expression (2-24) plotted for three different times for conditions typical of the  $\text{CO}_2$  laser.

We now turn to the evaluation of the step-response of an amplifier constructed of the two-level system. Denote the impulse response function in (2-24) by  $h(t, z)$ . If we denote the step response by  $E_{\text{step}}$  then we have by superposition



RESPONSE TO UNIT FIELD IMPULSE

$G_0 = 4.5 \text{ dB/m}$

$T_2 = 3 \text{ nanosecond}$

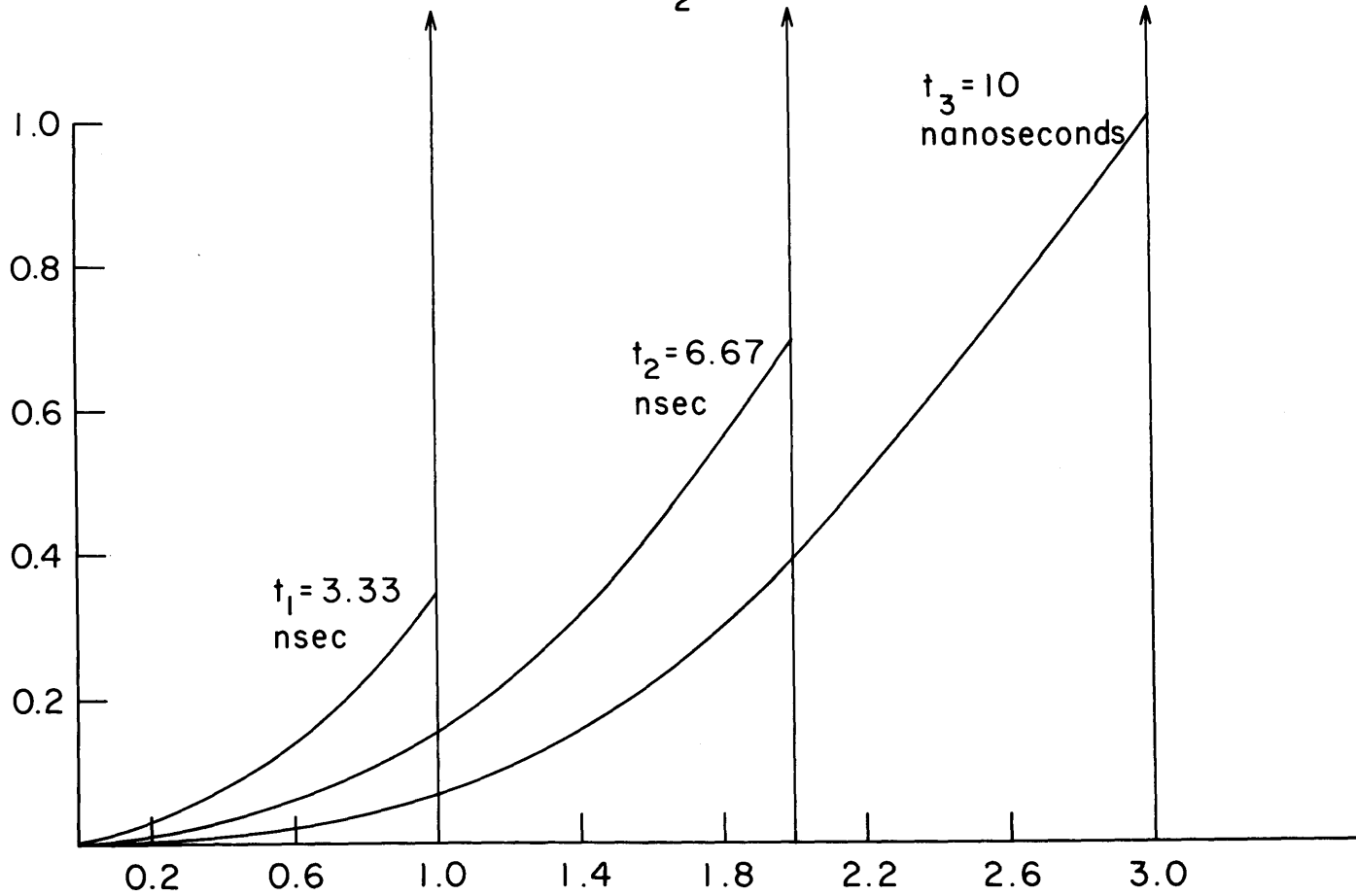


FIGURE 2-1

METERS

$$E_{\text{step}} = \int_{-\infty}^{\infty} h(t-\tau; z) \mu_{-1}(\tau) d\tau$$

where  $h(t-\tau; z) = cE$  impulse response because of our initial condition being an impulse in space.

$$E_{\text{step}} = \int_{\tau=0}^{t-z} \left\{ \mu_0 [c(t-\tau) - z] + \exp\left(\frac{t-\tau-\frac{z}{c}}{t_2}\right) \right. \quad (2-25)$$

$$\cdot \left. \frac{1}{c^{\frac{1}{2}} t_2} \left(\frac{zA}{t-\tau-\frac{z}{c}}\right)^{\frac{1}{2}} I_1 \left[ \frac{2}{t_2} \left(\frac{zA}{c}\right)^{\frac{1}{2}} \left(t-\tau-\frac{z}{c}\right)^{\frac{1}{2}} \right] \right\} d\tau$$

$$= S\left(t-\frac{z}{c}\right) + \int_0^{\frac{2}{t_2} \left(\frac{zA}{c}\right) \left(t-\frac{z}{c}\right)^{\frac{1}{2}}} e^{-\beta \chi^2} I_1(\chi) d\chi \quad (2-26)$$

where  $S$  is the unit step function,  $\chi$  is the normalized variable

$$\frac{2}{t_2} \left(\frac{Az}{c}\right)^{\frac{1}{2}} \left(t-\tau-\frac{z}{c}\right)^{\frac{1}{2}}, \text{ and } \beta = ct_2/4zA.$$

Note that this response shows an unperturbed step propagating through the medium. This means that the amplifier cannot respond to an infinitely fast risetime step; however, the amplifier adds to the remaining part of the step, which is indicated by the second term in equation (2-26). This step response can also be expressed in terms of Lommel functions defined as<sup>11</sup>

$$U_{\nu}(\omega, z) = \frac{\omega^{\nu}}{z^{\nu-1}} \int_0^1 J_{\nu-1}(z, t) \cos\left\{\frac{1}{2}\omega(1-t^2)\right\} t^{\nu} dt$$

$$U_{\nu-1}(\omega, z) = \frac{\omega^\nu}{z^{\nu-1}} \int_0^1 J_{\nu-1}(z, t) \sin\left\{\frac{1}{2}\omega(1-t^2)\right\} t^\nu dt$$

By adding the Lommel functions  $U_1$  and  $iU_2$  for pure imaginary argument, one gets an integral identical in form to the last term in (2-26). Hence, one finds

$$\begin{aligned} E_{\text{step}} &= e^{-(t-z/c)/t_2} \left\{ I_0 \left[ \left( \frac{Az}{c} \right)^{\frac{1}{2}} \left( t - \frac{z}{c} \right)^{\frac{1}{2}} \right] \right. \\ &\quad + iU_1 \left[ -\frac{2i}{t_2} \left( t - \frac{z}{c} \right), 2i \left\{ \frac{Az}{ct_2^2} \left( t - \frac{z}{c} \right) \right\}^{\frac{1}{2}} \right] \\ &\quad \left. - U_2 \left[ -\frac{2i}{t_2} \left( t - \frac{z}{c} \right), 2i \left\{ \frac{Az}{ct_2^2} \left( t - \frac{z}{c} \right) \right\}^{\frac{1}{2}} \right] \right\} \end{aligned} \quad (2-27)$$

It is an interesting check to look for the step response as  $t \rightarrow \infty$ . To do this consider equation (2-26) as to  $t \rightarrow \infty$ .

$$\begin{aligned} E_{\text{step}}(t \rightarrow \infty) &= 1 + \int_0^\infty e^{-\beta \chi^2} I_1(\chi) d\chi \\ &= 1 + \frac{\pi^{\frac{1}{2}}}{2\sqrt{\beta}} e^{1/8\beta} I_{\frac{1}{2}} \left( \frac{1}{8\beta} \right) \\ &= 1 + 2 e^{1/8\beta} \sinh \frac{1}{8\beta} \\ &= e^{1/8\beta} = e^{\frac{zA}{ct_2}} = e^{\alpha z/2} \end{aligned}$$

where we have used the relation  $A = \alpha ct_2/2$ . From this we infer that

$$I_{\text{step}}(t \rightarrow \infty) = e^{\alpha z} \quad (2-28)$$

where a unit step was applied. This is as expected. The step response integral was done numerically on a computer; the program can be found in Appendix A.

Figure 2-2 shows a series of plots of the normalized intensity response  $(E_{\text{step}})^2/e^{\alpha z}$  for typical parameters of a CO<sub>2</sub> laser amplifier. In these plots, the gain is held constant, while the bandwidth ( $t_2$ ) is changed.

Figure 2-3 shows normalized intensity step responses when the bandwidth is kept constant and the gain is changed. In this case the amplifier exhibits gain narrowing; that is, as the gain is made larger, and due to exponential dependence of the gain with distance, the center of line (hence a smaller effective bandwidth) contributes more heavily to the gain leading to a longer risetime for the larger gain cases. Any paradox in the reader's mind can be resolved easily if he realizes that if Fig. 2-3 were plotted without being normalized to unity, curve C would have a greater value than curve B which would be greater than curve A.

#### Linear amplification off line center for homogeneous broadened line

It is also necessary to consider the amplification process at frequencies away from line center since this may be the case in an experiment. The equations of interest are (2-19) and (2-20).

$$\frac{\partial K}{\partial T} = -AF - i\Omega K - \frac{K}{T_2} \quad (2-29)$$

$$\frac{\partial F}{\partial T} + \frac{\partial F}{\partial Z} = -K \quad (2-30)$$

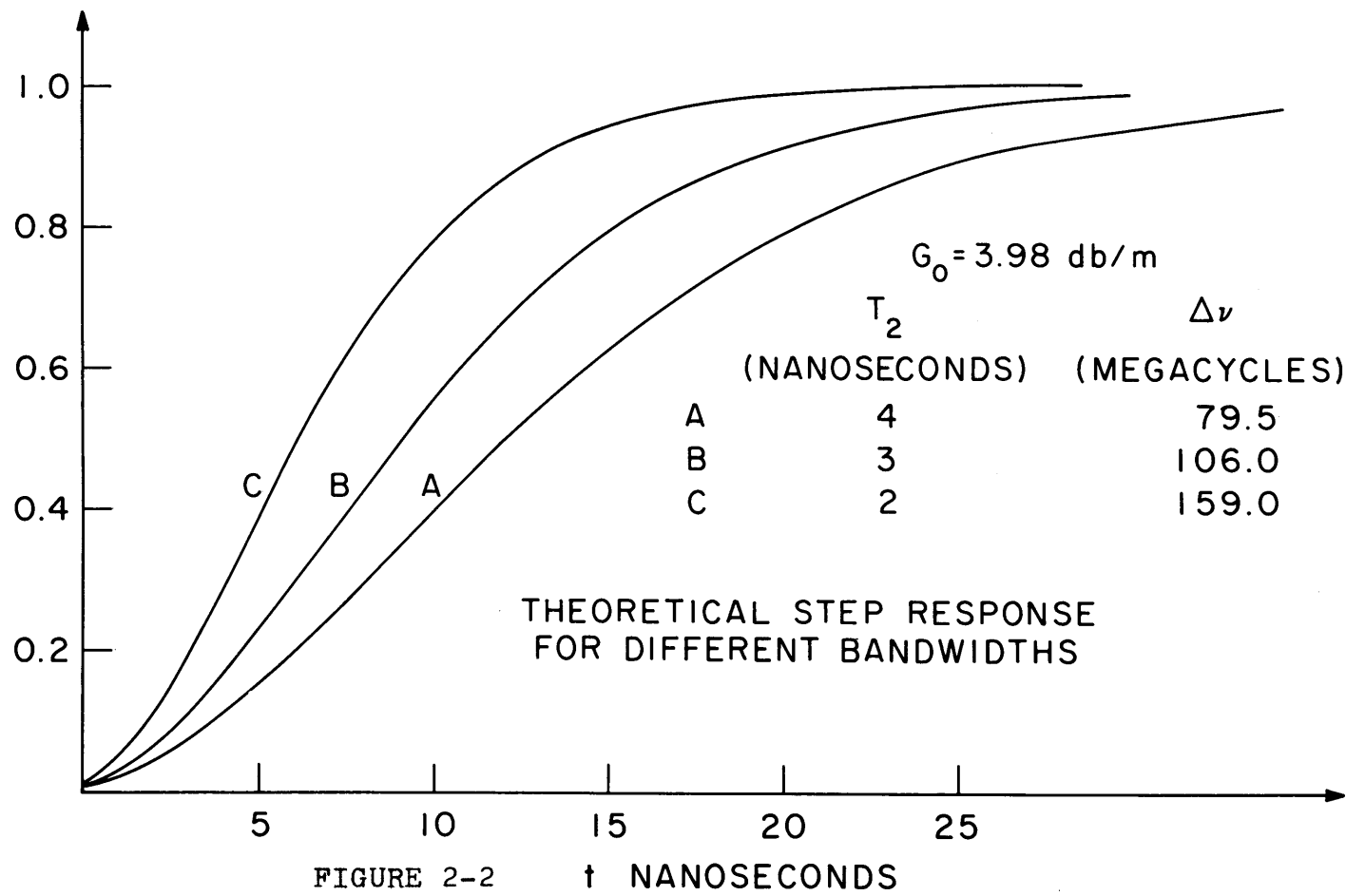


FIGURE 2-2

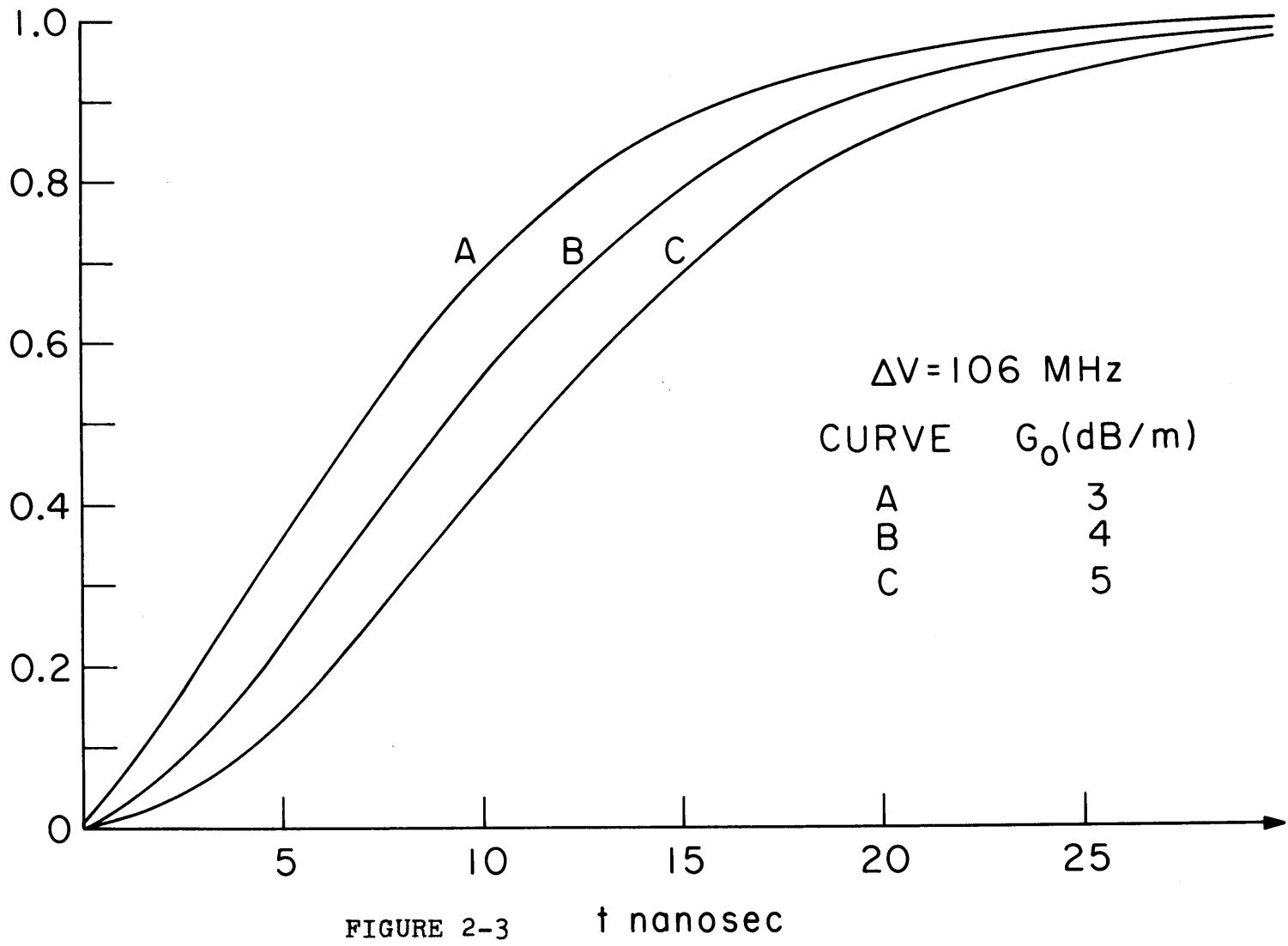


FIGURE 2-3  $t$  nanosec

where we are again using the normalized notation and  $F$  and  $K$  are complex. This problem can be simplified considerably by making the substitutions

$$F' = F e^{i\Omega(T - Z)}$$

$$K' = K e^{i\Omega(T - Z)}$$

whereupon equations (2-29) and (2-30) become

$$\frac{\partial K'}{\partial T} = -AF' - \frac{K'}{T_2}$$

$$\frac{\partial F'}{\partial T} + \frac{\partial F'}{\partial Z} = -K'$$

which are the same equations which were solved earlier.  $F'$  impulse =  $e^{i\Omega(T - Z)}$   $F$  impulse on resonance. The off resonant behavior multiplies the resonant behavior by a dephasing term which rings faster the further off resonance that the interaction takes place. Using unnormalized notation, the off resonance step response becomes

$$\begin{aligned} E_{\text{step}} = & 1 + \int_0^{\frac{2}{t_2} \left(\frac{zA}{c}\right)^{\frac{1}{2}} \left(t - \frac{z}{c}\right)^{\frac{1}{2}}} \cos \sigma \chi^2 e^{-\beta \chi^2} I_1(\chi) d\chi \\ & + i \int_0^{\frac{2}{t_2} \left(\frac{zA}{c}\right)^{\frac{1}{2}} \left(t - \frac{z}{c}\right)^{\frac{1}{2}}} \sin \sigma \chi^2 e^{-\beta \chi^2} I_1(\chi) d\chi \end{aligned} \quad (2-31)$$

where  $\sigma = t_2^2 c / 4Az (\omega - \omega_m)$  and  $\chi = 2/t_2 (Az/c)^{\frac{1}{2}} (t - \tau - z/c)^{\frac{1}{2}}$ .

Figure 2-4 shows theoretical intensity step responses for various values of off-resonant amplification. The other parameters are those

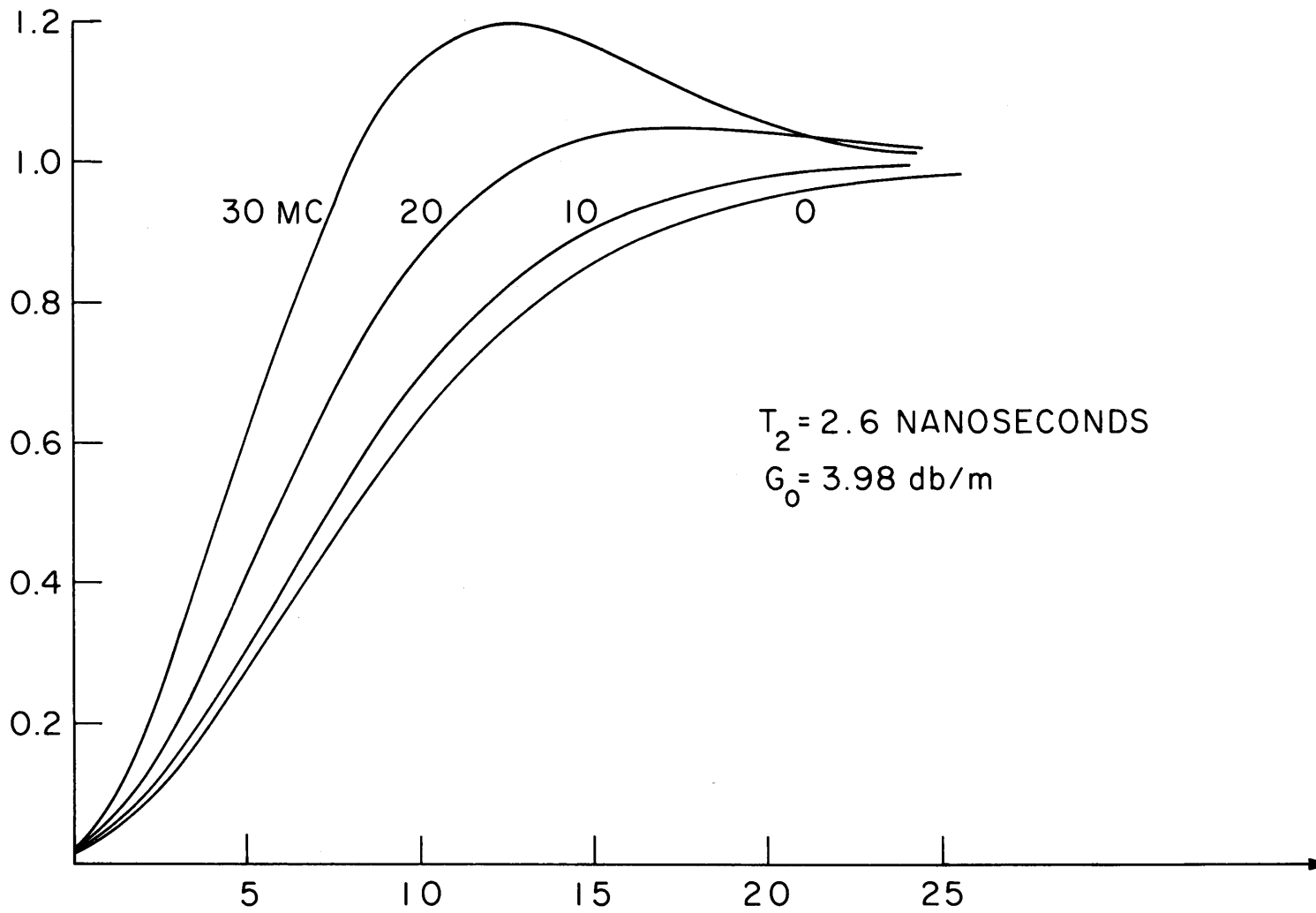


FIGURE 2-4 t NANOSECONDS



typical for a CO<sub>2</sub> laser. The curves were normalized for the values of the cw low signal amplification.

$$I_{\text{step}} = \frac{|E_{\text{step}}|^2}{\exp\left(\frac{\alpha z}{1 + \left(\frac{\omega - \omega_m}{t_2}\right)^2}\right)}$$

An important feature exhibited here is the ringing of the step response to a low-level signal when the amplification is far off resonance. One must be careful to distinguish this ringing from the nonlinear ringing of the population (a nutation effect). In experiments it is possible that one may confuse the two phenomena unless one is careful to ascertain whether the power levels used experimentally warrant the occurrence of nutation or whether the amplification is on resonance. This will be discussed in greater detail in the next chapter.

#### Linear amplification with inhomogeneous broadening

As mentioned earlier, we are faced with the problem of a mixture of broadening mechanisms in a CO<sub>2</sub> laser amplifier. Classically this has always been considered by a Voigt profile; the homogeneous linewidth would be convolved with an inhomogeneous linewidth which, in the case of a CO<sub>2</sub> laser, is Doppler-shaped due to the thermal velocities of the molecules. Of course, to analyse the fast time response of an inhomogeneously broadened system requires a modification of the original density matrix equations; this is done by considering a group of homogeneous systems which are continuously distributed by the Gaussian inhomogeneous linewidth and are coupled by their common interaction with the electric field.<sup>12</sup> To describe the continuous distribution of the

population inversion and polarization current for each velocity group, we modify equations (2-19), (2-20), and (2-21) to the following:

$N$ , the population difference, is replaced by a differential population inversion in frequency space which accounts for the inhomogeneous spread.

$$\begin{aligned}
 N &\rightarrow M(\nu) \, d\nu \text{ such that} \\
 \int_{-\infty}^{\infty} M(\nu) \, d\nu &= N \text{ and} \\
 M_e(\nu) &= \frac{2}{\sqrt{\pi} \Delta\nu} e^{-(2\nu/\Delta\nu)^2} \\
 K &\rightarrow Q(\nu)
 \end{aligned}$$

The inhomogeneous equations then become

$$\frac{\partial F}{\partial T} + \frac{\partial F}{\partial Z} = - \int_{-\infty}^{\infty} Q(\nu) \, d\nu \quad (2-32)$$

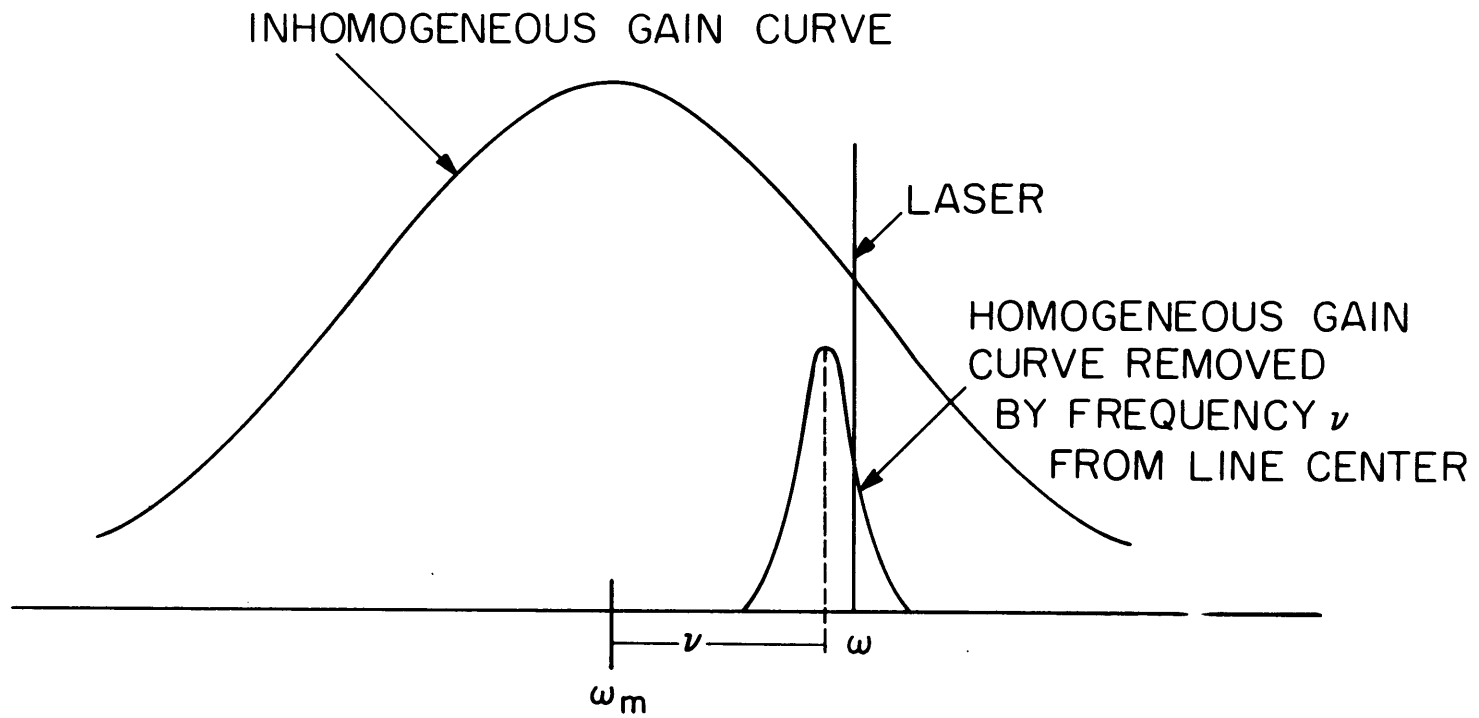
$$\frac{\partial Q(\nu)}{\partial T} = -A M(\nu) F - i\Omega' Q(\nu) - \frac{Q(\nu)}{T_2} \quad (2-33)$$

$$\frac{\partial M(\nu)}{\partial T} = 2(F^* Q(\nu) + F Q^*(\nu)) - \frac{M(\nu) - M_e(\nu)}{T_1} \quad (2-34)$$

$\Omega'$  is now defined as the frequency separation between the electric field and the particles in a velocity group centered at frequency  $\nu$

$$\Omega' = T_n(\omega + \nu - \omega_m) \quad (2-35)$$

This is easily shown in Fig. 2-5.



## INHOMOGENEOUS AMPLIFICATION

FIGURE 2-5

In addition,

$$A = \frac{\mu^2 \omega_m T_n^2 n}{2 \hbar \epsilon}$$

The linearized equations become, setting

$$\frac{\partial M(\nu)}{\partial T} = 0, \quad \frac{1}{T_1} = 0$$

$$\frac{\partial Q(\nu)}{\partial T} = A M(\nu) F - i\Omega'(\nu) - \frac{Q(\nu)}{T_2} \quad (2-36)$$

$$\frac{\partial F}{\partial T} + \frac{\partial F}{\partial z} = - \int_{-\infty}^{\infty} Q(\nu) d\nu \quad (2-37)$$

and

$$\int_{-\infty}^{\infty} M(\nu) d\nu = 1 \quad (2-38)$$

Note that complexity of the  $i\Omega'$  term could be reduced by using a total time derivative instead of the partial time derivative. It permits one to integrate for the impulse response without solving first for the poles and zeros. This has been done elsewhere and has led to some surprising, yet at the same time, intuitively appealing results.<sup>13</sup> There is no distinguishable difference (less than 4% difference in the two curves) between the step response for the homogeneously broadened medium and the inhomogeneously broadened medium provided

- (1) the amplification is at line center;
- (2) the half power bandwidth is the same for both cases;
- (3) the low signal gain at line center is the same for both cases;

(4) the total low signal gain is high,  $> 10$  db.

The intuitive reason for this surprising agreement is readily apparent when one realizes that this is an amplifying medium, not an attenuating one. Since the gain is exponential in character with distance, the center of the line contributes most strongly for a high gain medium (a manifestation of gain narrowing), whereas the tails contribute only a small portion to the resulting amplified pulse. It is precisely near the line centers that the homogeneous (Lorentzian) and inhomogeneous (Gaussian) lineshapes agree; therefore, for this linear exponential-type gain the amplified pulses agree. In the linear amplification it is only the shape of the linewidth near line center that counts, not the mechanisms that produce it. Of course, if the pulse were to saturate the medium, everything would change completely, and these arguments could no longer be made.

Similarly, if the linear pulse is put through an absorbing medium, the center of the linewidth absorbs most strongly, and the tails contribute most strongly to the output pulse. A Lorentzian shape and a Gaussian shape differ most strongly at the tails, so the pulse out of an absorber would be different for the two broadening mechanisms.

This result will be used extensively in our  $\text{CO}_2$  linear pulse experiment described in the next chapter.

One final word about our theoretical model for linear amplification before describing the experiment. The equations we have written here are for the interaction taking place through a single dipole moment. Unfortunately the  $\text{CO}_2$  laser has a degeneracy problem, since there exist a number of dipole moments corresponding to the different angular orientations of the molecule. If we were considering amplification at

times much longer than  $t_2$  (not the case here) collisional effects would cause the system to behave as though it had one dipole moment.

However, since in this experiment we only consider linear amplification, and we are adding the linear responses of groups of particles that have different strengths of interaction with the field, but whose behavior is identical except for the low signal gain. Therefore, we can consider this linear multi-level case to be equivalent to a two-level case with an average gain.

### CHAPTER III

#### EXPERIMENTAL SMALL-SIGNAL STEP RESPONSE AND MEASUREMENT OF BANDWIDTH

Since the theoretical step response has been described in detail, a brief description of the experiment will be given followed by a detailed description of the various components in the experiment. Figure 3-1 shows the complete experimental equipment layout.

The signal from a cw oscillator operating in the P(16) line is passed through a gallium arsenide polarization switch. The switch is followed by a polarizer, which reflects out the radiation when the switch is not activated. When a voltage is applied, the incoming wave becomes elliptically polarized and is partially transmitted through the polarizer. Light pulses with a risetime of 1 ns and lengths adjustable up to 100 ns result.<sup>14</sup>

The radiation is then passed through a multipass amplifier of five passes of the type used by Kogelnik and Bridges.<sup>15</sup> A 5-meter amplifying path is provided and gains as high as 23 dB can be obtained in a mixture of CO<sub>2</sub>, N<sub>2</sub>, and He. The flow rates and total pressures in the amplifier are measured, and from this data the partial pressures are evaluated. After amplification, the signal is detected in a Ge:Cu:Sb detector at liquid He temperature. The detector is terminated in 50 ohms, and the detected output is observed on a sampling oscilloscope with a 0.35 ns risetime.

#### The GaAs electro-optic modulator

The electro-optic modulator achieves pulses with risetimes much less than  $\pi t_2$ , which is on the order of 10 nanoseconds. The GaAs

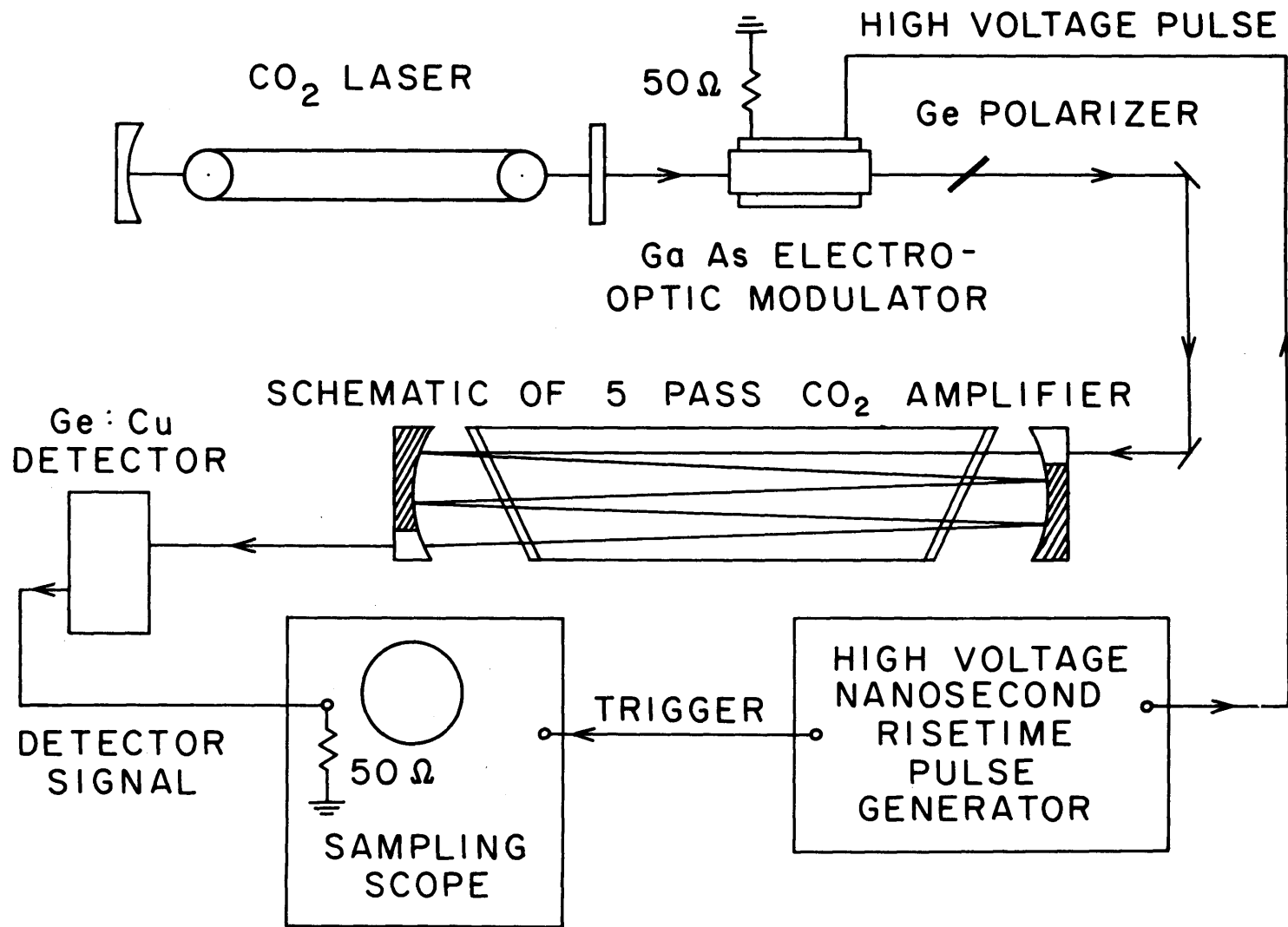


FIGURE 3-1



modulator works with the electro-optic effect in  $\text{Cr}^+$  doped single crystal GaAs.<sup>16</sup> The electro-optic effect here is a rotation of the polarization of the electric field with the application of a dc or rf electric field.

Intuitively this can be seen to take place if the electric field puts a force on the crystal which causes it to contract or expand along a certain axis; the refractive index then changes differently for each of the two polarizations. Figure 3-2 shows the GaAs electro-optic modulator used in this experiment; the refractive index is increased along  $\vec{i}_x$  and decreased along  $\vec{i}_y$  when an rf voltage is applied to the gold-coated surface. Consider an optical field at the input to the crystal

$$\begin{aligned}\vec{E}_{\text{input}} &= \vec{E} \sin(\omega t - kz) \\ &= E \sin(\omega t - kz) (\vec{i}_x + \vec{i}_y)\end{aligned}$$

so that

$$E_{\parallel} = E$$

and

$$E_{\perp} = 0$$

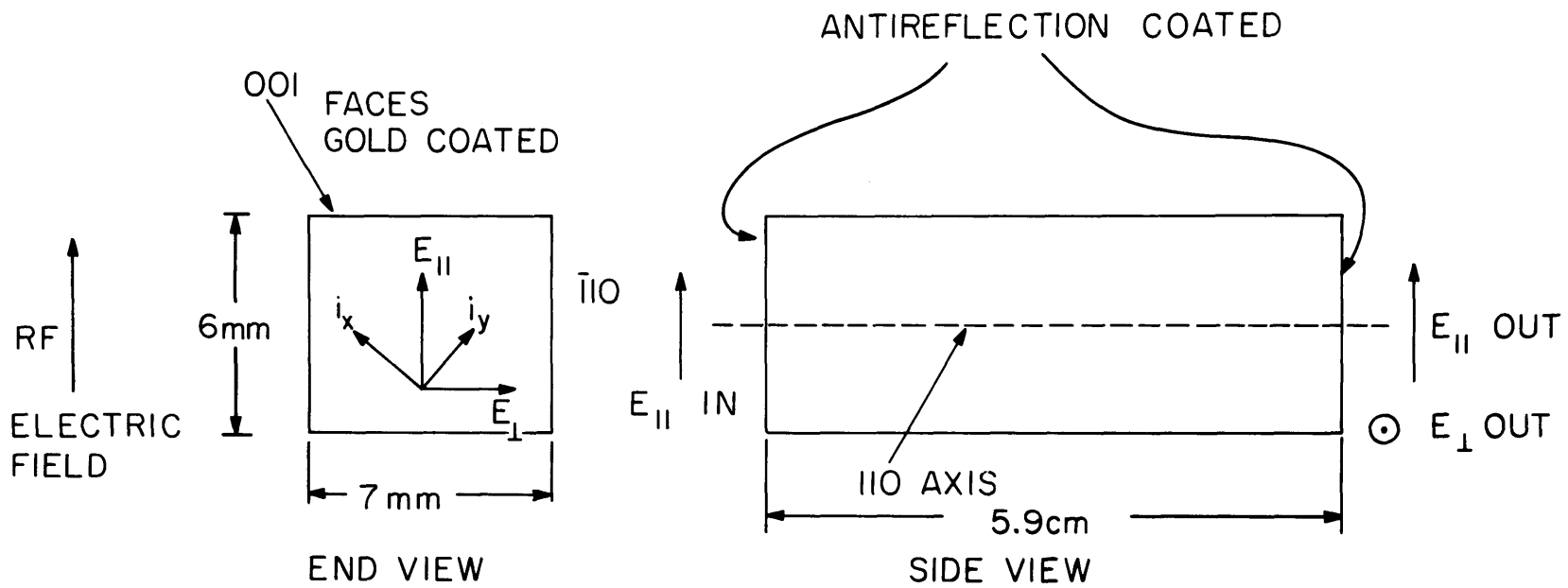
after going through the crystal.

$$\vec{E}_{\text{output}} = \frac{E}{\sqrt{2}} \left[ \vec{i}_x \sin\left(\omega t - kz + \frac{\phi}{2}\right) + \vec{i}_y \sin\left(\omega t - kz - \frac{\phi}{2}\right) \right]$$

then

$$E_{\parallel} = E \sin(\omega t - kz) \cos \frac{\phi}{2}$$

$$E_{\perp} = E \cos(\omega t - kz) \sin \frac{\phi}{2}$$



$n = 3.3, r_{41} = 1.3 (10^{-10}) \text{cm/VOLT}$   
**Ga As ELECTRO-OPTIC MODULATOR**

FIGURE 3-2

where  $\varphi$  is the total phase difference; therefore the power in the various polarizations is

$$P_{\parallel} = \cos^2 \frac{\varphi}{2}$$

$$P_{\perp} = \sin^2 \frac{\varphi}{2}$$

$\varphi$  goes linearly with the applied rf electric field and length of crystal, and for the size of crystal used in this experiment we can calculate from reference 16 an rf (or dc) voltage of 11.6 kV would be required for  $\varphi = \pi$ , which corresponds to  $P_{\parallel} = 0$  and  $P_{\perp} = 1$  ( $90^\circ$  rotation).

The GaAs modulator is used in conjunction with a Ge polarizer. Since the index of refraction of Ge is 4, if it is set at a Brewster angle, it rejects 85% per face of the radiation of polarization perpendicular to the polarization it passes completely.

In this experiment the oscillator was built with NaCl Brewster windows so that the output power (internally apertured to a single transverse mode) was vertically polarized. The Ge polarizer was placed after the GaAs modulator and passed only horizontally polarized radiation. When no voltage was applied to the GaAs, it behaved as an isotropic material ( $\varphi = 0$ ), and the polarizer shunted 98% of the radiation off to the side.

The voltage driver for the GaAs modulator and trigger for the Tektronix 1S1 sampling scope was an SKL Model 503A high voltage wave generator which produced voltage pulses of 1 kV magnitude with approximately 0.5 nanoseconds risetime by discharging a charged 50 ohm line through a mercury reed switch into another 50 ohm line. The GaAs formed a 50-ohm transmission line terminated in a match. The radiation after the GaAs is elliptically polarized, and the Ge polarizer picks out the

horizontally polarized component and passes that onto the multipass amplifier.

### The multipass amplifier

In both the linear and nonlinear pulse amplification experiments, it was found helpful to use an amplifier of relatively long length. In the linear amplification it was advisable because only when  $\exp(\alpha z) \gg 1$  did the difference between the homogeneous and inhomogeneous amplification become minimal. In the nonlinear case, as we shall show, the nonlinear interaction was not linear in length of amplification, i. e., the effect we were looking for did not merely halve in halving the amplifier distance - it may have been nonexistent. In both cases a 5-pass amplifier was used, providing 5 meters of amplification with no beam overlap in the amplifier. An excellent description of this amplifier follows (from reference 15):

" A multipass structure adapted from that described in Herriott, et al. was used, as shown in Fig. 3-1. It consists of two spherical mirrors of curvature radius  $R = 1$  meter, spaced at a distance of  $d = 1.5$  meters. This choice of parameters provides for ray systems that are re-entrant after six traversals. The IR beam is injected at an angle that arranges the impact points on the mirrors in coaxial circular patterns. As indicated in Fig. 3-1, the beam enters the amplifier through an opening in the input mirror and exits after five traversals through an opening in the output mirror.

Each opening is a  $120^\circ$ -sector cut out of the circular mirror and the input and output openings are set at an angle of  $120^\circ$  to each other as shown in Fig. 3-3. In the figure, the areas of beam impact on each mirror are marked by numbers which also indicate the completed

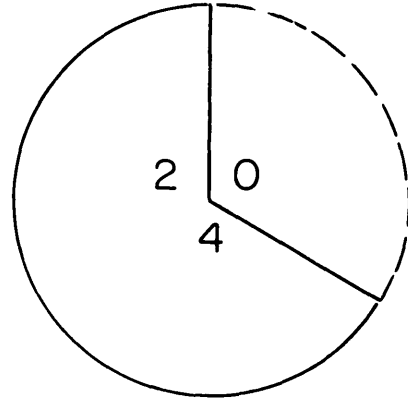
traversals.

It is known that two concave mirrors (without openings) form an optical resonator which can provide feedback for laser oscillations; these oscillations must be prevented in the present case. An obstacle inserted inside such a resonator will quench multimode oscillation patterns not only in the obstacle areas but also in areas that are axisymmetrical to that obstacle. The two rotated mirror openings can be regarded as obstacles. In the aperture of the system there is no area that is not covered by an opening or its axisymmetrical image. One expects, therefore, that the diffraction losses of this structure for oscillating modes are very high. Experimentally it was found that when the single pass gain exceeded 3 dB, accurate adjustment of the mirrors was necessary to prevent oscillations. To increase the diffraction losses even further, masks with circular holes, as shown in Fig. 3-4, were inserted in front of each mirror. Holes of 8.5 mm diameter insured freedom from oscillations in the present experiments. The masks increased the insertion loss of the amplifier by about 0.5 dB. The overall insertion loss of the amplifier varied between 1 and 2 dB depending on the age of the Brewster windows and the gold-plated mirrors, and on the quality of the alignment.

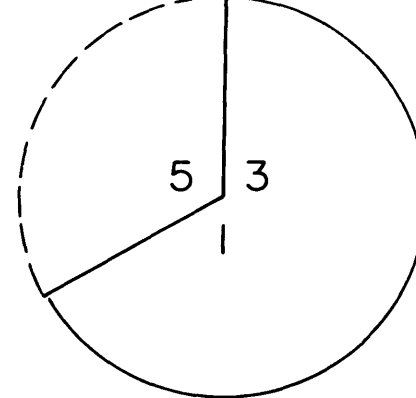
For these low insertion losses a zero-order Gaussian beam must be injected, and the beam parameters must be matched<sup>17</sup> to the parameters of a mode of the multipass mirror structure. Under matched conditions all five beams passing through the amplifier have the same contour. The beam waists are formed in the midplane of the structure where the beam radius (or spot size)  $w_0$  assumes a

### MULTIPASS AMPLIFIER MIRRORS

INPUT MIRROR

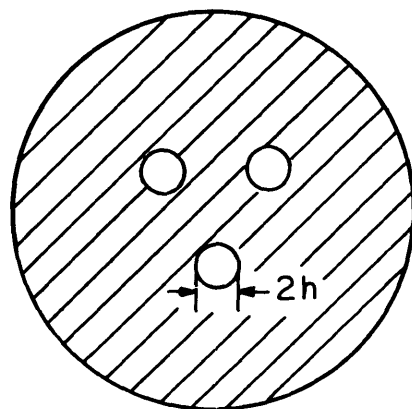


OUTPUT MIRROR



ORIENTATION FROM INPUT END  
NUMBER IS ORDER OF REFLECTION

FIGURE 3-3



$$2h = 8.5 \text{ mm}$$

MIRROR MASK

FIGURE 3-4

value of

$$w_o = \sqrt{\frac{\lambda}{2\pi}} \cdot \sqrt[4]{d(2R - d)} = 1.21 \text{ mm}$$

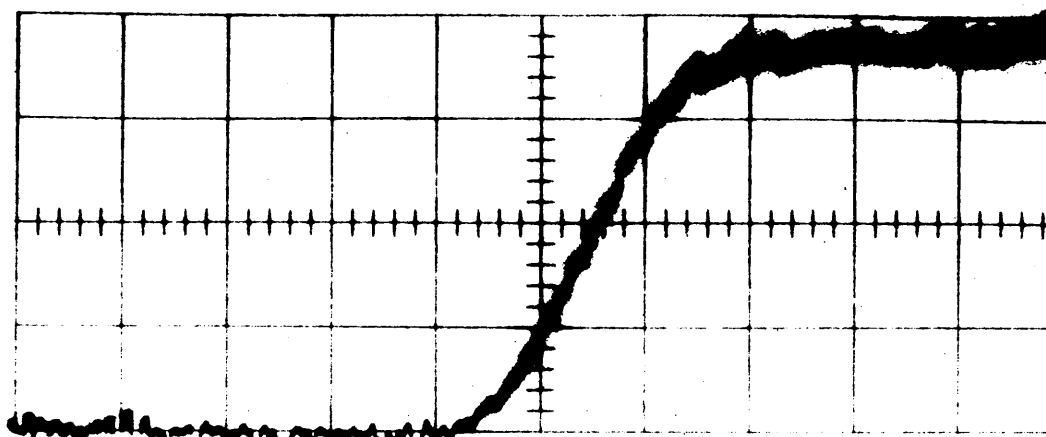
The corresponding beam radii at the mirrors have a value of  $w = 2.42 \text{ mm}$ .

The oscillator was comprised of a 2-meter radius of curvature gold-coated mirror and an 80% reflecting Irtran IV mirror (used for output coupling) separated by 1.7 meters. The mode matching between the oscillator and amplifier was accomplished by using a 2-meter radius of curvature gold-coated mirror (instead of a transmitting lens) which was placed 2.56 meters away from the Irtran IV output mirror and 0.90 meters before the input to the multipass amplifier. The beam was reflected off the curved mirror at an angle of less than  $10^\circ$  to minimize aberrations.

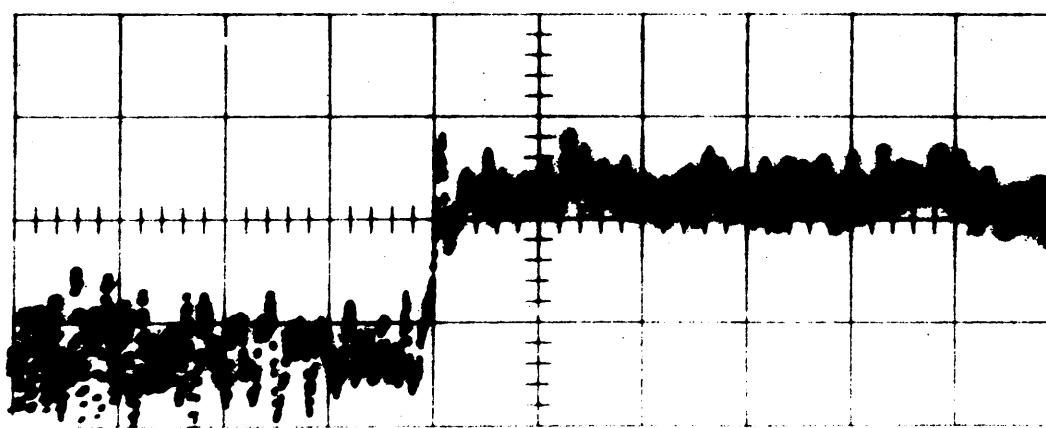
Figure 3-5 shows a typical response of the input pulse and of the response of the amplifier. Only the risetime of the amplifier was studied. The scale is 10 ns/div. The input signal was comparatively small and was partially obscured by sampling scope noise. The gain was measured from the steady-state portion of the oscilloscope trace. The amplified trace was sufficiently strong so that noise did not affect it.

Attenuators were used before and after the amplifier to insure linearity of amplification. By using attenuators and noting the oscilloscope settings, the steady state low signal gain could be measured, and  $\alpha$ , the low signal gain coefficient, could be determined. Once  $\alpha$  was known, computer curves were generated by the method outlined in Chapter 2 and were fitted to the experimental curve. The best value of  $t_2$  to achieve this fit was chosen on a trial-and-error basis.





Amplified output



Step input

FIGURE 3-5

An example of such a fit is shown in Fig. 3-6. The circles indicate the experimental points taken from a photograph. The three curves correspond to step responses computed from three different assumed values of  $t_2$  for a measured value of  $\alpha$ .

Several experimental step responses were measured for varying total pressures, but in each case the proportions of  $\text{CO}_2$ ,  $\text{N}_2$ , and He were fixed. Each time a value of  $t_2$  was found by the procedure just described.

Figure 3-7 shows a plot of the bandwidth,  $(\pi t_2)^{-1}$ , that was calculated in this manner vs total pressure in the amplifier. Note that the matched  $t_2$  was an effective  $t_2$  that included inhomogeneous contributions also. A straight line fits very well and has zero pressure intercept of 59 MHz. Since the bandwidth we are plotting is full width at half intensity, this zero pressure intercept corresponds to the Doppler width. A 59 MHz Doppler width in  $\text{CO}_2$  corresponds to a gas temperature of  $372^\circ\text{K}$ . Furthermore, a linear bandwidth curve is to be expected since the actual lineshape is the convolution of a Lorentzian and a Gaussian curve, and the total linewidth is approximately equal to the sum of the two linewidths.

The collisional part of this linewidth increases at 4.67 MHz/torr. This should check with collisional cross section data since  $t_2$  is a dephasing "collision" time of the polarization (equation (2-23)). Using the latest values of cross sections for  $\text{CO}_2 - \text{CO}_2$ ,  $\text{CO}_2 - \text{N}_2$ , and  $\text{CO}_2 - \text{He}$  collisions,<sup>18</sup> we get a linewidth broadening of 4.84 MHz/torr for a gas temperature of  $372^\circ\text{K}$ . Appendix B shows these calculations.

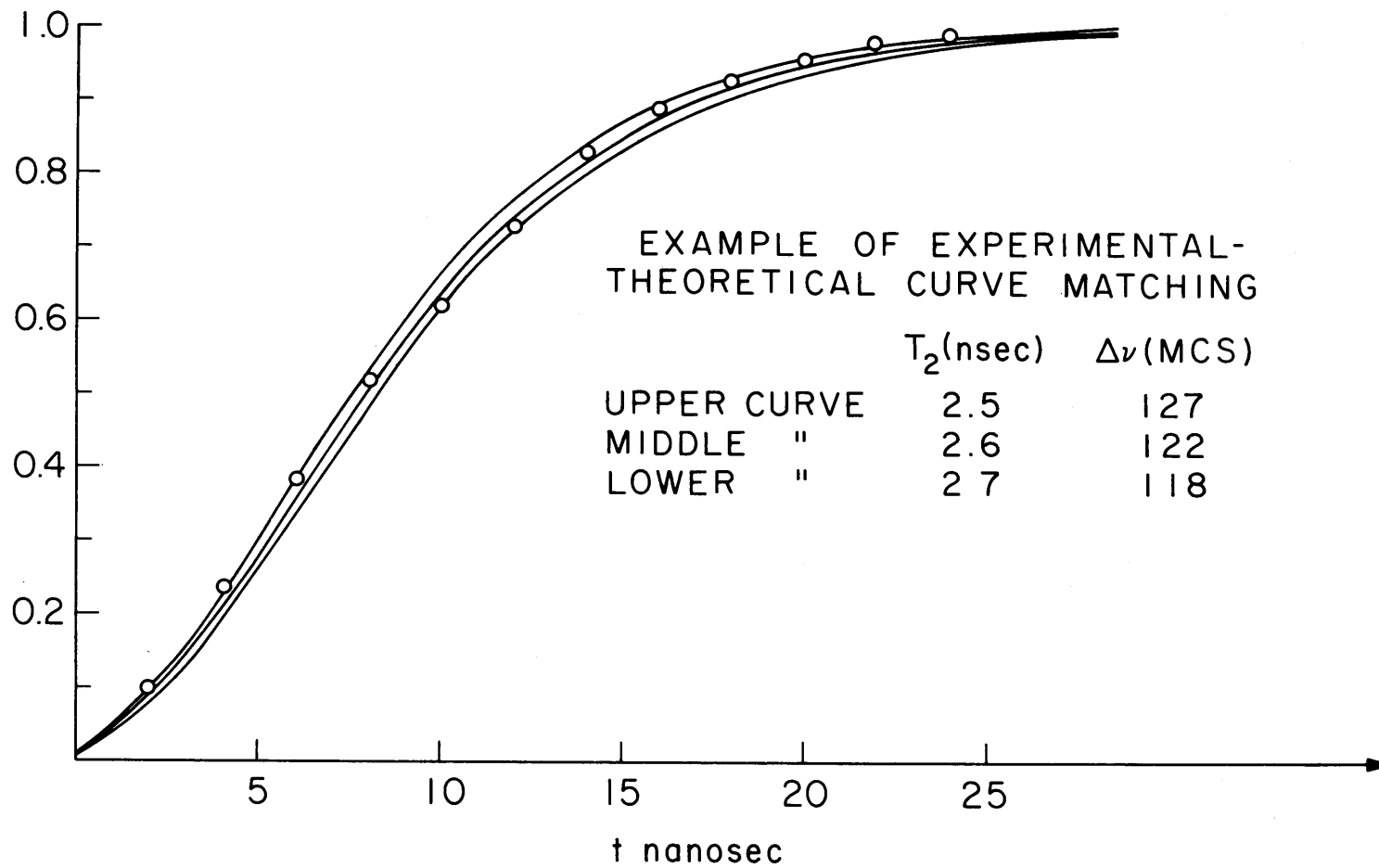
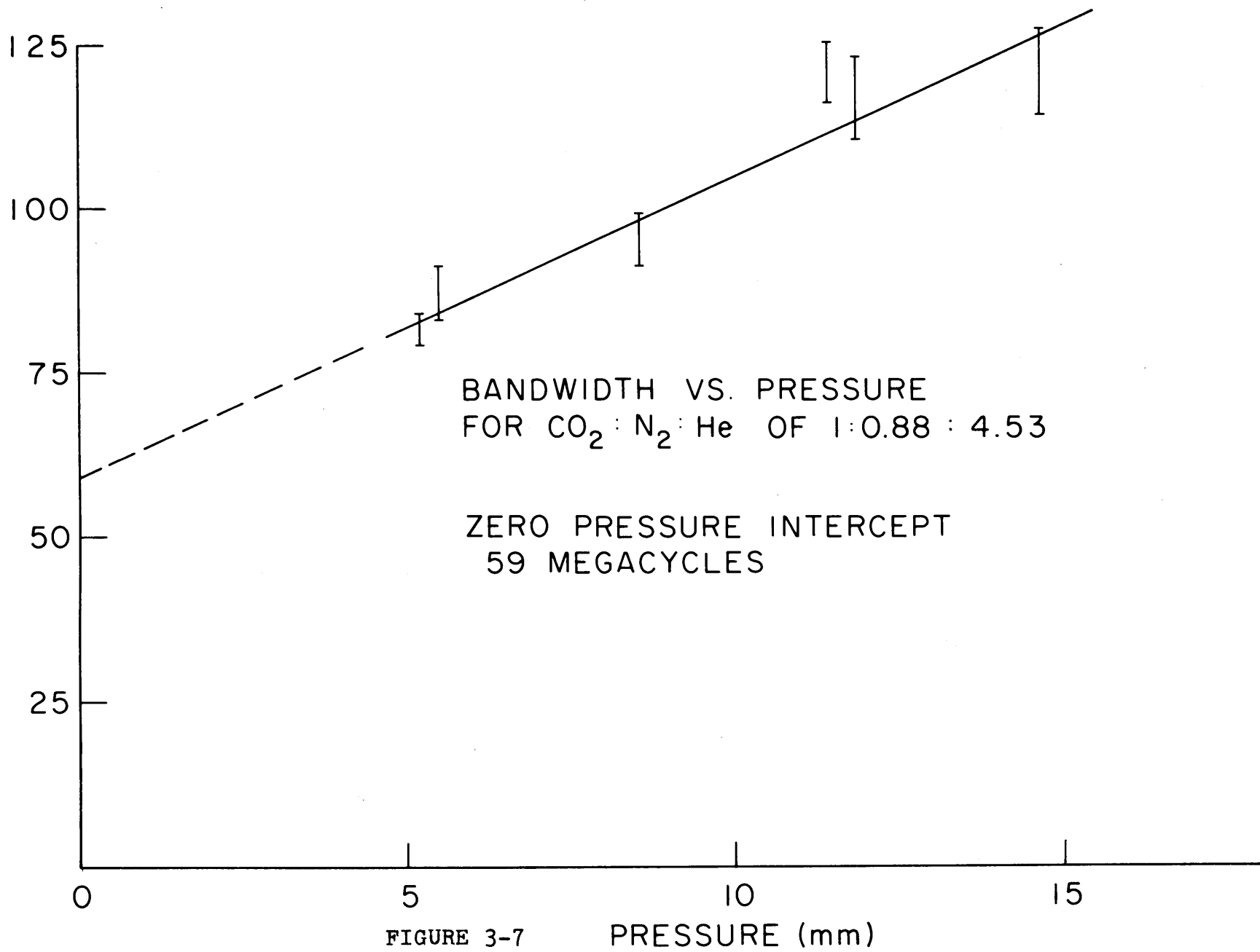


FIGURE 3-6



### Sources of experimental error

There are several sources of error in this experiment; they may be ascribed to either the laser oscillator or the GaAs crystal.

The GaAs modulator was of poor optical quality;<sup>19</sup> the beam after passing through it was not a TEM<sub>00</sub> Gaussian mode. If we were using a single pass amplifier, this would present no problem, since by definition all portions of the beam experience the same linear amplification. However, the multipass amplifier is designed to accept only a TEM<sub>00</sub> mode, and there was a 2 dB insertion loss when the beam of poor optical quality was passed through the amplifier. The error comes about in the manner in which the data was analyzed. The low signal gain coefficient was measured from the electronic steady state gain of the amplifier, when the theory was designed for the actual  $\alpha$ . Introduction of loss modifies equation (2-19)

$$\frac{\partial F}{\partial T} + \frac{\partial F}{\partial Z} + \frac{F}{T_0} = -K \quad (3-1)$$

where  $T_0$  is the normalized field loss coefficient which changes the result for  $E_{\text{step}}$

$$E_{\text{step}} (\text{with loss}) = e^{-\alpha_l Z} E_{\text{step}} (\text{without loss})$$

But even if this extra step were taken in the data analysis, the result would still not be completely accurate since equation (3-1) describes a continuous resistive loss, whereas the insertion loss consists of lumped diffraction losses at the apertures in the amplifier. Using a single pass amplifier of necessarily shorter length presents problems in the matching, since a high gain ( $e^{\alpha Z} \gg 1$ ) system is necessary to minimize differences

between the homogeneous and inhomogeneous amplification. No severe detuning effects such as the 30 MHz curve in Fig. 2-4 were observed, but the oscillator could have been 10 MHz off resonance quite easily even though it was tuned for peak power. This off resonant amplification could change the effective  $t_2$  used in the matching. Furthermore, any errors in measuring the effective  $t_2$  are made worse when trying to compute the collisional (homogeneous) linewidth because of the large fraction contribution of the Doppler width to the effective  $t_2$ .

Possible cures for these problems are:

- (1) The use of a GaAs crystal that is boat-grown instead of pulled. A boat-grown crystal has less optical striations than a pulled one, where the  $\text{Cr}^+$  dopant atoms form periodic concentrations and rarifications.
- (2) The use of an oscillator stabilized onto line center. This would give accurate results on line center, and a second oscillator could be locked off line center (using the first as a reference) to check the off-resonant amplification theory.

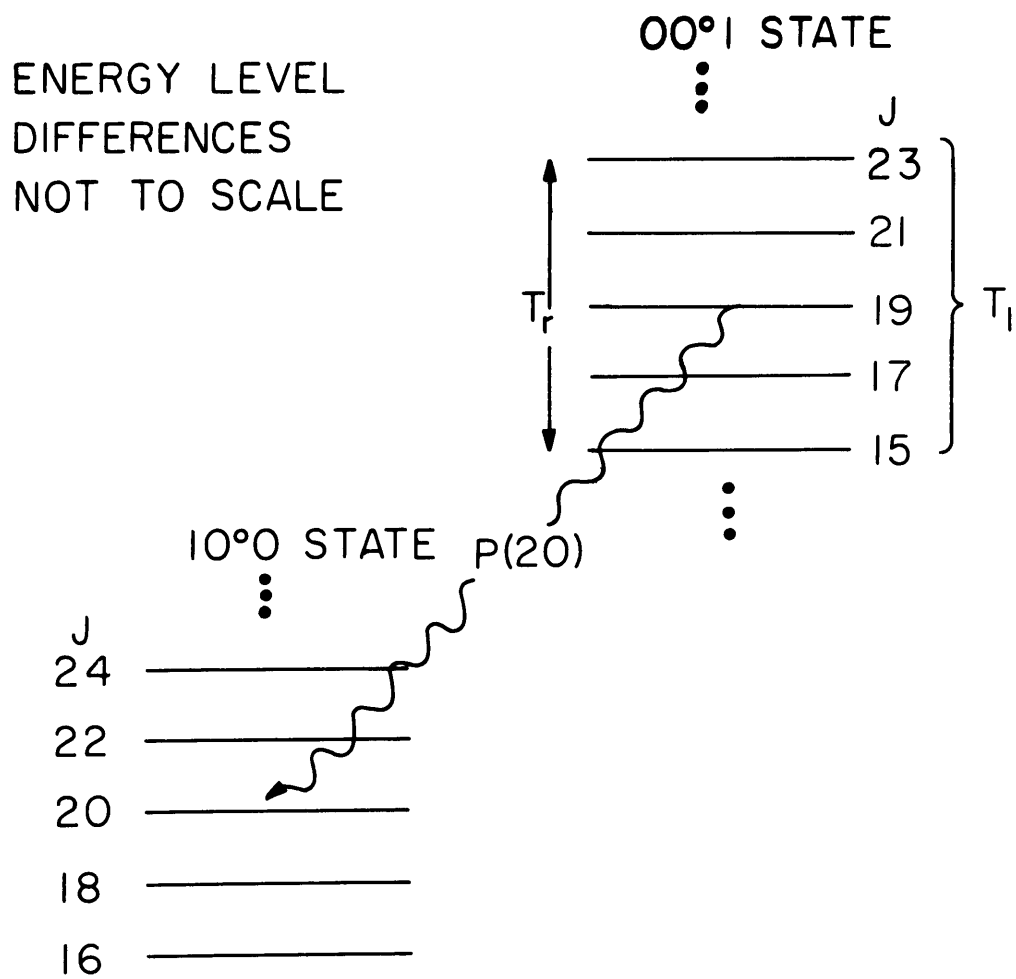
## CHAPTER IV

NON-LINEAR AMPLIFICATION IN A CO<sub>2</sub> LASER AMPLIFIER

Before considering any particular model for nonlinear amplification in CO<sub>2</sub>, we must first consider many of the different mechanisms complicating the amplification process. It is convenient to consider these at different pressure regimes since collisional effects change the amplification most drastically.

High pressure case

Let us first consider the high pressure regime, approximately 10 torr total pressure. At this pressure we may consider the line to be predominantly homogeneously broadened; furthermore, there is no degeneracy problem even for transitions operating between two levels with high J values since the collisions "couple" the different degenerate M-levels of a particular rotational level into one effective level. However, since the collision times begin to be small, and there are other rotational levels, relaxation from other rotational levels into the two levels between which the laser is operating becomes important.<sup>20</sup> Figure 4-1 shows an energy level diagram depicting this rotational relaxation problem. It shows a laser operating at P(20) and how the other rotational levels tend to relax into the 001 J = 19 and 100 J = 20 states. A further complication here is the fact that the electromagnetic field in any experiment has a nonuniform cross section. The nonlinear interaction is dependent on the strength of the electric field, so in any experiment we would find the time evolution of the pulse amplification to vary from the center to edge of the beam.



## ROTATIONAL RELAXATION

FIGURE 4-1



### Low pressure case

The other pressure regime where appreciably different amplification effects occur is when the total pressure is less than one torr; at these low pressures, relaxation from other rotational levels becomes important, and it becomes easier to drive the nonlinear interaction. However, we are still faced with the problem of the nonuniform intensity profile of the electromagnetic field, and since the collisional times are so long, the system no longer behaves with an average dipole moment, but rather we have to concern ourselves with the nonlinear interaction occurring through many different dipole moments. The medium is also predominantly inhomogeneously broadened.

### Intermediate pressures

At pressures between the two regimes discussed above, the experimental results are not especially startling, and the analysis is extremely complex; all the problems above have to be contended with. The medium is neither homogeneously nor inhomogeneously broadened. In addition, rotational relaxation exists, and multiple dipole moments relax into a single dipole in these time regimes. The nonuniform structure of the electromagnetic field presents problems also. This case will not be studied here.

### Theoretical model for the high pressure case

For the reasons mentioned earlier we may use the homogeneously broadened equations from Chapter 2.

$$\frac{\partial F'}{\partial T} + \frac{\partial F'}{\partial Z} = -K' \quad (4-1)$$

$$\frac{\partial K'}{\partial T} = -ANF' - \frac{K'}{T_2} \quad (4-2)$$

$$\frac{\partial N}{\partial T} = 4K'F' - \frac{N-1}{T_1} \quad (4-3)$$

where

$$F' = F e^{i\Omega(T-Z)} \quad (4-4)$$

$$K' = K e^{i\Omega(T-Z)} \quad (4-5)$$

For convenience we will only consider amplification at line center, i. e.,  $\Omega = 0$ . Furthermore, we are using a two-level system, which is only an approximation to the multi-level  $\text{CO}_2$  system. From Fig. 4-1 we can see that, strictly, there is a set of equations for each two-level system coupled by a rotational relaxation time  $T_r$  and together relaxing back to their equilibrium value with a time  $T_1$ . Instead we are going to replace  $T_1$  in equation (4-1) with an effective rotational relaxation time,

$$\frac{1}{T_1'} = \frac{1}{T_1} + \frac{1}{T_{r \text{ eff}}} \approx \frac{1}{T_{r \text{ eff}}}$$

The boundary condition for the partial differential equations is the initial electric field,  $F(T, Z = 0)$ . Then the equations can be numerically integrated on a computer, using the Runge-Kutta technique; the program (developed by T. K. Gustafson) is in Appendix C. The pulse is integrated along the path described in Chapter 2, and is stopped at a distance  $\ell$  corresponding to the length of the amplifier in the experiment. In addition to the input pulse and amplifier length, the medium parameters

have to be specified; these consist of the low signal gain coefficient, the phase interruption time  $t_2$ , and population recovery time,  $t_1$ .

Let us now consider two theoretical examples of this nonlinear amplification for fast risetime nonlinear pulses. The first will be representative of a typical experiment involving a  $\text{CO}_2$  laser amplifier, except that it will completely neglect rotational relaxation. By doing this simpler case first we can see the impetus for doing nonlinear amplification. The second will be the same as the first, except that it will include rotational relaxation. Also included on the first graph will be a curve corresponding to a linearly amplified step (equation (2-26)) for this gain and bandwidth. The linearly amplified step will, of course, be bandwidth limited.

Figure 4-2 shows our first example of pulse amplification. The pulse and medium parameters are summarized here:

$$\begin{aligned} \text{Peak intensity input pulse} &= 9.8 \text{ kW/cm}^2 \\ t_2 &= 2.8 \text{ nanoseconds, which corresponds to a} \\ &\quad \text{homogeneous bandwidth } \Delta\nu_n = 114 \text{ MHz} \\ \alpha &= 4 \text{ dB/m} \\ \ell &= 5 \text{ m, which means the low signal gain is} \\ &\quad 20 \text{ dB or a factor of 100} \\ \frac{1}{t_1} &= 0, \text{ no rotational relaxation.} \end{aligned}$$

In Fig. 4-2 we see the pulse intensity plotted versus time for  $z = 0$ , 2.5 meters, and 5 meters of amplification. The linearly amplified step is indicated by dashed lines on this graph. The intensity values on the graph do not pertain to the linear amplification, which, by definition, is done with extremely small intensity input pulses. The salient features

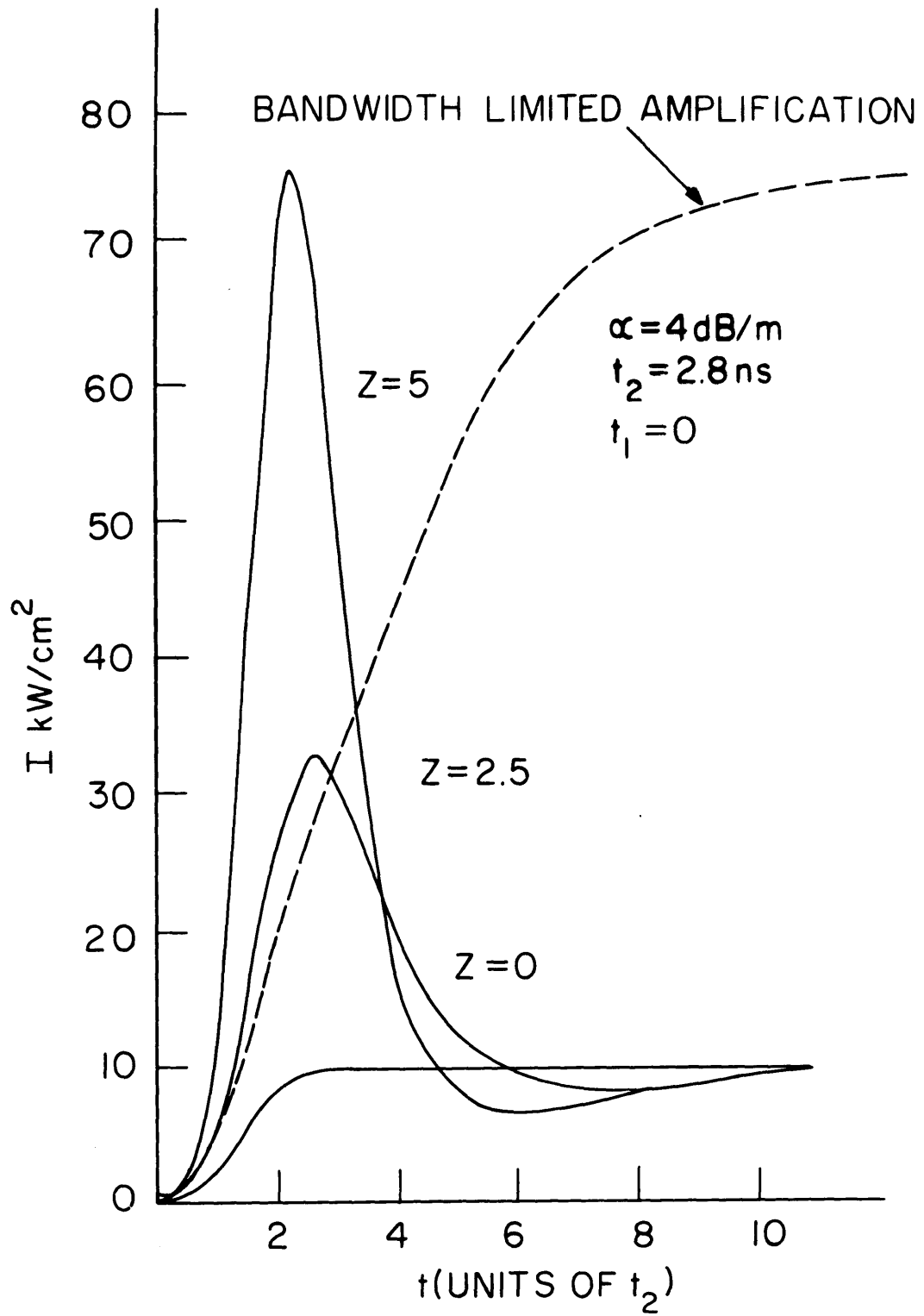


FIGURE 4-2

of the nonlinear pulse amplification are:

- (1) The pulse is amplified by a factor of 7.68, while the low signal gain is a factor of 100.
- (2) The pulse is amplified without distortion ("smearing" effects) at rates greater than the bandwidth. After five meters of amplification we see the risetime of the pulse to be 6.1 nanoseconds, and the inverse bandwidth,  $\pi t_2$ , is 8.89 nanoseconds. However, the risetime of the bandwidth limited pulse (dashed line) is approximately 20 nanoseconds. The intense pulse could be amplified even further without losing its fast risetime, whereas the low intensity pulse would have a longer risetime with further amplification due to gain narrowing.
- (3) The tail end, or lagging edge, of the pulse has been absorbed by the medium instead of being amplified. From 12.9 nanoseconds onward, the pulse at the output of the amplifier is less than it was at the input.

The last two points are related by the fact that the pulse acts upon the medium and the medium then acts back upon the pulse. That is, the intense pulse hits the medium very hard in a time comparable to the inverse bandwidth and is amplified to a value about a factor of 13 less than its low signal gain, but as though it has a much larger bandwidth than in the linear case. Another way to appreciate how this larger bandwidth comes about is to view it as saturation broadening; that is, the intense pulse induces transitions between the upper and lower laser level

at a rate comparable to the bandwidth of the medium.

$$\frac{\mu E}{\hbar} \geq \Delta\nu_n = (\pi t_2)^{-1} \quad (4-6)$$

When this occurs it is like flattening the Lorentzian lineshape to a lower value but with a much larger linewidth. However, this simplistic view has its limitations, since we cannot simply draw a new lineshape and then resort to linear amplification. Rather let us consider equations (4-1), (4-2), and (4-3). Note that the application of an intense pulse to the medium can drive the polarization  $K$  and inversion  $N$  in a nonlinear manner since they are coupled via equations (4-2) and (4-3). Finally, the resulting polarization drives the electromagnetic field via equation (4-1). If  $K$  were set equal to zero, we would have a propagating wave with an amplification. In fact if we satisfy condition (4-6),  $\partial K/\partial T \neq 0$ , and the optical pulse can drive the initial inversion into an absorbing state. When this occurs the lagging edge of the pulse is attenuated (the third observation of this theoretical pulse).

Figure 4-3 shows the variable  $N$  (the normalized inversion) versus time for the amplification of the pulse of Fig. 4-2. We can see the population go negative.

This population reversal in an amplifier is not merely an intellectual curiosity. Haus, Wagner, and Gustafson have expounded these results excellently,<sup>3</sup> but they can be summarized here. By applying a pulse that satisfies condition (4-6), pulse sharpening and shortening may be effected. In fact the further the pulse is amplified, the more pronounced the sharpening and shortening become.

The importance of condition (4-6) can be seen as follows; if it is not

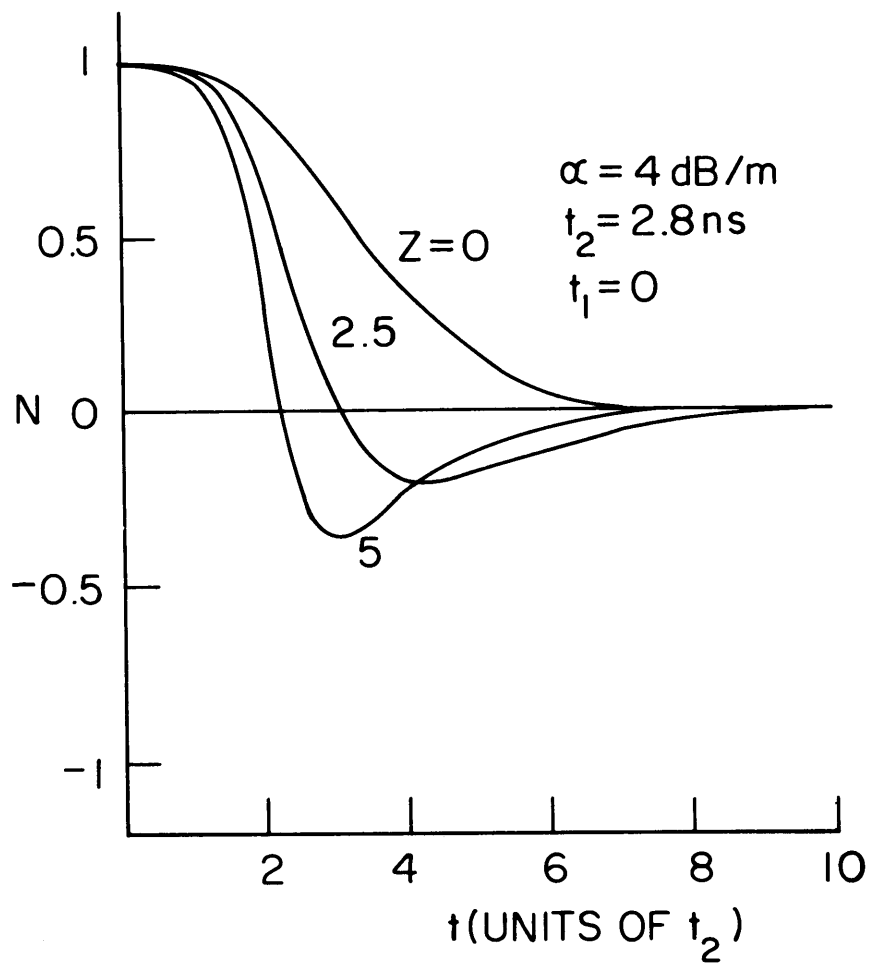


FIGURE 4-3

satisfied,  $\partial K/\partial T = 0$ , and the equations reduce to the rate equations

$$\frac{\partial F}{\partial T} + \frac{\partial F}{\partial Z} = T_2 ANF \quad (4-7)$$

$$\frac{\partial N}{\partial T} = -4 T_2 ANF^2 - \frac{N-1}{T_1} \quad (4-8)$$

A most important result can be shown from these rate equations; population reversal can never be achieved and the strongest nonlinear effect that can be done is to bleach the medium, that is,  $\rho_{22} = \rho_{11}$  or  $N = 0$ .

Consider equation (4-8). The equilibrium value of N is

$$N_{eq} = \frac{1}{1 + 4 T_2 T_1 A F^2}$$

N is driven towards this positive equilibrium value with a driving term that goes as the field squared; however, N is always greater than zero. If population reversal is not achieved, active pulse sharpening cannot be achieved.

There are some further limitations on the nonlinear amplification. If the electric field becomes so strong as to make  $\mu E/\hbar \gg \Delta\nu_n$ , then the field is probably so strong that the pulse propagates through the medium without the medium changing the pulse appreciably. Or, if the gain is very small ( $A \ll 1$ ), then condition (4-6) can be satisfied and the medium will not affect the pulse much either.

However, in a  $\text{CO}_2$  amplifier, the pulse intensities are not so intense as not to be amplified at all, and the gain is high enough for an effective interaction to exist. Satisfying condition (4-6) is the chief experimental



difficulty.

Now that we understand the basic processes behind the nonlinear pulse amplification, let us recompute our theoretical pulse amplification of Figs. 4-2 and 4-3, and include rotational relaxation. Figure 4-4 shows  $N$ , the normalized inversion, when a rotational relaxation time of 10 nanoseconds is included in the computation. The population reversal is reduced considerably from Fig. 4-3, and the result of this is shown in Fig. 4-5 where the pulse amplification is plotted. There is no absorption of the lagging edge of the pulse since the medium is not sufficiently absorbing.

We will now consider amplification at the low pressures where rotational relaxation is not a problem.

#### Theoretical model for the low pressure case

Let us begin by considering the equation for an inhomogeneously broadened medium, (2-32), (2-33), and (2-34).

$$\frac{\partial F}{\partial T} + \frac{\partial F}{\partial Z} = \int_{-\infty}^{\infty} Q(\nu) d\nu$$

$$\frac{\partial Q(\nu)}{\partial T} = -A M(\nu) F - i\Omega' Q(\nu) - \frac{Q(\nu)}{T_2}$$

$$\frac{\partial M(\nu)}{\partial T} = 2(F^* Q(\nu) + F Q^*(\nu))$$

where  $1/T_1 = 0$ .

These equations must be modified to include the effects of the rotational degeneracy of the laser levels. Consider a  $\text{CO}_2$  P transition

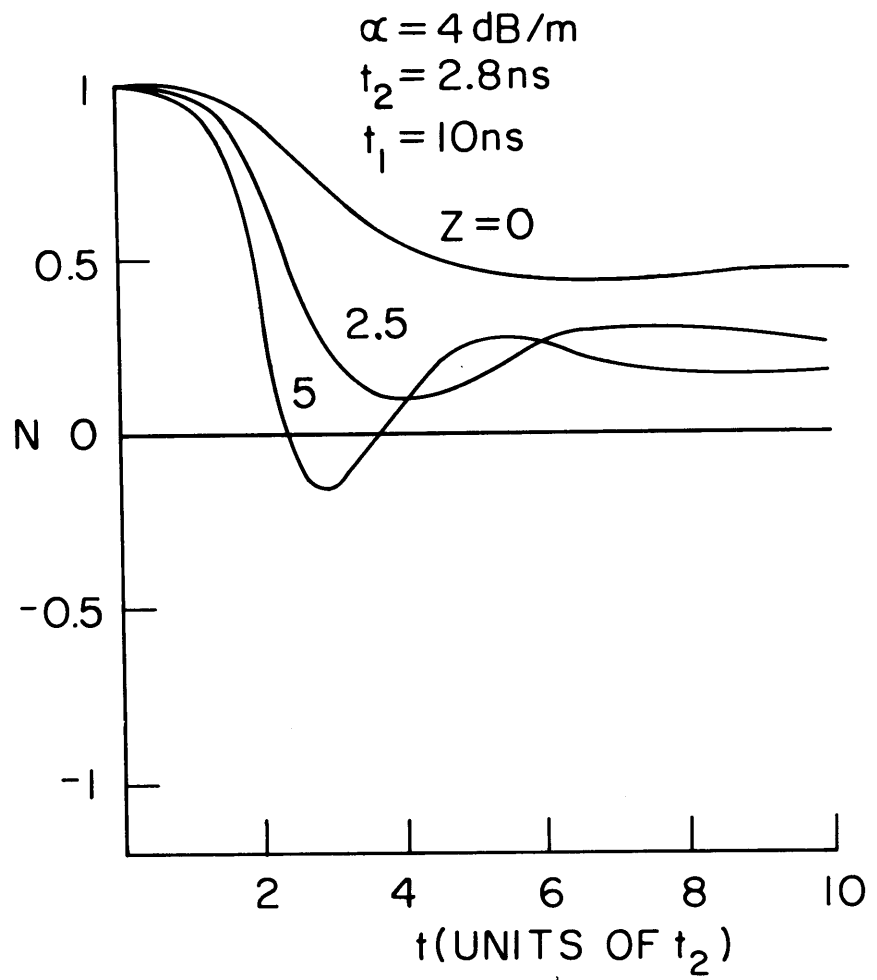


FIGURE 4-4

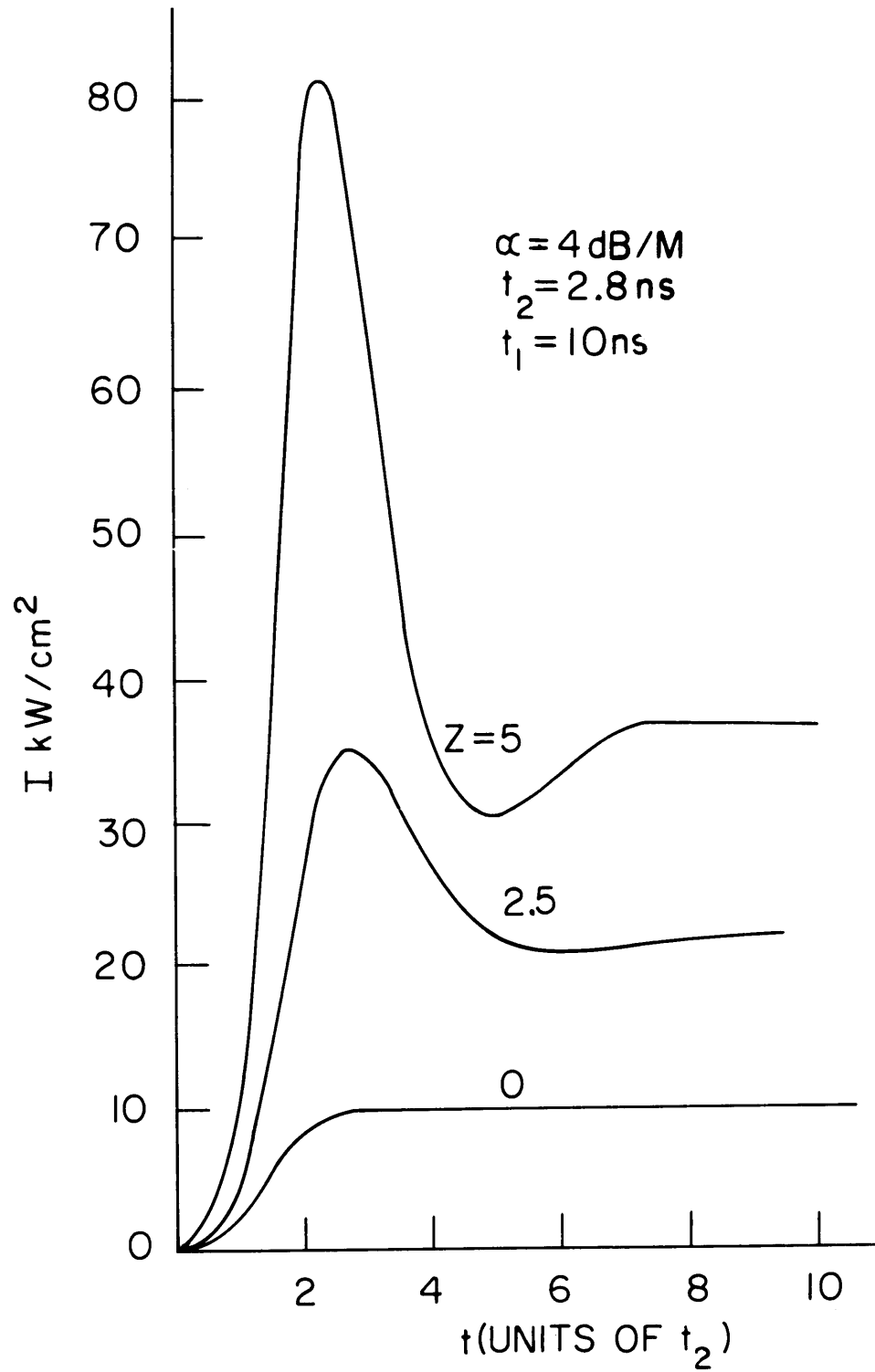


FIGURE 4-5

operating between J-1 and J. Figure 4-6 shows a model of the amplification process. There exists a set of  $2J-1$  independent populations with different dipole moments (actually our calculations are made simpler since  $\mu_{-m} = \mu_m$ ). Furthermore,

$$\frac{\mu_m}{\mu_{m=0}} = \left(1 - \frac{m^2}{J^2}\right)^{\frac{1}{2}}$$

This is true for a rigid molecule; including the effects of a non-rigid vibrator would only make small second-order correction here.

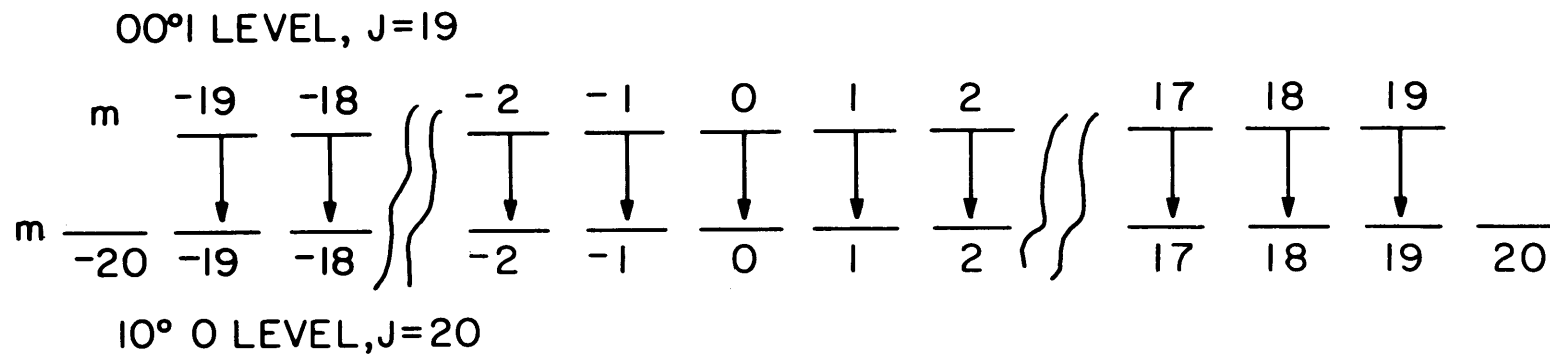
Equations (2-32), (2-33), and (2-34) must be modified as follows:

- (1)  $M(\nu)$ , the normalized population inversion per unit frequency for a group of particles centered a frequency  $\nu$  away from line center, must be further split to include the different populations for the different dipole moments  $M \rightarrow M_m$ .
- (2)  $Q(\nu)$ , the normalized polarization current for a group of particles centered at frequency  $\nu$  away from line center, has in its normalization a dipole  $\mu$ ; it must be separated into the different polarizations pertaining to the different orientations. Therefore

$$Q(\nu) \rightarrow \frac{\mu_m}{\mu_{m=0}} Q_m(\nu)$$

- (3)  $A$ , the normalized gain coefficient, is proportional to  $\mu^2$

$$A \rightarrow \left(\frac{\mu_m}{\mu_{m=0}}\right)^2 A_0$$



ARROWS INDICATE ALLOWED TRANSITIONS

DEGENERATE AMPLIFICATION

FIGURE 4-6

The value of  $A_0$  is calculated by summing over the degeneracy quantum number,  $\mu$ .

$$A_0 = \frac{A}{\sum_{m=-J}^J \left( \frac{\mu_m}{\mu_{m=0}} \right)^2}$$

Using all these new variables, the equations which describe the intense pulse amplification are:

$$\frac{\partial F}{\partial T} + \frac{\partial F}{\partial Z} = \sum_{m=-J}^J \int_{-\infty}^{\infty} Q_m(\nu) d\nu \quad (4-9)$$

$$\frac{\partial Q_m(\nu)}{\partial T} = -\frac{\mu_m}{\mu_{m=0}} A_0 M_m(\nu) F - i\Omega' Q_m(\nu) - \frac{Q_m(\nu)}{T_2} \quad (4-10)$$

$$\frac{\partial M_m(\nu)}{\partial T} = \frac{2\mu_m}{\mu_{m=0}} (F^* Q_m(\nu) + F Q_m^*(\nu)) \quad (4-11)$$

The initial conditions which must be specified are:

- (1) The frequency distribution of the initial population distribution  $M_m(\nu)_e$  ( $Z = 0$ ).
- (2) The initial pulse at  $Z = 0$ ,  $F(T, Z = 0)$ .
- (3) The gain coefficient  $A_0$ .
- (4) The rotational quantum number and the values of the dipole moments.
- (5)  $T_2$ .

The equations have been numerically integrated on a computer by C. K. Rhodes.<sup>21</sup> Figure 4-7 shows a typical pulse amplification done on a computer for 2.5 and 5 meters of amplification. The parameters used in the computation were:

$$\text{Peak input pulse intensity} = 2.38 \text{ kW/cm}^2$$

$$t_2 = 85 \text{ nanoseconds}$$

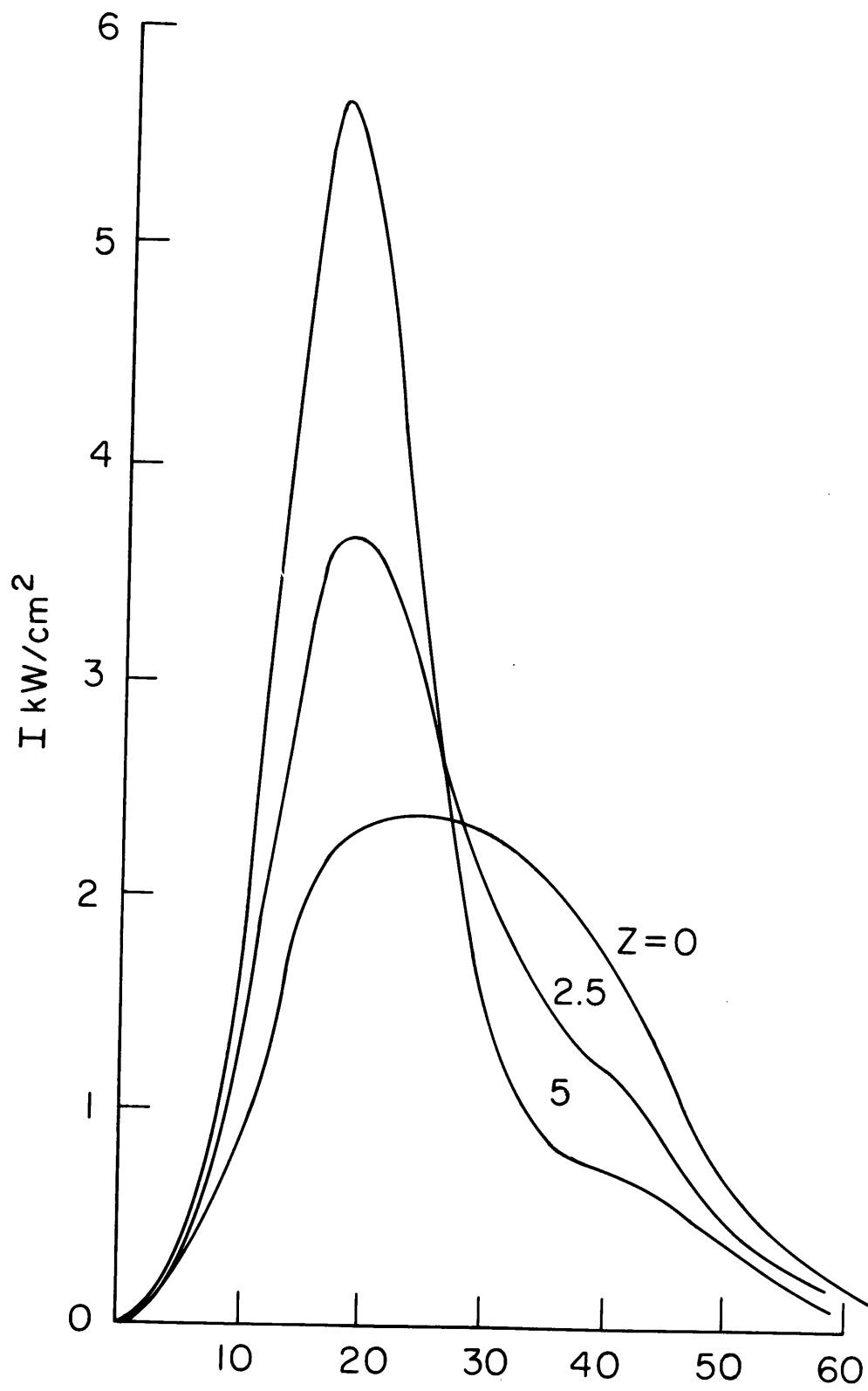
$$A_0 = 0.0295/\text{m}, \text{ which corresponds to an } \alpha \text{ of } 1.5 \text{ dB/m} \\ \text{and a low signal gain of } 5.62 \text{ for the length of} \\ \text{amplification} = 5 \text{ m.}$$

$$J = 20, \text{ and the corresponding dipole moments}$$

An inhomogeneous Doppler broadened line of 60 MHz

Active pulse sharpening does occur and attenuation of the lagging edge is observed. Note that these numbers are representative of a  $\text{CO}_2$  laser at these pressures and hence we can expect to see these effects at the low pressures.

Figure 4-8 shows a comparison between the pulse amplification of Fig. 4-7 and the same pulse amplification neglecting the rotational degeneracy. The pulses after 5 meters of amplification are not appreciably different, because for a high  $J$  value most of the dipole moments are centered about some average value; an extremely high pulse intensity is required then to make the products of the dipole moments and electric field noticeably different. However, if we were considering amplification on a  $P(4)$  transition, the values of the dipole moments would be considerably different, and these intensity values would be sufficiently strong to cause appreciable differences between the single dipole amplification and multiple-dipole moment amplification.

FIGURE 4-7  $t(\text{ns})$



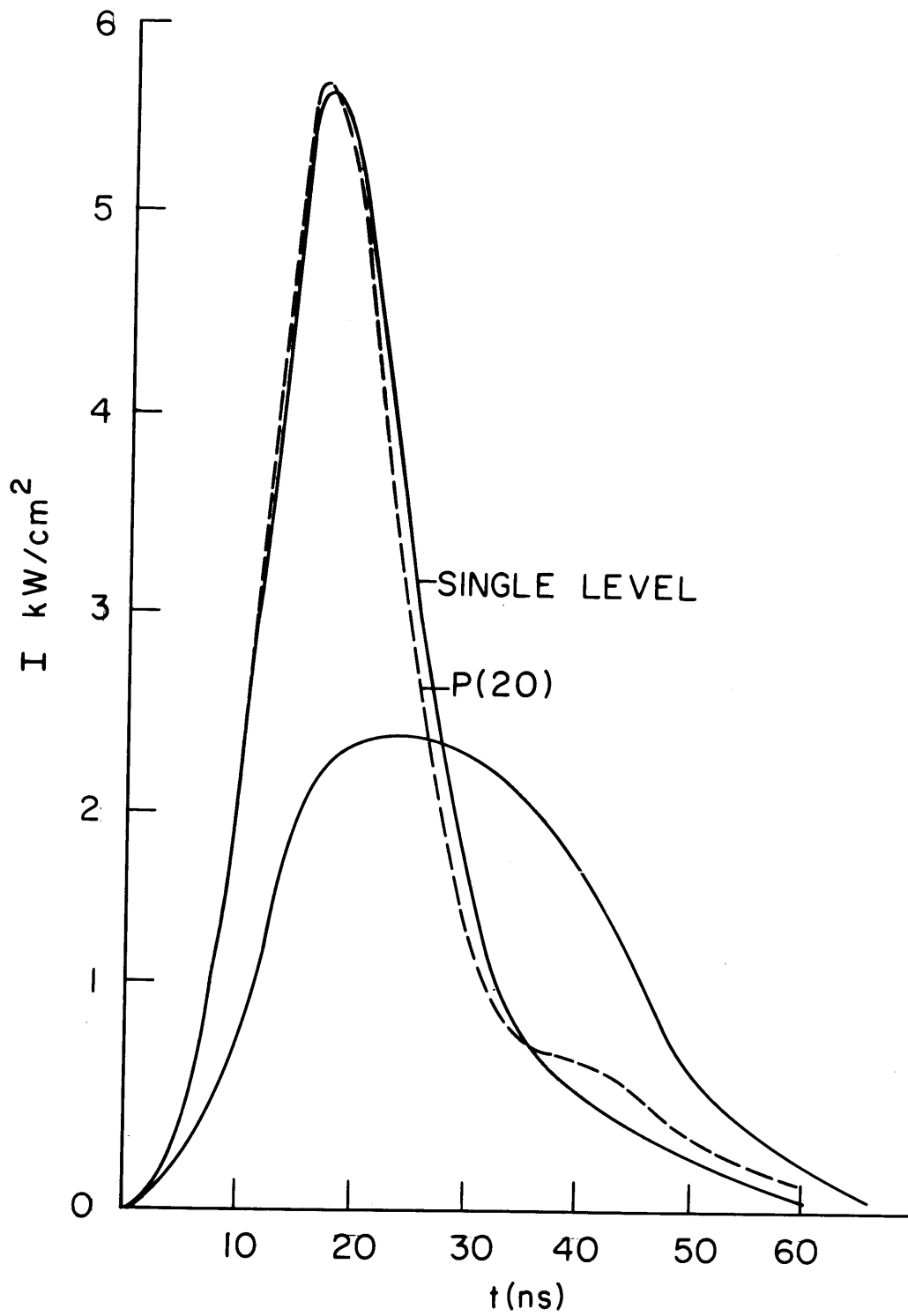


FIGURE 4-8

### Comparison with analytic $\pi$ -pulse solutions

Most of the theoretical work done in fast optical pulse amplification has been concerned with analytic solutions of the equations. That is, if we include the loss term in the field equation

$$\frac{\partial F}{\partial T} + \frac{\partial F}{\partial Z} + \frac{F}{T_0} = -K \quad \text{or} \quad - \sum_m \int_{-\infty}^{\infty} Q_m(\nu) d\nu$$

a steady state pulse with a hyperbolic secant shape will evolve; it is called a  $\pi$ -pulse because it satisfies the condition<sup>22</sup>

$$\frac{\mu}{\hbar} \int_{-\infty}^{\infty} E dt = \pi$$

However, this pulse does not come about until the loss from the term  $F/T_0$  becomes comparable to the energy put into the field from the amplifying medium. This is not satisfied at all here; the loss is so small that we will not consider it in our model.

### Effect of nonuniform electric field

It has constantly been mentioned that the nonuniform structure of the electric field causes variations in the rate of population reversal,  $\mu E/\hbar$ . All the theories described thus far use a plane electromagnetic wave.

This problem has plagued workers in this field for quite some time. For example, Hahn and McCall in their work on self-induced transparency in ruby were limited in their analysis of the observed transparency by the fact that the beam in the absorber was self-trapping and forming small filaments.<sup>23</sup>

For the particular experiment done here, the problem is every bit as complex because of the diffraction of the beam in the amplifier. First

consider the case of a pulse propagating in an amplifier such that there is very little diffraction; that is, the beam may have any transverse intensity distribution (in our case a TEM<sub>00</sub> Gaussian), but this intensity profile will not change very much while the beam is propagating through the amplifier when the amplifier is off ( $\alpha = 0$ ). In this limit (ray optics), the computation can be done for several values of input intensities, and the resulting output intensities can be summed after being multiplied by appropriate weighting factors for the areas that the various input intensities occupied. The resulting sum will give the output power, and the computed result can be made to simulate reality by increasing the number of input intensity levels used.

But the amplifier used in this experiment has a beam which diffracts appreciably while passing through it; in linear amplification with a Gaussian beam profile the spot size,  $w$ , the radius of the  $e^{-2}$  intensity value, varies between 2.42 mm on the mirrors of the multipass amplifier, and 1.21 mm in the center of the amplifier. This refocussing condition on each pass is necessary to achieve five passes of amplification without appreciable spreading of the beam, which is necessary to observe strong nonlinear effects within a reasonable amplifier length.

However, the method used in generating the short intense pulses produced pulses which did not have a pure Gaussian intensity cross section, but rather they resembled a plane wave of finite aperture. Of course, the insertion loss increased in attempting to couple these pulses to the multipass amplifier which in this case behaved as a mode filter. So although a plane wave treatment could be used, the diffraction of the beam and its being apertured could not be included in the theoretical model.

## CHAPTER V

## NONLINEAR PULSE AMPLIFICATION EXPERIMENT

The main problem in achieving any kind of interesting nonlinear pulse amplification in a CO<sub>2</sub> laser amplifier with pulse sharpening and attenuation of the lagging edge is the fulfillment of condition (4-6).

$$\mu E/\hbar \geq \Delta\nu, \text{ the bandwidth of the system}$$

The CO<sub>2</sub> laser can be Q-switched since it is a high gain system ( $\alpha > 3$  dB/m at normal operating pressures) and has a long lifetime of the upper laser state ( $\approx 10^{-3}$  seconds). The normal method of Q-switching is by rotating one of the cavity mirrors. The risetime of the Q-switched pulse is approximately 100 nanoseconds, which is too long; the long risetime of the pulse is strong enough to saturate the amplifier before the strongest part of the pulse can begin to drive the medium (flip the population) at a very fast rate. The rotating mirror Q-switched pulses could only achieve population reversal severe enough to lead to attenuation of the lagging edge of the pulse if an amplifier of extraordinary length were used (about 25 meters for typical parameters of a CO<sub>2</sub> laser). Obviously a method of extracting the energy from the cavity, other than transmission coupling through a cavity mirror, is needed.

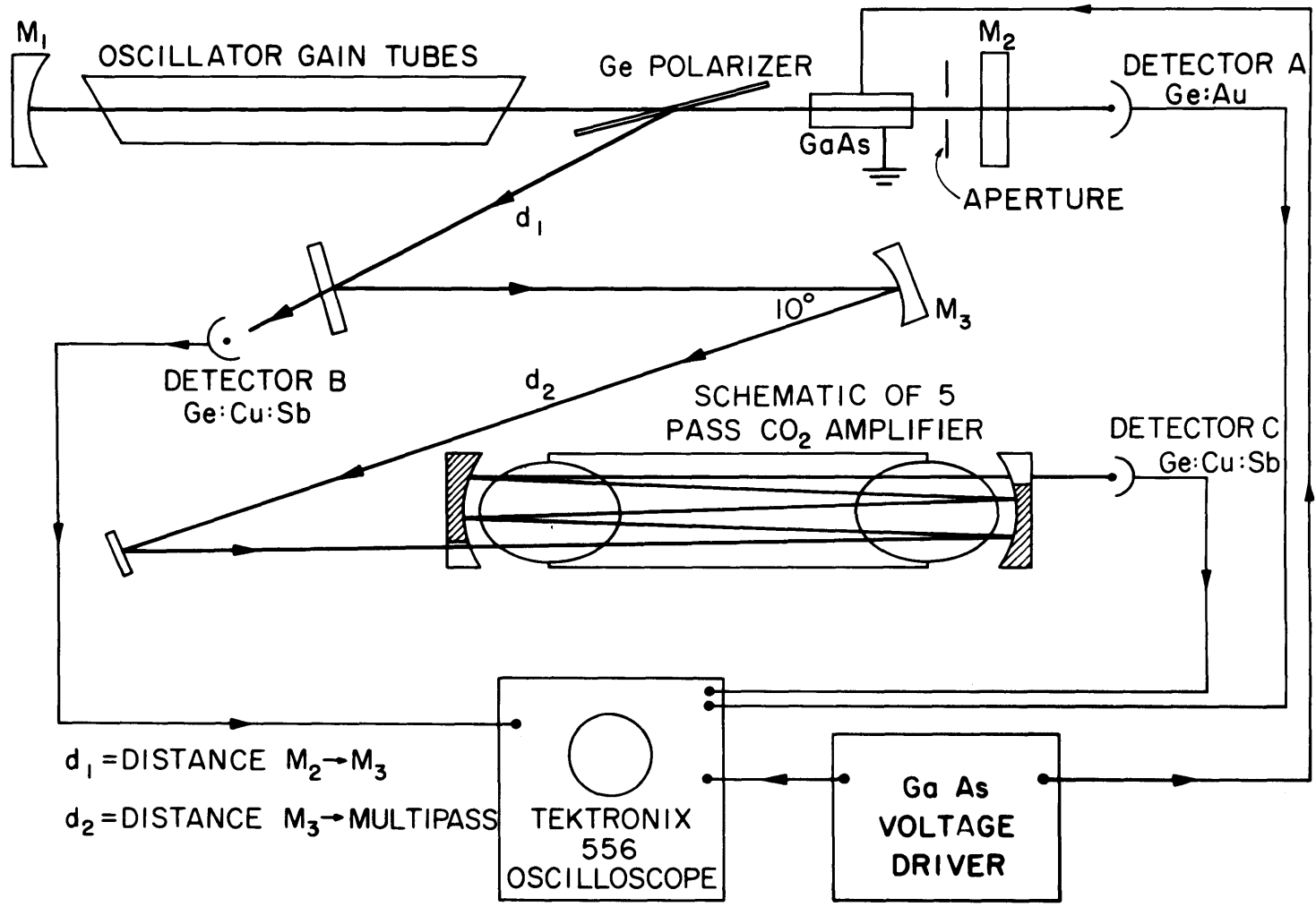
Considerable attention has been given to the production of short CO<sub>2</sub> pulses by introducing a saturable absorber, such as SF<sub>6</sub>, into the cavity.<sup>5</sup> Unfortunately these pulses do not have very short risetimes either ( $\approx 50$  nanoseconds), and do not exist singularly; rather they are emitted in trains with approximately 20 pulses in each train. Amplifier experiments cannot be done with 20 successive pulses; after each pulse,

the amplifying medium needs a chance to recover, i. e.,  $N$ , the normalized inversion, must return to unity.

One solution to this problem is to place our GaAs modulator and Ge polarizer, a device with which we can achieve nanosecond switching times, external to the cavity. Using the arrangement described in the linear experiment, the pulse input to the amplifier could be switched on with a nanosecond risetime. But to get 100% transmission through the Ge polarizer, the GaAs modulator would have to have an electro-optic rotation of  $90^\circ$ , requiring a voltage of 11.6 kV.

The method finally used for short pulse production is shown in Fig. 5-1. The GaAs modulator and Ge polarizer are used inside the cavity, both to achieve Q-switching and pulse extraction, in this case called cavity dumping, since when the voltage signal is applied to the GaAs to extract the pulse, the cavity behaves as though one of the mirrors were removed, and the energy was "dumped" out.<sup>24</sup> The operation is simple in theory but difficult to perform in practice.

When no voltage is applied to the GaAs modulator, it behaves like an isotropic material, and the laser oscillates cw with a polarization in the plane of the paper. Consider what happens when a quarter wave voltage is applied to the modulator ( $\varphi = \pi/2$ ). Any radiation traveling toward  $M_2$  passes through the crystal, becomes circularly polarized, bounces off  $M_2$ , goes through the GaAs modulator again, becomes linearly polarized (polarization vertical to the paper), and is reflected off the Ge polarizer. In this manner, the GaAs acts as an internal cavity switch to stop the laser oscillation. But now consider if the voltage is suddenly dropped to zero as in Fig. 5-2a. The laser will begin to Q-switch with an experimentally observed risetime of 300 nanoseconds on detector A, Fig. 5-2b;



NONLINEAR PULSE AMPLIFICATION

FIGURE 5-1

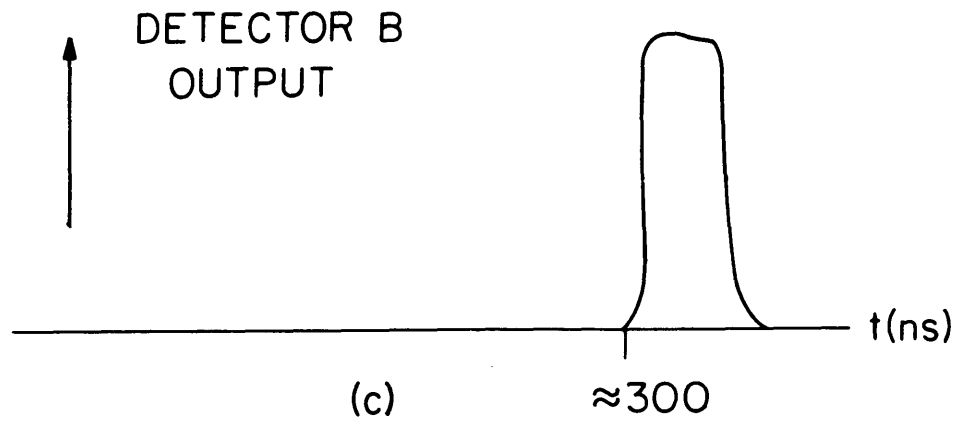
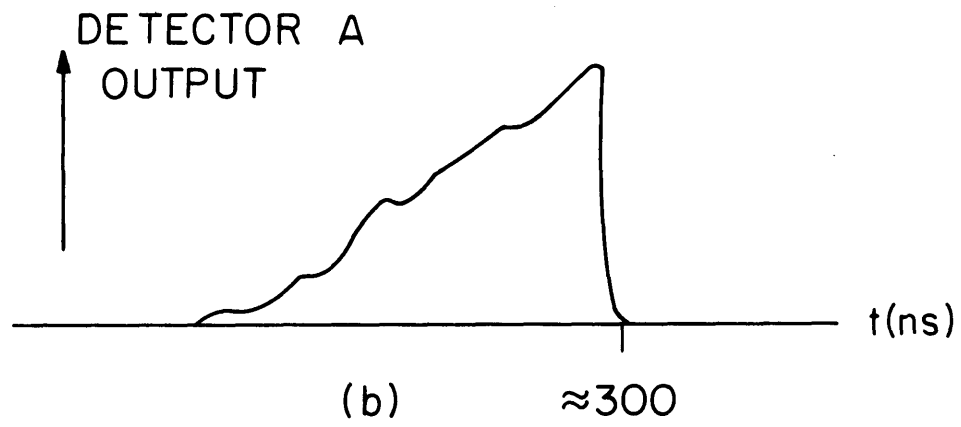
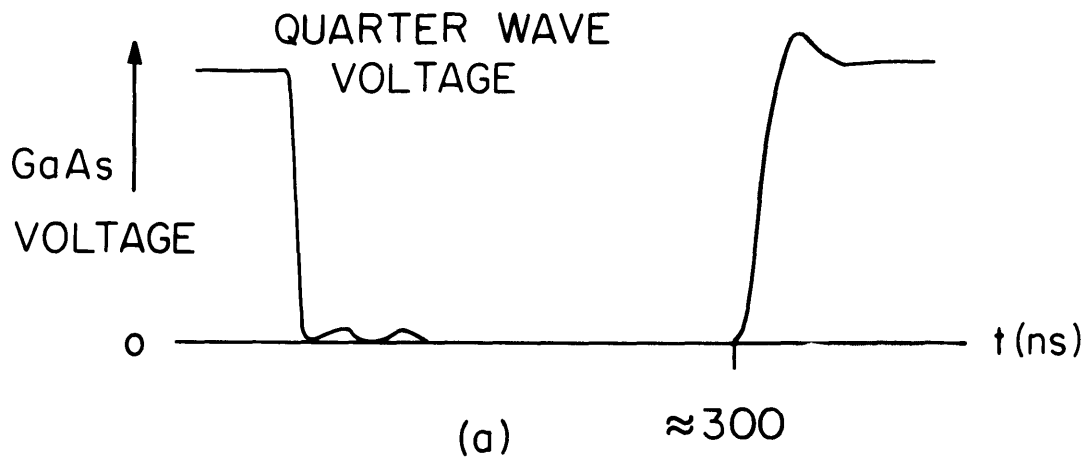


FIGURE 5-2

$M_2$  was an Irtran IV flat with 5% transmission. The voltage is re-applied to the Ga-As modulator when the cavity intensity is at its maximum, Fig. 5-2a; then the Q-switched pulse is shuttled out of the cavity by reflection off the Ge polarizer. The pulse has a length of twice the round trip transit time of the cavity,  $2l/c$ , in this case 48 nanoseconds, and its risetime is limited only by the voltage risetime of the GaAs driver ( $\approx 5$  nanoseconds). The output pulse is monitored by detector B, Fig. 5-2c.

Figure 5-3 is an oscilloscope photograph of the intensity inside the cavity (upper trace) and the voltage on the GaAs crystal (lower trace).

Figure 5-4 shows the dumped pulse (upper trace) and intensity inside the cavity (lower trace). The risetime of the pulse is approximately 5 nsec, and its peak power approximately 1.5 kW.

Figure 5-5 is a multiple exposure of Fig. 5-3, but during one Q-switching sequence the voltage was not re-applied to the GaAs. On that one occasion, the intensity in the cavity leaked out through  $M_2$ ; this is evident in the upper trace.

Figure 5-6 is like Fig. 5-3, except that proper axial tuning of the cavity has led to spontaneous mode-locking behavior. The ringing of the upper trace is  $2l/c$ , and the width of the pulses indicates that only 3 modes are being locked. The mode-locking was not repetitive enough, however, and most of our amplifier work was done without trying to induce mode-locking to achieve shorter pulses.

The cavity was 7.2 meters long and Z-shaped so that it could fit on our optical table. Three separate gain tubes were used; a three-foot-long  $1\frac{1}{2}$ " diameter, a four-foot-long 1" diameter, and a four-foot-long  $3/4$ " diameter.  $M_1$  was a total reflector, 7.32 m radius of curvature,



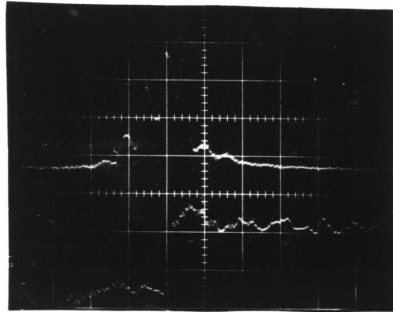


FIGURE 5-3

Time scale 100 nsec./major division

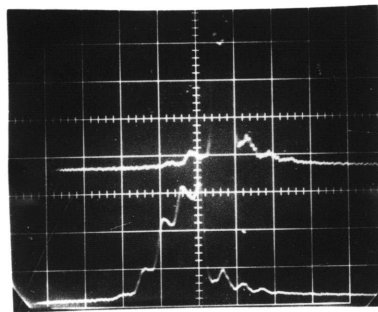


FIGURE 5-4

Time scale 100 nsec./major division

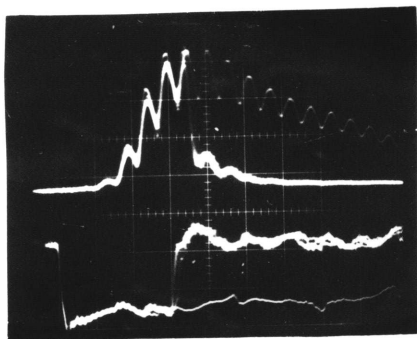


FIGURE 5-5

Time scale 100 nsec./major division

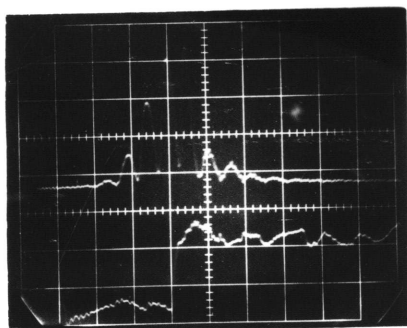


FIGURE 5-6

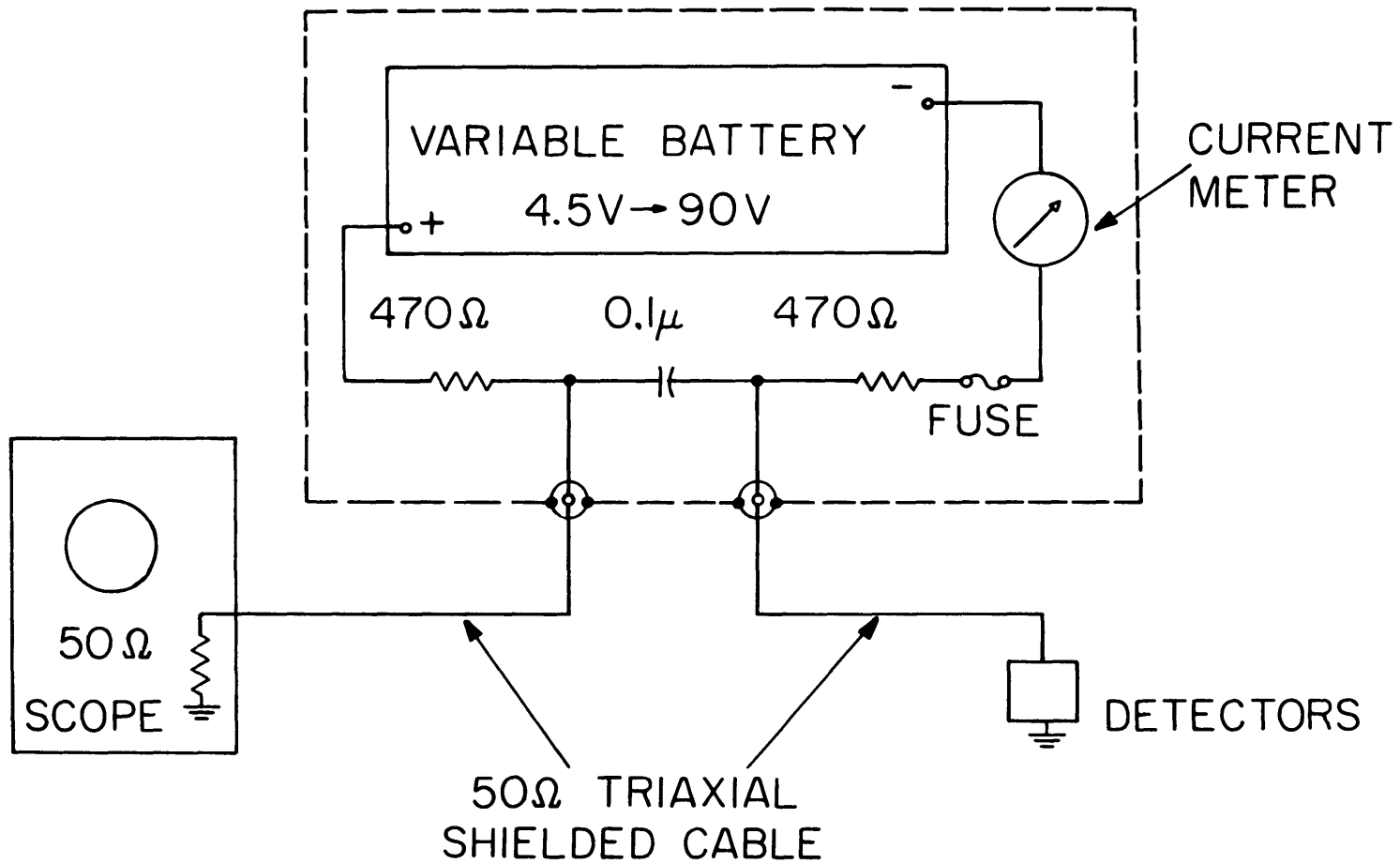
Time scale 100 nsec./major division

making the cavity nearly semi-hemispherical. This was necessary so that the cavity mode would be small enough to fit through the GaAs, which was near the  $M_2$ , the flat mirror.

The same multipass amplifier was used here as was used in the linear experiment. The mode coupling parameters were  $d_1 = 1.245$  m;  $M_3 = 2.08$  m radius of curvature, and  $d_3 = 0.853$  m. In addition to the previously mentioned fact that the extra length is of critical importance when looking for nonlinear effects, the multipass amplifier offers other advantages for nonlinear pulse amplification experiments as well:

- (1) No overlap from pass to pass. Whereas this could have been tolerated in a linear experiment, it definitely could not be in a nonlinear experiment when the population inversion varies with time.
- (2) The beam is repeatedly refocused. This keeps the intensity (and the electric field) at a high level, which drives the nonlinear interaction at a faster rate.

The experiment here involves taking power measurements from our detectors B and C, which were Ge:Cu:Sb cooled to  $4.2^{\circ}\text{K}$  having measured risetimes of 1 nanosecond or better (Fig. 3-5). Let us now consider the bias circuit for the detectors as shown in Fig. 5-7. Note that with this circuit the voltage across the load is the same for either pulse or cw radiation impinging upon the crystal, because the capacitor maintains a constant voltage even when the impedance of the crystal changes suddenly to a burst of radiation. The detectors were calibrated and plots of  $\Delta I$ , the change in the detector current due to the presence of laser radiation, versus power input to the detector were made. These calibrations were done for a series of bias currents. It was found that  $\Delta I \sim P^{0.76}$ .



DETECTOR BIAS CIRCUIT

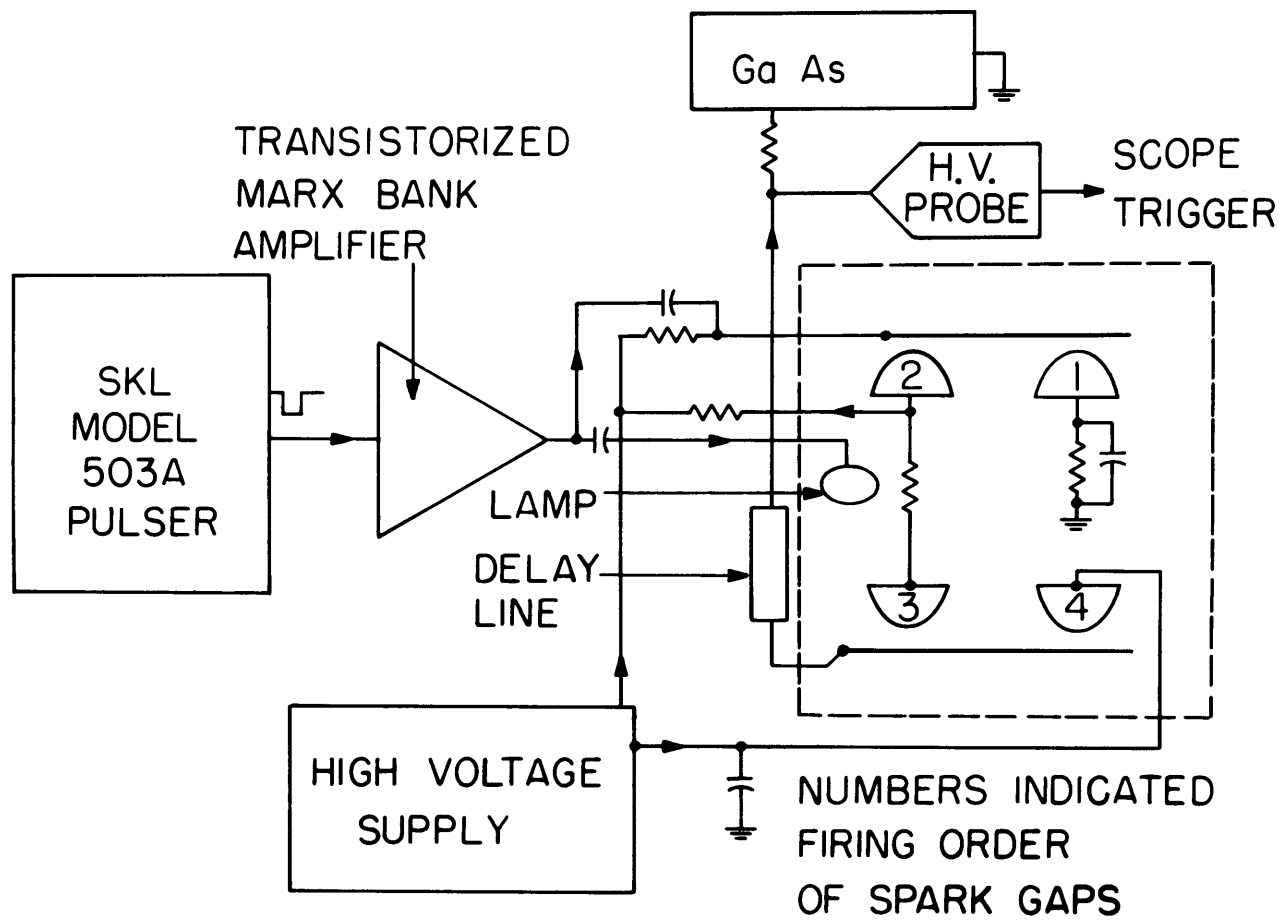
FIGURE 5-7

Calibrated attenuators were placed at the inputs to detectors B and C so they would not be saturated. The oscilloscope curves were corrected for the nonlinear detector characteristics.

Since the pulse risetime is limited by the voltage risetime onto the GaAs (Fig. 5.2a), let us discuss how this was done. Figure 5-8 shows a schematic of the electronics. An SKL Model 503A pulser emits a 70 volt, 0.5 nanosecond risetime pulse which triggers a Marx-Bank amplifier (roughly successive stages of transistors run in the avalanche mode).<sup>25</sup> A high voltage pulse triggers a burst of ultraviolet light (tungsten wire on a barium titanate disk) in a spark gap chamber and the ultraviolet breaks down a set of spark gaps which are nearly close enough to break down spontaneously. The first set of gaps breaking down reduce the voltage to zero on the GaAs, trigger the oscilloscope, and send a voltage surge along a variable delay line. When this surge hits the second set of spark gaps ( $\approx 300$  nanoseconds later) they break down and the quarter wave voltage is re-applied to the GaAs.

#### Experimental limitations in intense short pulse production

The main limitation in producing pulses in the manner just described was the presence of dc voltage on the GaAs; the dc voltage heated the crystal, which necessitated cooling of the crystal to prevent thermal runaway. However, there was still a temperature distribution in the GaAs causing it to behave like a thermal lens. Since the cavity was near semi-hemispherical so that the  $TEM_{00}$  mode could fit into the GaAs, the thermal lens effect caused laser oscillations with a non-Gaussian mode pattern. Experimentally the mode appeared to be an aperture-limited plane wave. For example, when the amplifier masks described



### GaAs VOLTAGE DRIVER

FIGURE 5-8

in Chapter II were inserted, it was found that the insertion loss increased by a substantial amount (up to 2.5 dB) which indicates the mode was not a Gaussian in cross section and that its diameter was greater than the aperture diameter, 8.5 mm.

A further complication is the fact that the oscillator emitted cw radiation since it was impossible to shut off the laser completely by applying a quarter wave voltage to the GaAs modulator. This was probably due to some imperfection in the crystal giving it some permanent birefringence. In that case, no value of voltage can turn off the laser completely.

But this cw radiation was not steady; as a result, the inversion in the oscillator was not the same from pulse to pulse, and the pulse amplitude varied a good deal more than one would gather from Fig. 5-5. The photograph in Fig. 5-5 was taken when the crystal was cooled by conduction through silicone vacuum grease applied to its sides and bottom. Later, the silicone grease was removed since it flowed over the optical faces; the crystal was then air cooled, which proved to be not as satisfactory from the point of view of laser performance.

The inherent trouble with the cw output is that it is amplified also, and once it is amplified enough to saturate the amplifier, the inversion in the amplifier can vary with time, making the problem even more difficult to analyze. If one records only large pulses, however, the cw output is then probably low, and the inversion is affected less. From the relatively high experimentally measured gains, one concludes that this had to be the case. The only requirement of the cw fluctuation is that it reduce to a low value a time interval equal to at least  $t_1$  before the pulse comes along, so that the amplifier inversion can return to its

(optical) field-free equilibrium value.

#### Low pressure amplification results and computer matching of curves

Using the techniques just described, pulse amplification was observed at low pressures; the partial pressures of  $\text{CO}_2$  and  $\text{N}_2$  were 0.25 and 0.55 torr, respectively. Figure 5-9 shows two photographs of oscilloscope traces; the upper photograph is for the amplifier off, the lower for the amplifier on. In each photograph the upper trace is detector C, the amplifier output, and the lower trace is detector B, the amplifier input. These two photographs were necessary because of the insertion loss of the beam into the amplifier. By noting the relative amplitudes and voltage settings in the upper photograph, one can determine for the lower photograph what the input power (lower trace) would have been at the output. In this manner the electronic gain of the amplifier was measured. The curve marked 'experimental' on Fig. 5-10 shows the resulting input and output powers after the detector characteristics had been taken into account. Here we now see sharpening of the front edge of the pulse, shortening of the pulse (from 34 nanoseconds full width at half power to 20 nanoseconds) and attenuation of the lagging edge. This is the first observation of population reversal in an active medium.

These curves show important practical results also:

- (1) Pulses can be amplified significantly at frequencies greater than their bandwidth. Here we have a pulse with a risetime of 18 nanoseconds being amplified significantly (peak pulse gain of 2.43) when the inverse Doppler width is 17 nanoseconds.
- (2) Pulse shortening can be achieved while amplifying



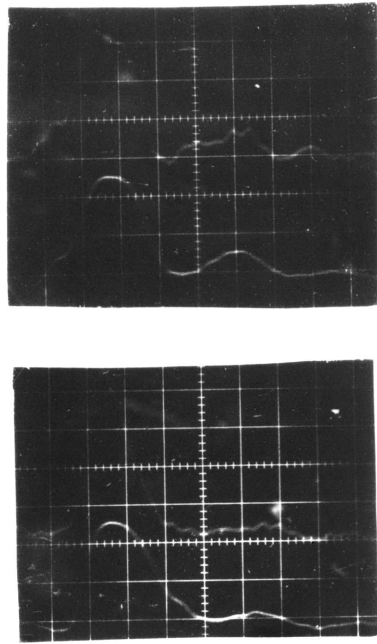
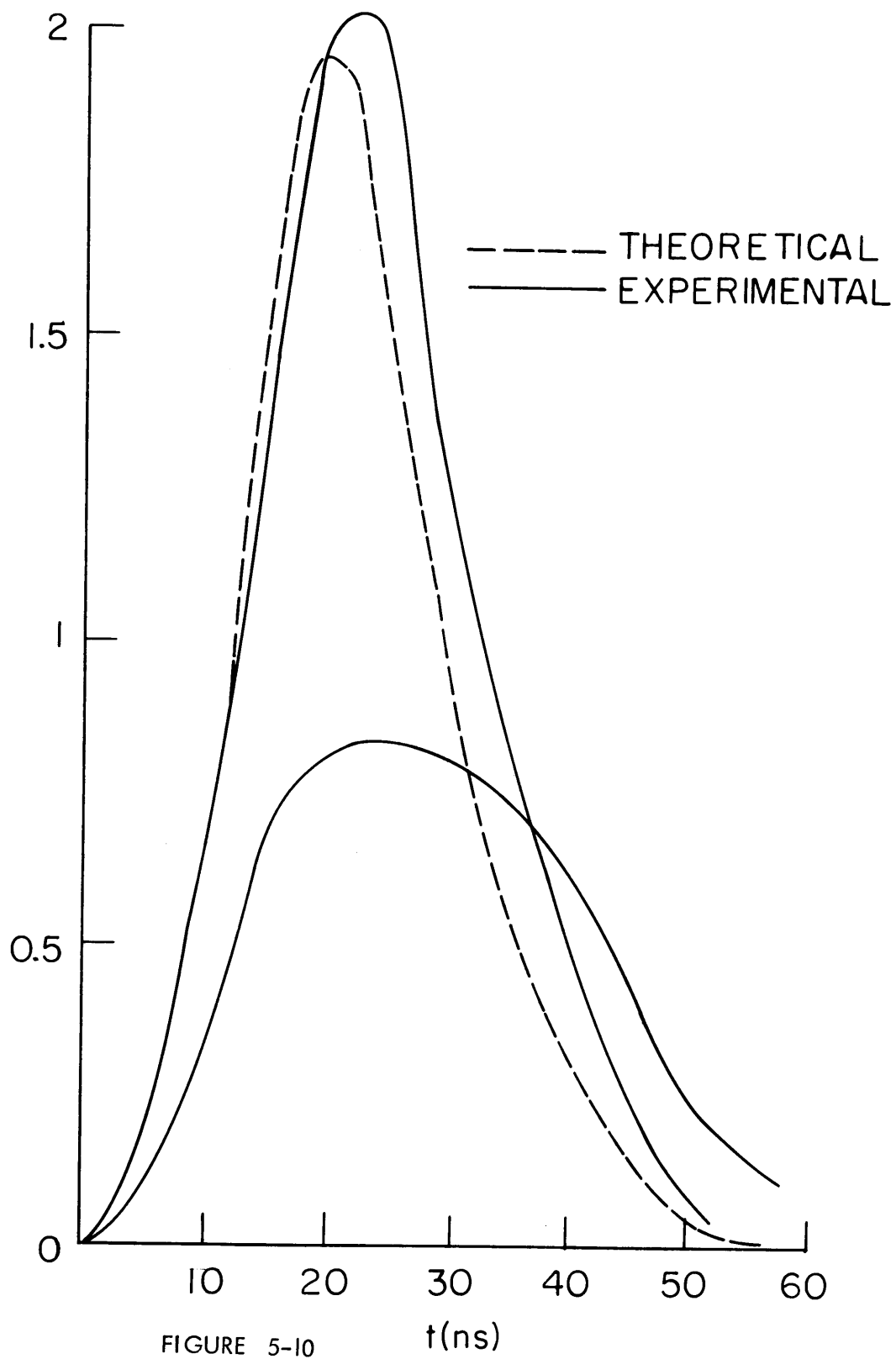


FIGURE 5-9

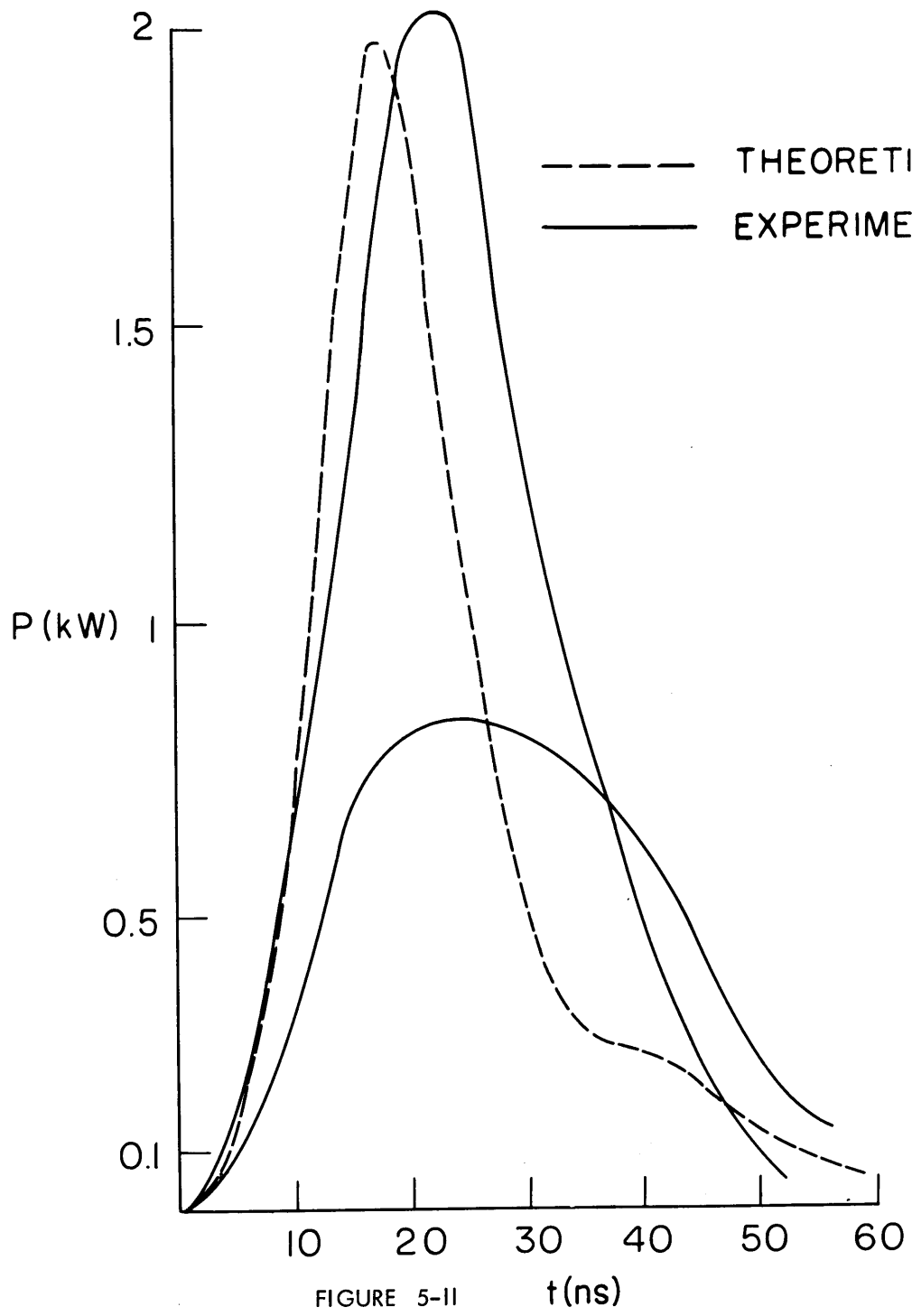
Time scale 20 nsec./major division



the pulse.

- (3) Since the lagging edge of the pulse experienced attenuation, due to population reversal, the shortening effect becomes more pronounced as the amplifier length is increased.

Computer curves were run to predict the amplification theoretically. The experimentally observed input pulse was used as one boundary condition for the equations which describe the pulse amplification, equations (4-9), (4-10), and (4-11). The pulse was observed to occur on P(20), and the appropriate dipole moments were used in the computer program. The other pertinent parameters were  $\Delta\nu_D = 59$  MHz and  $t_2 = 85$  nanoseconds. Figure 5-11 shows the computer generated curve labelled 'theoretical' and the experimental result when a low signal gain coefficient of 1.5 dB/m and an intensity of  $2.38 \text{ kW/cm}^2$  (corresponding to a beam diameter of 3.6 mm) were used. A plane wave model was used for the reasons mentioned in the previous section. The most obvious observation of this theoretical-experimental fit is that the energy in the experimental output pulse is higher than the one predicted using the above parameters in the computation. Whereas we could not hope to have the computer program predict the pulse behavior exactly, it should at least predict the energy gain of the pulse. From experimental observations, we know the pulse to be larger than the 3.6 mm used here, because of the previously mentioned difficulties with the GaAs. If we use the aperture size, 8.5 mm, as the size of the beam, the peak input intensity is lowered to  $1.47 \text{ kW/cm}^2$ , and using  $\alpha = 1.4$  dB/m, the curve labelled 'theoretical' on Fig. 5-10 results. This is as expected because the medium can do more to the radial portion of the pulse of low intensity



than the central portion of high intensity. This fit, Fig. 5-10, is our best fit.

Figure 5-12 shows another experimental observation and theoretical match of low pressure amplification. The pressures were the same as in the previous case. The input pulse is exceptionally long because the dumping did not work perfectly. The parameters used to obtain this best fit were the same as before, except the low signal gain was 1.5 dB/m and the peak intensity of the input pulse was  $0.809 \text{ kW/cm}^2$ . The computer matching was done for a single level instead of P(20) to conserve computer time. Note that for the input power level of 1.4 kW an intensity of  $2.18 \text{ kW/cm}^2$  is necessary for an aperture size of 8.5 mm. The rather large discrepancy between the two intensity values could be due to the "quality" of the mode when the experiment was performed; diffraction in the final pass could have caused the intensity to be lower than expected (most of the nonlinear amplification would occur there also). Our pulse power measurement technique could have been wrong also.

However, both of these examples consistently show the pulse sharpening and absorption of the lagging edge of the pulse. The absorption is frequently referred to as a nutation effect. This is the same phenomenon, except there is no periodic ringing which is normally associated with the nutation effect. If the pulse is much shorter than  $t_2$ , much longer than  $(\Delta\nu_D)^{-1}$ , and of the correct intensity, it may cause a ringing (nutation) in the inversion, which in turn may cause the pulse power to indent (have a localized minima) and, if amplified sufficiently, to break into two parts. Consequently, many observers fallaciously assume any observation of ringing in a pulse to be a nutation

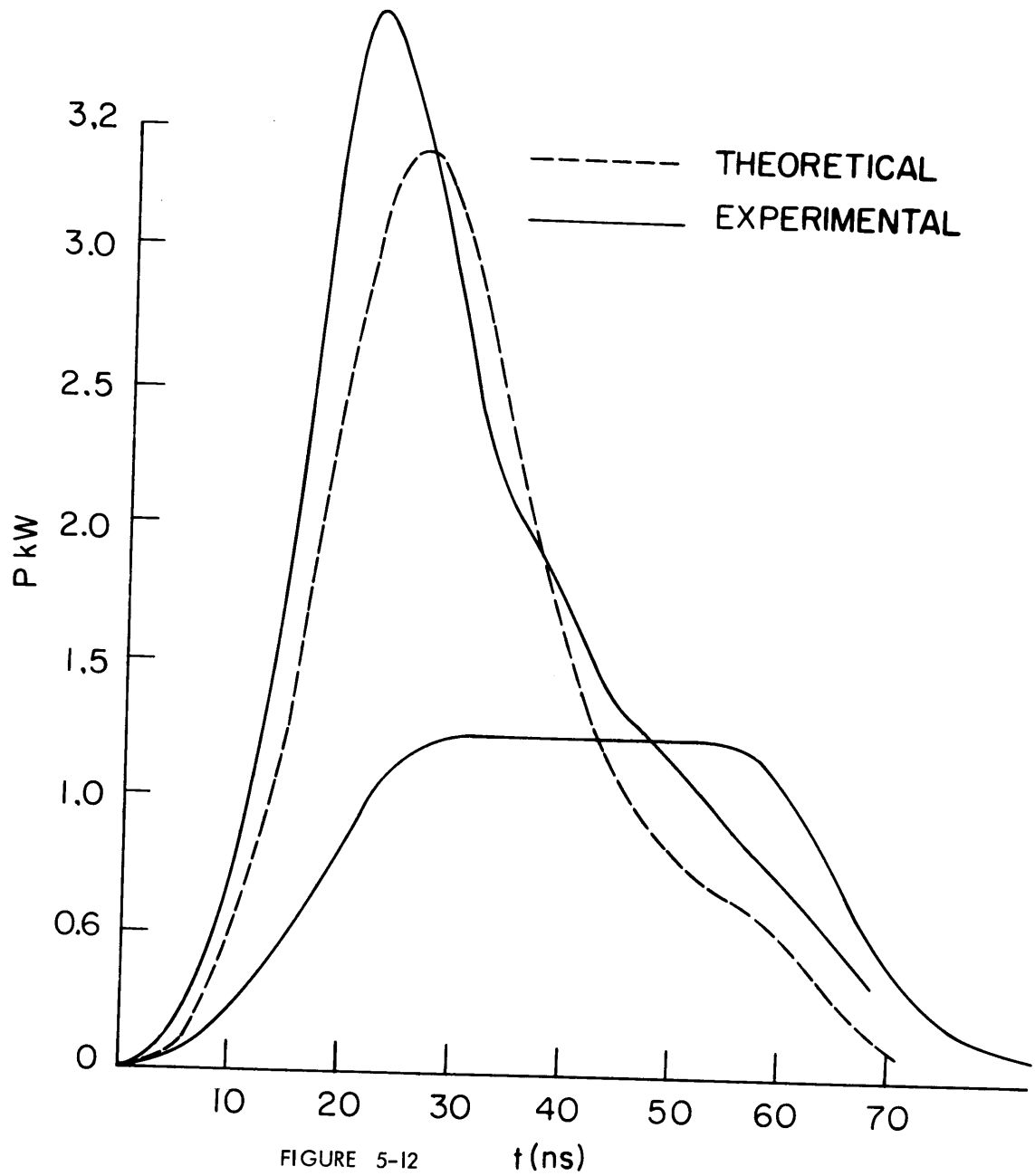


FIGURE 5-12 t(ns)

effect,<sup>8</sup> when in actuality pulse ringing may be caused by many other effects, such as off-resonance linear pulse amplification (Fig. 2-4).

Other observers also incorrectly believe that no nutation effect has been observed unless there is ringing in the pulse intensity.<sup>26</sup>

In our particular example, we have caused the initially inverted population to become noninverted, and the medium to become absorbing (since the lagging edge was absorbed), but the power itself did not begin to indent. We were slightly low in the intensity required to observe pulse ringing. Consider Fig. 5-11, which shows a computer fit for a peak input intensity of  $2.38 \text{ kW/cm}^2$ . Now consider Fig. 5-13, which shows the same computer result if the peak input intensity is increased to  $9.66 \text{ kW/cm}^2$ ; the output clearly shows pulse ringing. Had the mode structure of our beam been more well-defined, the intensity of experimental pulse would have been high enough (in theory) to observe pulse ringing.

#### High pressure amplification results and computer matching curves

Pulse amplification was also attempted at high pressures,  $p \text{ CO}_2 = 1.83 \text{ torr}$ ,  $p \text{ N}_2 = 1.6 \text{ torr}$ , and  $p \text{ He} = 8.23 \text{ torr}$ . Figure 5-14 shows the corrected input and output power curves obtained by using the techniques described in the previous sections. Also on Fig. 5-14 is the theoretical output curve obtained from Equations (4-1), (4-2), and (4-3) by using the input pulse as a boundary condition on the differential equations. The medium parameters used in the computation were  $\alpha = 2.5 \text{ dB/m}$ ,  $t_2 = 2.8 \text{ nanoseconds}$ , and  $t_1 = 22.4 \text{ nanoseconds}$ .  $t_1$ , one may recall, is the effective rotational relaxation time.

Again a plane wave interaction was assumed with a beam diameter

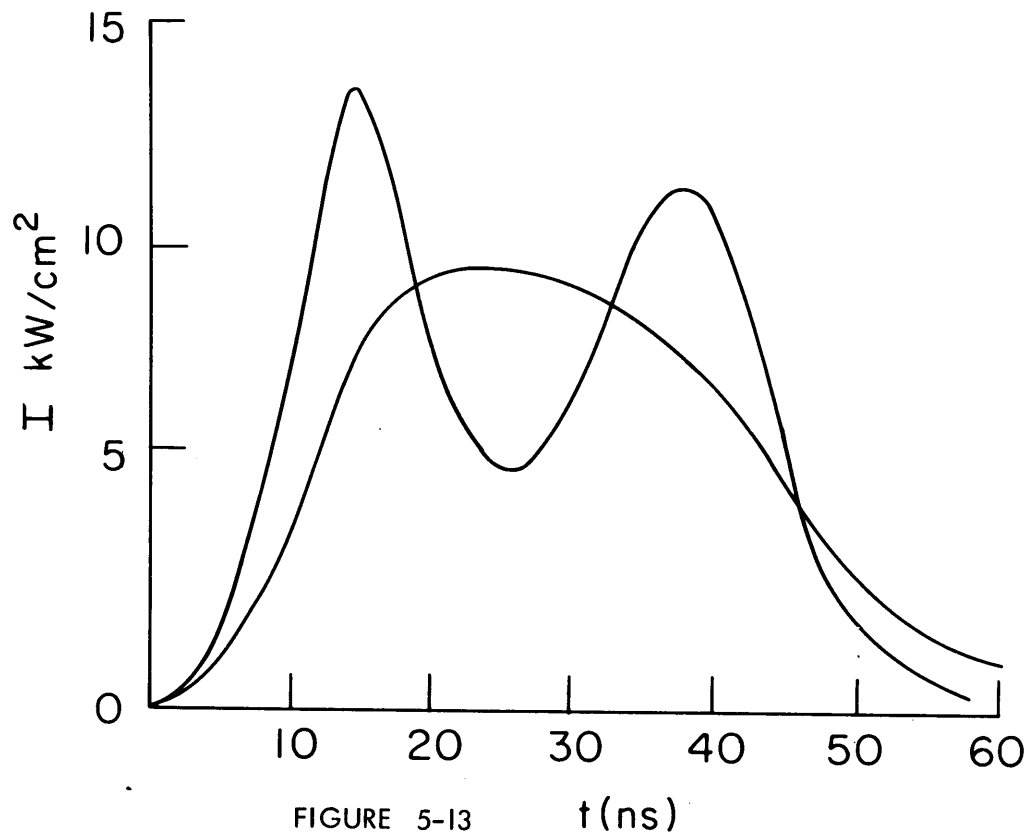


FIGURE 5-13  $t(\text{ns})$



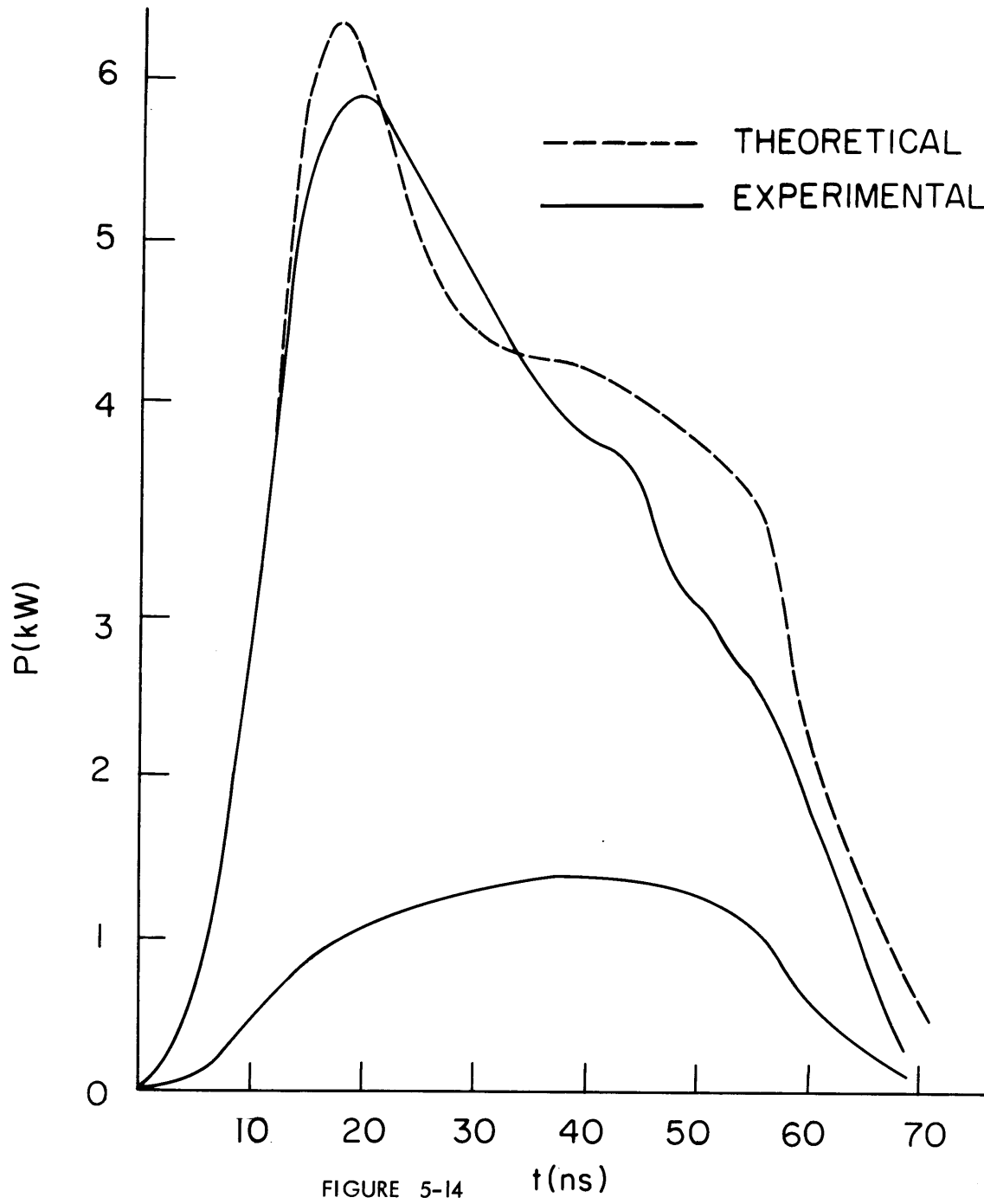


FIGURE 5-14

of 8.5 mm corresponding to a peak input intensity of  $2.46 \text{ kW/cm}^2$ .

Due to the problems with the cw input to the amplifier, the cw output was high enough to alter the bias current in the detector, causing its sensitivity to change significantly. Although this was accounted for in the plotting of the pulse power, the accuracy of the power of the amplified pulse is only good to 25%.

Nevertheless, the experimental-theoretical match is rather good, considering the non-idealized state of the experiment. The most important fact to be learned here is that the lagging edge of the pulse is not absorbed because of rotational relaxation. However, since the low signal gain is so much larger at the high pressures than at the low pressures, the peak power gain is higher also.

Using these considerations, one can design an oscillator-amplifier combination for any particular use. For example, one may use an oscillator of moderate pulse output power to drive a low pressure amplifier so that active pulse sharpening could be achieved and shorten the pulse to a desired length in time. The shortened pulse could be then amplified in a high pressure amplifier which would amplify the shortened pulse to the desired power level.

## CHAPTER VI

### CONCLUSIONS

This work has investigated both the experimental and theoretical aspects of linear and nonlinear short pulse amplification. However, in no sense can this be regarded as the final definitive work in this field. Rather it should be regarded as a first investigation of these interesting phenomena.

For example, the linear pulse response experiment showed the bandwidth of the laser could be measured by observing the step response. By performing the experiment more accurately, as discussed in Chapter III, one could determine the collision broadening linewidths of the constitutive gases in the  $\text{CO}_2$  laser. Also by studying the behavior of the linear response at low pressures one can observe the Landau-type damping which is present in an inhomogeneously broadened line.

The theory derived for the linear experiment is applicable not only to  $\text{CO}_2$  lasers, but could be used to predict the behavior of other laser amplifiers to fast-risetime linear pulses. Bandwidth information could be derived from such experiments even for lasers in the visible region. Also note that the theory derived in Chapter II for the inhomogeneous linear response could be used for solid state lasers if the inhomogeneous broadening profile were changed from a Gaussian to whatever is necessary for the particular broadening mechanism that may exist.

However, the nonlinear pulse experiment yielded the most interesting experimental results by far. Without belaboring the results already discussed thoroughly in Chapter V, one can see that pulse amplification is not limited by the bandwidth of the medium, and that active pulse sharpening can be achieved via resonant amplification.

The nonlinear experiment could be made more successful if a rotating mirror were used to initiate Q-switching in the oscillator. This would eliminate the need for the dc voltage on the GaAs. Dumping could be achieved by applying a short pulse of voltage to the crystal. The advantages would be no cw radiation from the oscillator and better mode definition of the beam.

Other interesting objectives to be studied here are: (1) mode-locking the oscillator to obtain pulses shorter than the round-trip transit time, and (2) using a pulsed amplifier to obtain higher gains.

The techniques learned here for studying nonlinear pulse interactions may be used in any high-gain laser amplifier.

## APPENDIX A

Program to compute equations 2-26 and 2-31.

```

DIMENSION FI(30)
INTEGER MN,N,J,KS,KT
LABEL SETBRK.(LABEL)
READ PRINT COMMENT STYPE N,J,TMIN,TINC,TMAX,ZAN,Z,T2,OMG
R'A
SAFE=2.0*SQRT.(ZAN)
THROUGH KEEP, FOR T=TMIN,TINC,T.G.TMAX
ENDPT=SAFE*SQRT.(T-Z)
BEGIN=0.0
SHORT BND=SIMPER.(BEGIN,ENDPT,R.,N,J,KS,KT,PF,PS)
AND=SIMPER.(BEGIN,ENDPT,Q.,N,J,KS,KT,PF,PS)
DND=(AND+1)*(AND+1)
NND=BND*BND
SND=(DND+NND)*EXP.(-2*ZAN*T2/(OMG*OMG*T2+1.))
WHENEVER KS.E.1 .AND. KT.E.1
PRINT FORMAT WHY,T,DND,NND,SND
OR WHENEVER KS.E.0
N=N+1
T=SHORT
OR WHENEVER KT.E.0
PRINT FORMAT HELP,T
KEEP E'L
CONTINUE
T=READ
V'S WHY=$3H T=F6.2,7H IREAL=E15.8,S2,5HIMAG=E15.8/,
:1,6HSTEP=E15.8*S
V'S HELP=$$1,H'FAILED TO CONVERGE FOR T = 'F6.2/'$
INTERNAL FUNCTION (A,B,X)
ENTRY TO Q.
Y=0.0
MN=1
MFIBES.(X,Y,MN,FI)
EXPR=EXP.(-X*X/(4.0*ZAN*T2))*FI(1)*COS.(X*X*OMG/(4.0*ZAN))
FUNCTION RETURN EXPR
END OF FUNCTION
INTERNAL FUNCTION (A,B,X)
ENTRY TO R.
Y=0.0
MN=1
MFIBES.(X,Y,MN,FI)
EXPS=EXP.(-X*X/(4.0*ZAN*T2))*FI(1)*SIN.(X*X*OMG/(4.0*ZAN))
FUNCTION RETURN EXPS
END OF FUNCTION
END OF PROGRAM

```

APPENDIX B  
CALCULATION OF AMPLIFIER BANDWIDTH FROM  
COLLISION CROSS SECTION MEASUREMENTS

The bandwidth can be computed from the collision frequency by

$$\begin{aligned}\Delta\nu_n &= \frac{1}{\pi T_2} = \frac{\nu_c}{\pi} \\ &= \sum_m \frac{p_m}{kT} \sigma_{cm} \left( \frac{8kT}{\pi m_{cm}} \right)^{\frac{1}{2}}\end{aligned}$$

where the sum is over the  $m$  constitutive gases,  $p_m$  is the partial pressure of the  $m^{\text{th}}$  gas,  $\sigma_m$  is the collisional cross section between  $\text{CO}_2$  and the  $m^{\text{th}}$  gas, and

$$m_{cm} = \frac{m_{\text{CO}_2} m_m}{m_{\text{CO}_2} + m_m}$$

where  $m_{\text{CO}_2}$  is the mass of the  $\text{CO}_2$  molecule and  $m_m$  is the mass of the  $m^{\text{th}}$  gas.

The cross sections used in these calculations were

$$\begin{aligned}\sigma_{\text{CO}_2 - \text{CO}_2} &= 13 \cdot 10^{-15} \text{ cm}^2 \\ \sigma_{\text{CO}_2 - \text{N}_2} &= 8.7 \cdot 10^{-15} \text{ cm}^2 \\ \sigma_{\text{CO}_2 - \text{He}} &= 3.7 \cdot 10^{-15} \text{ cm}^2\end{aligned}$$

Using these numbers we find the various collision broadening frequencies to be

$$\Delta\nu_n(\text{CO}_2) = 6.43 \text{ MHz/torr}$$

$$\Delta\nu_n(\text{N}_2) = 4.88 \text{ MHz/torr}$$

$$\Delta\nu_n(\text{He}) = 4.49 \text{ MHz/torr}$$

using a temperature of 373<sup>o</sup>K obtained from the Doppler width (zero pressure intercept) of Fig. 3-7. Using the partial pressures listed on Fig. 3-7, we find the collision linewidth measurements using these cross sections to be 3.7% higher than the pulse amplification linewidth measurements.

APPENDIX C

Program to compute nonlinear pulse response for a  
homogeneously broadened amplifier.

```

DIMENSION X(1000),Y(1000),Z(1000),ZII(101)
INTEGER N,KM,I,J,MODE,HM,V,CJ,JLIM
REAL LO,L1,L2,NE
999 READ (5,901) LO,L1,L2,A,ZL,CK,MMM
READ (5,902) N,KM,HM,KN,W,CN,X(1)
READ (5,903) NE,V,TM,KN,CJ,MODE
WRITE (6,904)
WRITE (6,901) LO,L1,L2,A,ZL,CK,MMM
WRITE (6,905)
WRITE (6,902) N,KM,HM,KN,W,CN,X(1)
WRITE (6,906)
WRITE (6,903) NE,V,TM,KN,CJ,MODE
H=KN/(N+0.)
NNN=N+1
F=H/2.
AC=1.
AA=1.
AB=1.
BA=1.
BB=1.
BC=1.
Z(1)=0.
Y(1)=0.
CC=EXP(L2*F)
CA=EXP(LO*F)
CI=CN*SQRT(CK)
CB=EXP(L1*F)
DA=CB/CA/CC
DB=CC/CA
DC=CC/CA/CB
R=0.
CCC=CC*CC
CAC=CA*CA
CBC=CB*CB
DAA=DA*DA
DRB=DB*DB

```



```

DCC=DC*DC
VCC=CCC**V
VAC=CAC**V
PR=0.
IF (MODE.NE.0) GO TO 101
DO 100 I=2,NNN
RR=H*(I-1.)
S=(-H/2.+RR)
AL=(RR-1.)/W-TM
BL=(S-1.)/W-TM
Z(I)=AA*(CAC)*CI/(1.+AL**CJ)
ZO=AA*CA*CI/(1.+BL**CJ)
XO=4.*Z(I-1)*H*BA*Y(I-1)
YO=-A*BB*(NE+X(I-1)/AB)*H*Z(I-1)
X(I)=XO/6.+X(I-1)
Y(I)=YO/6.+Y(I-1)
DO=ZO*DA*BA
DP=ZO*DB*BB
XI=4.*DO*(Y(I-1)+YO/2.)*H
YI=-A*DP*(NE+(X(I-1)+XO/2.)/(AB*CB))*H
X(I)=X(I)+XI/3.
Y(I)=Y(I)+YI/3.
XO=4.*DO*(Y(I-1)+YI/2.)*H
YO=-A*DP*(NE+(X(I-1)+XI/2.)/(AB*CB))*H
X(I)=X(I)+XO/3.
Y(I)=Y(I)+YO/3.
AC=AC*CCC
AA=AA*CAC
AB=AB*CBC
BA=BA*DA
BB=BB*DB
BC=BC*DCC
XI=4.*Z(I)*BA*(Y(I-1)+YO)*H
YI=-A*Z(I)*BB*(NE+(X(I-1)+XO)/AB)*H
X(I)=X(I)+XI/6.
Y(I)=Y(I)+YI/6.

```

```

WR=Z(I)*Z(I)*H/AA/AA
PR=PR+WR
IF (((I-1)/HM*HM).NE.(I-1)) GO TO 100
T=H*(I-1.)
GT=SQRT(A)*2.
GR=2./(SQRT(A))
GRT=GT*GT
ZY=Z(I)*GT/AA
XIAB=X(I)/AB
GRAC=Y(I)*GR/AC
ZYZY=ZY*ZY
PRRT=PR*GRT
WRITE (6,907) R,T,XIAB,GRAC
WRITE (6,909) ZYZY,PRRT
100 CONTINUE
GO TO 200
101 IF (MODE.NE.1) GO TO 199
DO 102 I=2,NNN
RR=H*(I-1.)
S=(-H/2.+RR)
AL=(RR-TM)/W
BL=(S-TM)/W
Z(I)=AA*(CAC)*EXP(-(AL*AL))*CI
ZO=AA*CA*EXP(-(BL*BL))*CI
XO=4.*Z(I-1)*H*BA*Y(I-1)
YO=-A*BB*(NE+X(I-1)/AB)*H*Z(I-1)
X(I)=XO/6.+X(I-1)
Y(I)=YO/6.+Y(I-1)
DO=ZO*DA*BA
DP=ZO*DB*BB
XI=4.*DO*(Y(I-1)+YO/2.)*H
YI=-A*DP*(NE+(X(I-1)+XO/2.)/(AB*CB))*H
X(I)=X(I)+XI/3.
Y(I)=Y(I)+YI/3.
XO=4.*DO*(Y(I-1)+YI/2.)*H
YO=-A*DP*(NE+(X(I-1)+XI/2.)/(AB*CB))*H

```

```

X(I)=X(I)+X0/3.
Y(I)=Y(I)+Y0/3.
AC=AC*CCC
AA=AA*CAC
AB=AB*CRC
BA=BA*DAA
BB=BB*DBB
BC=BC*DCC
XI=4.*Z(I)*BA*(Y(I-1)+Y0)*H
YI=-A*Z(I)*BB*(NE+(X(I-1)+X0)/AB)*H
X(I)=X(I)+XI/6.
Y(I)=Y(I)+YI/6.
WR=Z(I)*Z(I)*H/AA/AA
PR=PR+WR
IF (((I-1)/HM*HM).NE.(I-1)) GO TO 102
T=H*(I-1.)
GT=SQRT(A)*2.
GR=2./(SQRT(A))
GRT=GT*GT
ZY=Z(I)*GT/AA
XIAB=X(I)/AB
GRAC=Y(I)*GR/AC
ZYZY=ZY*ZY
PRRT=PR*GRT
WRITE (6,907) R,T,XIAB,GRAC
WRITE (6,909) ZYZY,PRRT
102 CONTINUE
GO TO 200
199 ZII(1)=0.
READ (5,908) (ZII(I),I=2,101)
WRITE (6,910)
WRITE (6,908) (ZII(I),I=2,101)
DO 400 I=2,NNN
Z(I)=AA*(CAC)*CN*SQRT(ZII(1+(I-1)/5)+((I-1-(I-1)/5*5)/5.)*(ZII(2+
1(I-1)/5)-ZII(1+(I-1)/5)))
Z0=AA*CA*CN*SQRT(ZII(1+(I-1)/5)+(((I-1-((I-1)/5*5))/5.)-.1)*(ZII

```

```

I(2+(I-1)/5)-ZII(1+(I-1)/5))
X0=4.*Z(I-1)*H*BA*Y(I-1)
Y0=-A*BB*(NE+X(I-1)/AB)*H*Z(I-1)
X(I)=X0/6.+X(I-1)
Y(I)=Y0/6.+Y(I-1)
D0=Z0*DA*BA
DP=Z0*DB*BB
XI=4.*D0*(Y(I-1)+Y0/2.)*H
YI=-A*DP*(NE+(X(I-1)+X0/2.)/(AB*CB))*H
X(I)=X(I)+XI/3.
Y(I)=Y(I)+YI/3.
X0=4.*D0*(Y(I-1)+YI/2.)*H
Y0=-A*DP*(NE+(X(I-1)+XI/2.)/(AB*CB))*H
X(I)=X(I)+X0/3.
Y(I)=Y(I)+Y0/3.
AC=AC*CCC
AA=AA*CAC
AB=AB*CBC
BA=BA*DAA
BB=BB*DBB
BC=BC*DCC
XI=4.*Z(I)*BA*(Y(I-1)+Y0)*H
YI=-A*Z(I)*BB*(NE+(X(I-1)+X0)/AB)*H
X(I)=X(I)+XI/6.
Y(I)=Y(I)+YI/6.
WR=Z(I)*Z(I)*H/AA/AA
PR=PR+WR
IF(((I-1)/HM*HM).NE.(I-1)) GO TO 400
T=H*(I-1.)
GT=SQRT(A)*2.
GR=2./(SQRT(A))
GRT=GT*GT
ZY=Z(I)*GT/AA
XIAB=X(I)/AB
GRAC=Y(I)*GR/AC
ZYZY=ZY*ZY

```

```

PRRT=PR*GRT
WRITE (6,907) R,T,XIAB,GRAC
WRITE (6,909) ZYZY,PRRT
400 CONTINUE
200 JLIM=(ZL+H*V)/(H*V)
DO 201 J=1,JLIM
R=R+H*V
PR=0.
AC=1.
AA=1.
AB=1.
BA=1.
BB=1.
BC=1.
DO 201 I=2,NNN
X0=4.*Z(I-1)*H*BA*Y(I-1)
Y0=-A*Z(I-1)*BB*(NE+X(I-1)/AB)*H
HH=H*V
Z00=Z(I)/VAC+Z(I-1)
X00=X(I-1)/AB/CB+NE
Y00=Y(I)/VCC+Y(I-1)
Z0=-HH*Y(I)/BB/VCC
XX=X0/6.+X(I-1)
YY=Y0/6.+Y(I-1)
ZZ=Z0/6.+Z(I)/(VAC)
D0=DA*BA
DP=DB*BB
XI=4.*H*(Z00+Z0)/2.*(Y(I-1)+Y0/2.)*D0
YI=-A*H*(Z00+Z0)/2.*(X00+X0/2./AB/CB)*DP
ZI=-HH*(Y00+Y0)/2./DP
XX=XX+XI/3.
YY=YY+YI/3.
ZZ=ZZ+ZI/3.
X0=4.*H*(Z00+ZI)/2.*(Y(I-1)+YI/2.)*D0
Y0=-A*H*(Z00+ZI)/2.*(X00+XI/2./AB/CB)*DP
Z0=-HH*(Y00+YI)/2./DP

```

```

XX=XX+X0/3.
YY=YY+Y0/3.
ZZ=Z7+Z0/3.
AC=AC*CCC
AA=AA*CAC
AB=AB*CBC
BB=BB*DBB
BA=BA*DAA
BC=BC*DCC
YI=-A*H*(Z(I)/(VAC)+Z0)*(NE+(X(I-1)+X0)/AB)*BB
ZI=-HH*(Y(I-1)+Y0)/BB
XI=4.*H*(Z(I)/(VAC)+Z0)*(Y(I-1)+Y0)*BA
Y(I)=YY+YI/6.
X(I)=XX+XI/6.
Z(I)=ZZ+ZI/6.
WR=Z(I)*Z(I)*H/AA/AA
PR=PR+WR
IF (((J/KM*KM).NE.J).OR.(((I-1)/HM*HM).NE.(I-1))) GO TO 201
T=H*(I-1)+R
ZX=Z(I)*GT/AA
XIAB=X(I)/AB
GRAC=Y(I)*GR/AC
ZXZX=ZX*ZX
PRRT=PR*GRT
WRITE (6,907) R,T,XIAB,GRAC
WRITE (6,909) ZXZX,PRRT
201 CONTINUE
IF (MMM.NE.0) GO TO 999
901 FORMAT (6F10.3,I5)
902 FORMAT (3I5,4E10.3)
903 FORMAT (E10.3,I5,2E10.3,2I5)
904 FORMAT ('  L0          L1          L2          A          ZL          CK')
905 FORMAT ('  N      KM      HM          TN          W          CN          X(0)')
906 FORMAT ('  NE          V          TM          KK          CJ          MODE ')
907 FORMAT ('0',3H Z=,F8.5,3X,3H T=,F12.8,3H N=,F16.7,4X,2HK=,F16.7)
908 FORMAT (5F10.4)

```

```
909 FORMAT (3H F=,E16.7,3X,3HPR=,E16.7)
910 FORMAT(' INPUT INTENSITIES ')
CALL EXIT
END
```

REFERENCES

1. F. T. Arecchi and R. Bonifacio, "Theory of Optical Maser Amplifiers," IEEE J. Quantum Electronics, QE-1, pp. 169-178, July 1965.
2. C. L. Tang and B. D. Silverman, "Dynamic Effects on the Propagation of Intense Light Pulses in Optical Media" in Physics of Quantum Electronics, edited by P. L. Kelley, B. Lax, and P. E. Tannenwald (McGraw-Hill Book Co., Inc., New York, 1966), pp. 280-293.
3. W. G. Wagner, H. A. Haus, and T. K. Gustafson, "High Rate Optical Amplification," IEEE J. Quantum Electronics, QE-4, pp. 267-273, May 1968.
4. A. Icsevgi and W. E. Lamb, Jr., "Propagation of Light Pulses in a Laser Amplifier," Phys. Rev. 185, pp. 517-545, September 10, 1969.
5. A. J. DeMaria, H. A. Heynau, "Investigation of Means for Generating High-Energy and Extremely Narrow Laser Pulses," United Aircraft Final Report for Contract No. DA-01-021-AMC-15514(Z), Report No. F-920475-5, March 1967.
6. C. K. N. Patel and R. E. Slusher, "Self-Induced Transparency in Gases," Phys. Rev. Letters, 19, pp. 1019-1022, October 20, 1967.
7. O. R. Wood and S. E. Schwarz, "Passive Q-Switching of a CO<sub>2</sub> Laser," Appl. Phys. Letters, 11, pp. 88-89, August 1, 1967.
8. C. Hocker and C. Tang, "Observation of the Optical Transient Nutation Effect," Phys. Rev. Letters, 21, pp. 591-594, August 26, 1968.
9. P. A. Miles and J. W. Lotus, "A High-Power CO<sub>2</sub> Laser Radar Transmitter," IEEE J. Quantum Electronics, QE-4, pp. 811-819, November 1968.
10. D. L. Bobroff and H. A. Haus, "Impulse Response of Active Coupled Wave Systems," J. Appl. Phys. 38, pp. 390-403, January 1967.
11. M. V. Cerrillo and E. F. Bolinder, "On Basic Existence Theorems in Network Synthesis," Technical Report No. 246, Research Laboratory of Electronics, M. I. T., August 15, 1952.
12. F. A. Hopf and M. O. Scully, "Theory of an Inhomogeneously Broadened Laser Amplifier," Phys. Rev. 179, pp. 399-416, March 10, 1969.



13. H. A. Haus and C. M. Watson, "Step Response of Inhomogeneously Broadened Laser Medium," Quarterly Progress Report No. 92, Research Laboratory of Electronics, M. I. T., pp. 201-203, January 15, 1969.
14. T. J. Bridges, T. Y. Chang, and P. K. Cheo, "Pulse Response of Electro-Optic Modulators and Photoconductive Detectors at  $10.6 \mu$ ," Appl. Phys. Letters, 12, pp. 297-300, March 1968.
15. H. Kogelnik and T. J. Bridges, "A Nonresonant Multipass CO<sub>2</sub> Laser Amplifier," IEEE J. Quantum Electronics, QE-3, pp. 95-96, February 1967.
16. I. P. Kaminow and E. H. Turner, "Electro-Optic Light Modulators," Proc. IEEE, 54, pp. 1374-1390, October 1966.
17. H. Kogelnik and T. Li, "Laser Beams and Resonators," Proc. IEEE, 54, pp. 1312-1329, October 1966.
18. D. N. Ducsik, "Determination of Collision Cross Sections of CO<sub>2</sub>, He, N<sub>2</sub>, O<sub>2</sub>, CO, H<sub>2</sub>O and the Radiative Lifetime of the (001 - 100) CO<sub>2</sub> Laser Transition," S. B. Thesis, Department of Electrical Engineering, M. I. T., June 1969.
19. M. E. Drougard, "Optical Inhomogeneities in Gallium Arsenide," J. Appl. Phys. 37, pp. 1858-1866, March 15, 1966.
20. R. L. Abrams and P. K. Cheo, "Collisional Relaxation of CO<sub>2</sub> Rotational Levels by N<sub>2</sub> and He," Appl. Phys. Letters, 15, 177-178.
21. F. A. Hopf, C. K. Rhodes, and A. Szoke, "Influence of Degeneracy on Coherent Pulse Propagation in an Inhomogeneously Broadened Laser Amplifier," to be published, Phys. Rev., April 1970.
22. J. A. Armstrong and Eric Courtens, "Exact Solution of a  $\pi$ -Pulse Problem," IEEE J. Quantum Electronics, QE-4, pp. 411-419, June 1968.
23. S. L. McCall and E. L. Hahn, "Self-Induced Transparency by Pulsed Coherent Light," Phys. Rev. Letters, 18, pp. 908-911, May 22, 1967.
24. T. J. Bridges and P. K. Cheo, "Spontaneous Self-Pulsing and Cavity Dumping in a CO<sub>2</sub> Laser with Electro-Optic Q-Switching," Appl. Phys. Letters 14, pp. 262-264, May 1, 1969.
25. R. N. Lewis, E. A. Jung, G. L. Chapman, L. S. Van Loon, and T. A. Ramanowski, "Some High Voltage Pulse Techniques in Use at Argonne," IEEE Trans. Nuclear Science, NS13, pp. 84-88, April 1966.

26. C. L. Tang and H. Statz, "Optical Analog of the Transient Nutation Effect," Appl. Phys. Letters, 10, pp. 145-147, March 1, 1967.

## BIOGRAPHICAL NOTE

Paul W. Hoff was born in Pitcairn, Pennsylvania, on September 14, 1943. He attended primary and secondary schools there and was graduated from the Gateway Senior High School in 1961. He entered Massachusetts Institute of Technology in September 1961 and participated in the Electrical Engineering Cooperative Program at Bell Telephone Laboratories, receiving the S. B. and S. M. degrees in June 1966. As a graduate student in the Electrical Engineering Department he held an N. S. F. Fellowship and was a research assistant in the Research Laboratory of Electronics.

Mr. Hoff has accepted a position as Assistant Professor at M. I. T. in the Electrical Engineering Department beginning September 1970.